Master's thesis

2021

Mary Elizabeth Hemler

NTNU
Norwegian University of
Science and Technology
Faculty of Medicine and Health Sciences
Department of Neuromedicine and Movement Sciences

Mary Elizabeth Hemler

Using microdialysis to administer and assess drugs aimed at attenuating Alzheimer's disease-related neuropathology

May 2021

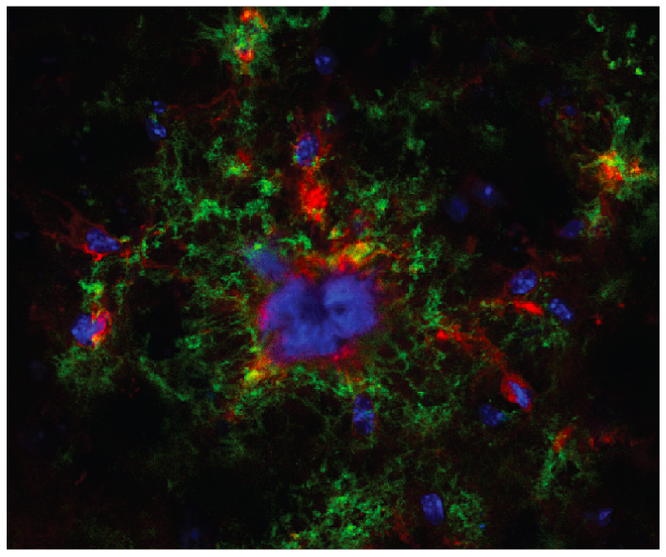

NTNU
Norwegian University of
Science and Technology

NTNU
Norwegian University of
Science and Technology

NTNU
Norwegian University of
Science and Technology

Using microdialysis to administer and assess drugs aimed at attenuating Alzheimer's disease-related neuropathology

Mary Elizabeth Hemler

Master of Science in Neuroscience
Submission date: May 2021
Supervisor: Ioanna & Axel Sandvig
Co-supervisor: Christiana Bjørkli

Norwegian University of Science and Technology
Department of Neuromedicine and Movement Sciences

Acknowledgements

First and foremost, I would like to thank Yanna and Axel Sandvig for taking me on as a master student in the Sandvig group; I feel extremely privileged to have experienced such a supportive and motivating lab environment while completing my thesis. I would also like to thank my daily co-supervisor, Christiana Bjørkli, for her unwavering kindness and expert guidance throughout every step of the master thesis process, and for inspiring me to continue in the Alzheimer's research field. I truly could not have dreamed up a more fantastic daily co-supervisor; words can do no justice to express my appreciation to you. I would also like to thank Bruno, Paolo, and Grethe at the Witter group for passing on their laboratory and microscope expertise. My deep gratitude also extends to my family back in the United States, who supported my dream to move to Norway and study a new field without hesitation. Finally, I would like to thank the greatest group of friends imaginable; to Ella, Ane, Raissa, Jørgen, Michael, Nora, Ivan, and Anita: thank you for your superb company, your love and support, for keeping me sane, and for making Trondheim a home.

Abstract

Alzheimer's disease is the most common form of dementia and is characterized by the neuropathological hallmarks amyloid-β and neurofibrillary tangles. Despite tremendous efforts in understanding the molecular, pathophysiological, and diagnostic criteria of Alzheimer's disease in the past 20 years, all disease-modifying therapies to date have failed to effectively treat patients. As the neuropathological alterations associated with the disease are estimated to appear up to two decades prior to the onset of clinical symptoms, initiating treatment in the preclinical stage may be necessary to halt the Alzheimer's disease biochemical cascade. While targeting the disease in the preclinical stage is not yet feasible in patients due to a lack of clear biomarkers, the use of preclinical animal models bypasses this limitation. Using a modified push-pull microdialysis methodology for the simultaneous infusion of disease-modifying drugs and collection of cerebrospinal fluid, we found that Fasudil reduces intracellular amyloid-β in young animals and amyloid plaques and cerebrospinal fluid amyloid-β in old animals, while Lonafarnib reduces tau neuropathology and cerebrospinal fluid tau biomarkers in young and old animals. However, an unexpected finding was that Lonafarnib treatment increased amyloid plaques and cerebrospinal fluid amyloid-β in old animals, suggesting that activating the endosomal-lysosomal system may inadvertently increase amyloid-β pathology if administered too late in the AD biochemical cascade. Taken together, these findings offer support for the application of repurposed drugs to attenuate Alzheimer's disease neuropathology at various timepoints in preclinical models to probe potential biochemical events that result in Alzheimer's disease.

Abbreviation list

3R/4R	3-repeat/4-repeat
3xTg	Triple-transgenic mouse model
AAV	Adeno-associated virus
Aβ	Amyloid-β
ABC	Avidin-biotin complex
AD	Alzheimer's disease
AKM/CoMed	Avdeling for Komparativ Medisin
APOE	Apolipoprotein E
APOE4	Apolipoprotein E ε4 allele
APP	Amyloid precursor protein
AV	Autophagic vacuole
BACE1	β-secretase cleavage enzyme 1
BBB	Blood-brain barrier
BCSFB	Blood-cerebrospinal fluid barrier
CA	Cornu ammonis
CNS	Central nervous system
CP	Choroid plexus
CSF	Cerebrospinal fluid
DAB	3,3'-diaminobenzidine
DAPI	4'6-diamidino-2-phenylindole
Dkk1	Dickkopf-1
DMSO	Dimethyl sulfoxide
DS	Down syndrome
dSub	Dorsal subiculum
EC	Entorhinal cortex
ELISA	Enzyme-linked immunosorbent assay
EOAD	Early-onset Alzheimer's disease
ER	Endoplasmic reticulum
FEP	Fluorinated ethylene propylene
GDP	Guanosine diphosphate
GFP	Green fluorescent protein
GSK-3β	Glycogen synthase kinase-3β
GTP	Guanosine triphosphate
HIAR	Heat-induced antigen retrieval
HPC	Hippocampi
iAβ	Intracellular amyloid-β
ISF	Interstitial fluid
LAMP1	Lysosomal-associated membrane protein 1
LANDO	LC3-associated endocytosis
LEC LII	Layer II of the lateral entorhinal cortex
LOAD	Late-onset Alzheimer's disease
LRP1	Lipoprotein receptor-related protein 1
LRP6	Low-density lipoprotein receptor-related protein 6
LTP	Long-term potentiation
LV	Lateral ventricle
MAP2	Microtubule-associated protein 2
MCI	Mild cognitive impairment
MRI	Magnetic resonance imaging
MTL	Medial temporal lobe
mTOR	Mammalian target of rapamycin
MVB	Multivesicular bodies
NFT	Neurofibrillary tangle
P-tau	Phosphorylated tau
PB	Phosphate buffer
PBT	PB containing 0.2% Triton-X-100
PET	Positron emission tomography
PFA	Paraformaldehyde
PSEN1	Presenilin-1
PSEN2	Presenilin-2
RAGE	Receptor for advanced glycation end products
ROCK	Rho-associated protein kinase
T-tau	Total tau
TBS-Tx	Tris-buffered saline with 2.5% Triton-X-100
TREM2	Triggering receptor expressed on myeloid cells 2
Tris-HCl	Tris(hydroxylmethyl)aminomethane
VLDLR	Very-low-density-lipoprotein receptor
Wnt	Wingless-related integration site
Wnt-PCP	Wingless-related integration site-planar-cell-polarity

Table of contents

1 Introduction

1.1 Introduction to Alzheimer's disease

The increasing life expectancy in Norway is estimated to more than double the number of people living with Alzheimer's disease (AD) and other forms of dementia by 2050[1]. AD affects approximately one in ten people and is pathologically characterized by brain volume loss, followed by impaired cognition, memory, and language[2, 3]. AD neuropathology is characterized by accumulation of extracellular amyloid-β (Aβ) plaques consisting of Aβ peptides, followed by the appearance of intracellular neurofibrillary tangles (NFTs) comprised of hyperphosphorylated tau proteins[4]. Despite tremendous efforts in understanding the molecular, pathophysiological, and diagnostic criteria of AD in the past 20 years, all disease-modifying therapeutic trials to date have failed to treat AD patients[5]. A central reason for failures in clinical trials aimed at altering the AD cascade is due to timing of administration; most trials begin at advanced stages of the disease, after irreversible neuronal death has already taken place[5, 6]. Converging evidence demonstrates that the pathophysiological processes of the disease initiate decades before the time of clinical diagnosis[7-9]. Therefore, initiating treatment early in the disease cascade, before cognitive impairment becomes apparent, may be necessary for protecting finely tuned neuronal circuits and consequently cognitive skills[10].

1.2 Pathophysiology of AD

AD is characterized by specific neuropathological changes that likely culminate in cerebral hypometabolism and widespread synaptic loss, eventually leading to neuronal death[11]. While Aβ and tau are considered the neuropathological hallmarks of the disease, it is important to note that AD pathophysiology has also been observed in cognitively normal individuals upon postmortem examination, although at significantly lower levels than observed in AD[12]. In addition to the accumulation of extracellular amyloid plaques and intracellular NFTs, the pathophysiology of AD is characterized by cortical atrophy[13, 14], enlarged brain ventricles[15], and widespread neuroinflammation[16, 17]. Although the inflammation observed in AD was initially thought to be a consequence of accumulating neurodegeneration, mounting evidence suggests that the sustained activation of the brain's resident immune cells, microglia, may exacerbate both Aβ and tau pathology and serve as a potential link in the pathogenesis of the disease[18, 19].

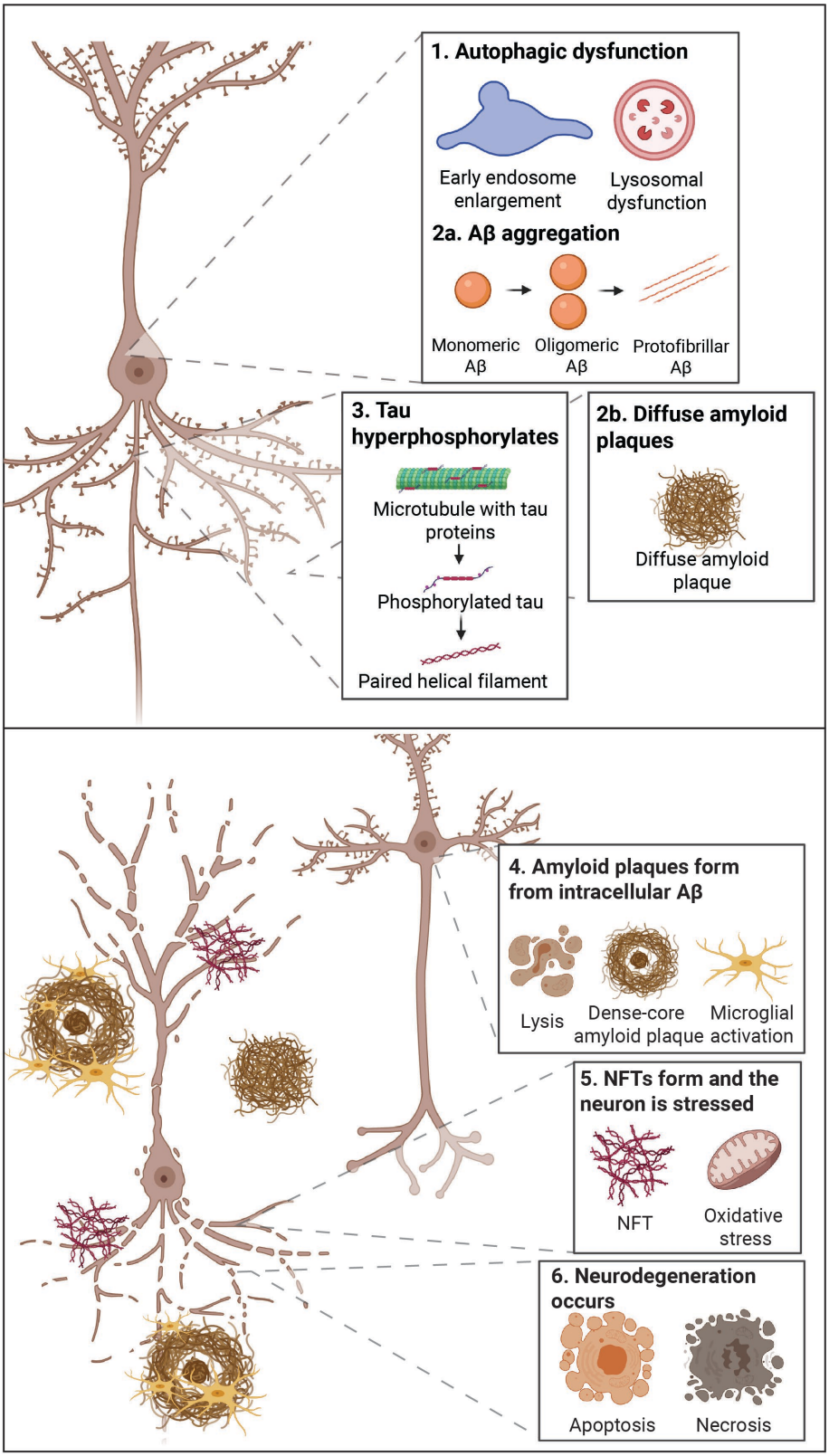

Figure 1.1. (A-B): Overview of the pathophysiology of AD. (A): Autophagic dysfunction first becomes apparent, particularly through an enlargement of early endosomes and accumulation of lysosomes. Next, Aβ progressively aggregates from monomeric to protofibrillar forms. At the same time, extracellular diffuse amyloid plaques appear. Tau protein then becomes hyperphosphorylated and detaches from the microtubule, ultimately aggregating into paired helical filaments. (B): A lysis event of the neuron occurs, forming a dense-core amyloid plaque and triggering microglial activation. Intracellular neurofibrillary tangles begin to appear, triggering oxidative stress. Finally, neurodegeneration of the neuron occurs, through both apoptotic and necrotic processes.

Figure adapted from Bjorkli et al.[20] and created with biorender.com. Abbreviations; Aβ: amyloid-β; NFT: neurofibrillary tangle.

1.2.1 Stages of pathological manifestation in AD

The pathophysiology of AD follows a predictable spatiotemporal pattern, with both animal models and patients first displaying intracellular Aβ (iAβ) accumulation in layer II of the lateral entorhinal cortex (LEC LII), followed by the deposition of amyloid plaques, first in the temporal neocortex, then in the entorhinal cortex (EC) and hippocampus, before ultimately involving the diencephalic nuclei and the cerebellum[21-23]. Aβ deposition expands anterogradely from regions exhibiting Aβ pathology into regions that receive neuronal projections from these areas[21]. Meanwhile, initial tau deposition begins in LEC LII, followed by the hippocampus and ultimately the neocortex[24]. Although the exact mechanisms behind the stereotyped propagation of tau misfolding remain to be elucidated, research suggests that tau aggregates can spread via transsynaptic propagation and in a cell-to-cell manner[25, 26]. In line with the progression of tau pathology, cortical atrophy appears first in the LEC and hippocampus of human patients, followed by atrophy of the posterior (i.e., temporal, parietal, and occipital) cortices and ultimately the frontal association cortices[27]. Magnetic resonance imaging (MRI) studies in humans have revealed that these brain alterations commence several years prior to the appearance of AD clinical symptoms[28].

1.2.2 The blood-brain barrier clearance pathways in AD

The blood-brain barrier (BBB) is a highly specialized, semi-permeable membrane composed of endothelial cells, astrocytic end-feet, and pericytes. The BBB prevents the entry of potentially toxic substances into the central nervous system (CNS) and represents the major interface for communication between neurons and circulating cells of the immune system[29, 30]. Additionally, transport across the BBB via receptor for advanced glycation end products (RAGE)-bearing cells represents a major clearance route for Aβ[31].

Soluble Aβ can be cleared from the brain through multiple routes, including transport across the BBB and blood-cerebrospinal fluid barrier (BCSFB), interstitial fluid (ISF) bulk flow, enzymatic degradation and cellular uptake via lysosomes, CSF absorption into the circulatory and lymphatic systems, and LC3-associated endocytosis (LANDO) in microglia[32]. While the continuous clearance of Aβ is vital for the maintenance of homeostasis within the CNS, clearance of Aβ and other potentially toxic substances may be reduced in AD due to BBB dysfunction[29]. Although research suggests that the breakdown of the BBB is at least partially a physiological consequence of aging[33], this process may be expedited by the deposition of Aβ into the vasculature and concomitant inflammation[29, 34]. Additionally, the deposition of tau

proximal to blood vessels may promote BBB dysfunction[35]. As the BBB controls and limits the entry of drug molecules into circulation, the disruption of the BBB associated with AD may affect pharmaceutical treatment of the disease.

1.2.3 Cleavage of APP and resulting APP-fragments

Aβ peptides, consisting of 36 to 43 amino acids, are natural products of metabolism resulting from the proteolysis of the amyloid precursor protein (APP). APP is a type-I transmembrane protein with its N-terminal within the extracellular space and its C-terminal within the cytosol[36, 37]. The proteolysis of APP occurs via two distinct processing pathways: the amyloidogenic pathway, which leads to Aβ generation, and the non-amyloidogenic pathway, which prevents Aβ generation[38]. In the amyloidogenic pathway, APP is first cleaved by β-secretase cleavage enzyme 1 (BACE1), generating APPβ and an APP carboxy-terminal fragment (C99). Further processing of C99 by ϒ-secretase generates Aβ fragments of several different peptide lengths, including Aβ40 and Aβ42. While the majority of secreted Aβ peptides are 40 amino acids in length (Aβ40), the less common longer, 42 amino acid species (Aβ42) have received more attention due to the increased propensity of these peptides to nucleate and drive the production of amyloid fibrils[39, 40]. In the non-amyloidogenic pathway, APP is cleaved by α-secretase approximately in the middle of the Aβ sequence, precluding Aβ formation[41]. Although the physiological functions of APP and Aβ have been heavily researched, clear consensus on the proteins' functions remain unresolved. APP has been reported to have trophic functions such as influencing cell proliferation, differentiation, neurite growth, and synaptogenesis[42], while Aβ has been reported to regulate synaptic transmission in mice[43] and demonstrates antimicrobial properties *in vitro* and *in vivo*[44, 45].

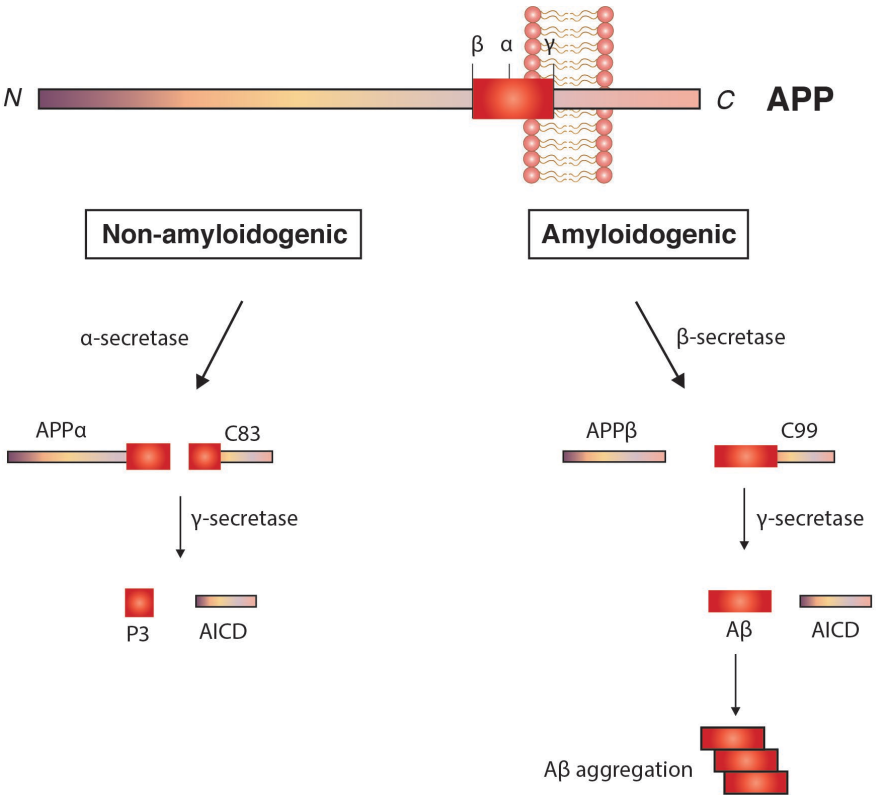

Figure 1.2. Cleavage of APP and its proteolytic products. APP can undergo proteolytic processing via 2 pathways. In the non-amyloidogenic pathway, cleavage by α-secretase occurs within the Aβ domain, precluding Aβ formation and generating the large, soluble APPα and a non-amyloidogenic C-terminal fragment (C83). Further proteolysis of this fragment generates the non-amyloidogenic fragment P3 and the APP intracellular domain (AICD). Alternatively, in the amyloidogenic pathway, cleavage by β-secretase occurs at the beginning of the Aβ domain and generates a shorter soluble N-terminus, APPβ, and an amyloidogenic C-terminal fragment (C99). Further processing by ϒ-secretase generates the AICD as well as Aβ fragments of several different peptide lengths, including Aβ40 and Aβ42. Figure adapted from Wilson et al.[46] Abbreviations; AICD: amyloid precursor protein intracellular domain; APP: amyloid precursor protein; Aβ: amyloid-β; C: carboxyl-terminus; N: amino-terminus.

1.2.4 Pathophysiology of tau

The microtubule-associated protein tau is encoded by a single gene, *MAPT*, which is located on chromosome 17. Mutations in the *MAPT* gene can cause frontotemporal dementia with parkinsonism linked to chromosome 17, providing clear evidence that tauopathy is causative of neurodegeneration[47]. However, major gaps in our knowledge remain regarding how these mutations promote tau aggregation and neurodegeneration in AD. Human brains express six molecular isoforms of tau, which are the result of alternative mRNA splicing, with or without exons 2, 3, and 10[48]. Insertion of exon 10 incurs 4-repeat (4R) tau isoforms, while exclusion of exon 10 incurs 3-repeat (3R) tau isoforms. Both 4R and 3R tau isoforms are found in the adult human brain, primarily in the axons of neurons in healthy physiological conditions, while 3R tau isoforms are not present in adult mice[49, 50].

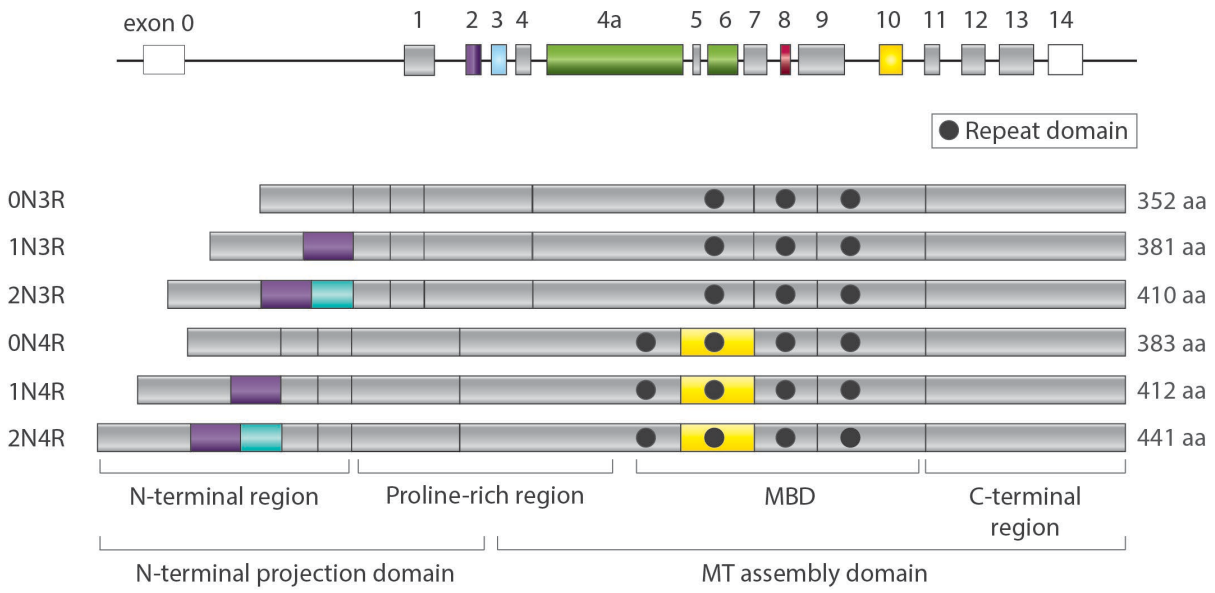

Figure 1.3. Tau isoform expression. In the human CNS, six isoforms exist that contain either no (0N), one (1N), or two (2N) amino-terminal inserts as a result of inclusion or exclusion of exons 2 and 3, and either three (3R) or four (4R) MBDs as a result of inclusion or exclusion of exon 10. Exons 4a and 6 have been reported in isoforms in the peripheral nervous system, while exon 8 has not been reported in any isoform. Figure adapted from Li et al.[51]. Abbreviations; aa: amino acids; C-terminal: carboxyl-terminal; MBD: microtubule binding domain; MT: microtubule; N-terminal: amino-terminal.

Although the physiological roles of tau in the human brain are continuing to be revealed, an established normal physiological function of the protein is to promote the assembly of tubulin subunits into microtubules[52]. Tau has frequently been stated in the literature as a stabilizer of microtubules[52-54]; however, recent research suggests that tau may instead increase the lability of microtubules by preventing the binding of genuine microtubule stabilizers, such as MAP6[55]. Tau is a natively unfolded protein containing 85 potential serine (S), threonine (T), and tyrosine (Y) phosphorylation sites. In addition to phosphorylation, tau protein can be modified in several ways, including N- and C-terminal proteolytic cleavage, nitration, glycosylation, acetylation, glycation, ubiquitylation, and filament formation[56]. Animal models of AD have demonstrated that abnormal phosphorylation (and eventual hyperphosphorylation) of tau may cause the protein to mislocalize from the axons of adult neurons to the somatodendritic compartment, where the protein aggregates into NFTs[57, 58]. Initial abnormal tau phosphorylation may be the result of altered activity of kinases such as glycogen synthase kinase-3β (GSK-3β)[59].

1.3 The role of amyloid-β in AD

The amyloid cascade hypothesis has been the prevailing explanation for the pathogenesis of Aβ for over 25 years[11, 60-62]. Although the amyloid cascade hypothesis has been revised multiple times throughout the decades, at its core, the hypothesis holds that Aβ production and/or Aβ fibril formation is the central pathogenic cause of AD. Early versions of the

hypothesis were focused on the adverse effects of large, insoluble amyloid plaques on surrounding dendrites, axons, and glia[61, 62], while more recent versions of the hypothesis have implicated the toxicity of soluble oligomeric Aβ and/or an imbalance between the production and clearance of Aβ[63].

The amyloid cascade hypothesis first originated out of the discovery that mutations in the *APP* gene were causative for a minority of early-onset autosomal dominant AD cases[64, 65]. Early-onset AD (EOAD) is differentiated from late-onset AD (LOAD), with the former having an age of onset ≤ 65 and typically displaying a more aggressive course and shorter survival time compared to LOAD[66]. Further support for the amyloid cascade hypothesis came from the link between the *APP* gene and down syndrome (DS); the *APP* gene is located on chromosome 21, and overexpression of *APP* results in a striking propensity for individuals with DS to develop EOAD[67]. Complete trisomy of chromosome 21 causes universal development of amyloid plaques and NFTs, with two-thirds of individuals with DS developing dementia by age 60[68]. In fact, no NFTs have been reported in individuals with DS and AD in the absence of dense-core amyloid plaque pathology, providing strong support for the amyloid cascade hypothesis[69]. Therefore, it is believed that the additional copy of the *APP* gene in individuals with DS may drive the development of AD by increasing levels of Aβ and ultimately tau.

Genetic mutations of *APP* are also common in EOAD, with pathogenic mutations typically clustered near β-secretase or ϒ-secretase cleavage sites. Other mutations observed in EOAD include mutations in *presenilins 1* and *2* (*PSEN1* and *PSEN2*), which are components of ϒ-secretase[70]. These three genetic loci associated with EOAD all culminate in an increased production of Aβ42, lending support to the amyloid cascade hypothesis. Although the mutations in *APP* and the presenilins are fully penetrant and guarantee onset of the disease, EOAD cases account for fewer than 5% of all AD cases[71].

Aβ dysregulation in LOAD is not well-understood. As research has demonstrated that individuals with LOAD exhibit approximately a 30% reduction in Aβ clearance, Aβ dysregulation in LOAD is believed to be a result of deficient clearance of Aβ rather than overproduction[72]. As mentioned previously, the functionality of the BBB and other clearance systems declines throughout the lifespan in humans[73, 74]. In line with this, the greatest overall risk factor for LOAD appears to be increased age[75]. The strongest identified genetic risk factor for LOAD is the *apolipoprotein E* (*APOE*) ε4 allele (*APOE4*)[76], which is associated with an earlier age of onset in LOAD[77] and leads to increased Aβ deposition in both animal models[78] and AD patients[79]. Research using animal models suggests that *APOE* may compete with Aβ for binding to lipoprotein receptor-related protein 1 (LRP1), instead directing the rapid

clearance of soluble Aβ to the very-low-density-lipoprotein receptor (VLDLR), which ultimately results in impaired Aβ clearance by astrocytes[80, 81]. Therefore, *APOE4* likely contributes to AD pathogenesis via both increased production and reduced clearance of Aβ.

According to the amyloid cascade hypothesis, the primary driving force in AD pathogenesis is the progressive accumulation of Aβ in the brain. In EOAD, this accumulation is the result of specific mutations that lead to an increased rate of the production of toxic Aβ species. The underlying mechanisms behind the accumulation of toxic Aβ in LOAD are less clear but likely involve faulty clearance mechanisms. While decades of research have led to the clear conclusion that Aβ peptides play a central role in the pathogenesis of AD, the amyloid cascade hypothesis has been increasingly challenged in recent years, primarily due to disappointing results from Aβ-targeting disease-modifying drugs[82-84].

1.3.1 Forms of Aβ

In the extracellular space, Aβ proteins can exist in multiple assembly states, ranging from monomeric to soluble, non-fibrillar oligomeric formations to insoluble, fibrillar structures present in amyloid plaques[85]. While some studies suggest that oligomers exist as an intermediate step between monomeric and fibrillar forms of Aβ[86-88], other studies have pointed to the formation of oligomers as an alternative assembly process to Aβ monomers directly forming protofibrils and fibrillar amyloid plaques[89, 90]. Therefore, it is currently unknown whether therapeutic interventions that reduce Aβ fibrils at the cost of augmenting nonfibrillar oligomeric Aβ species would be helpful or harmful[90].

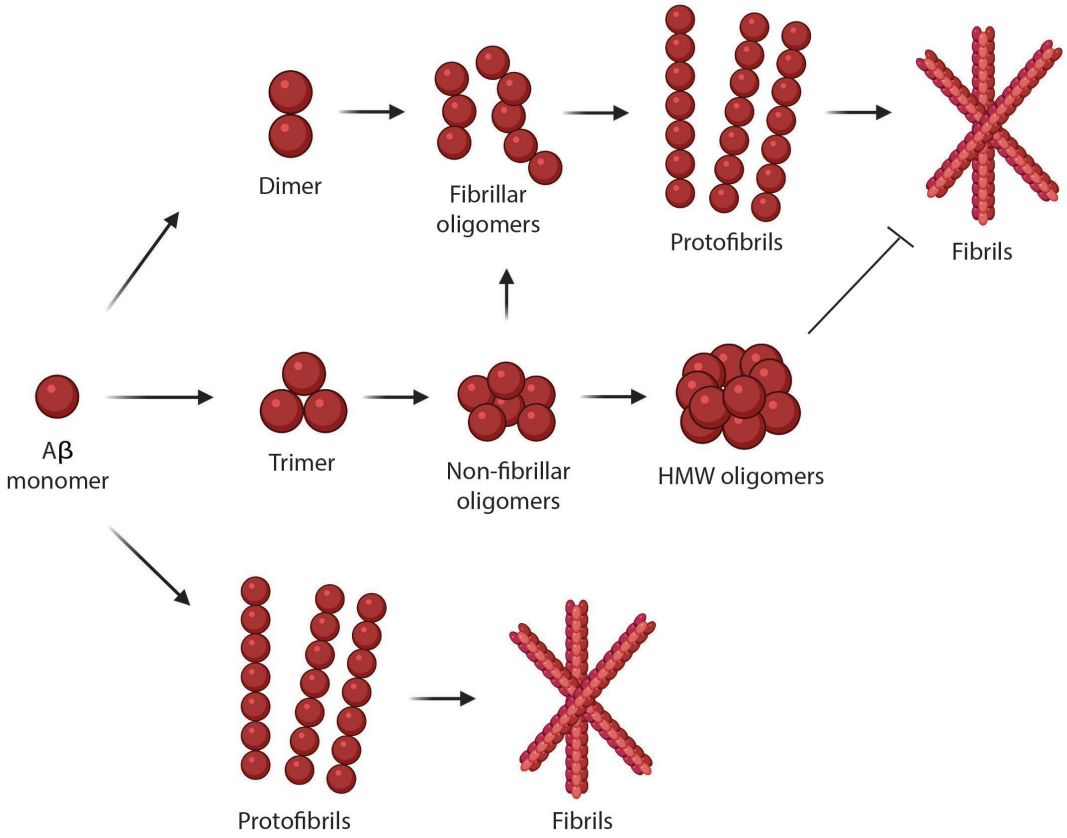

Figure 1.4. Schematic representation of potential Aβ aggregation pathways. In one pathway, Aβ monomers form into dimers then quickly form protofibrils and mature fibrils (top). Other Aβ oligomers such as trimers and globulomers pool as stable non-fibrillar oligomers (middle). However, research has suggested that Aβ monomers can also directly aggregate into protofibrils and fibrils (bottom), with oligomer formation existing as an alternative assembly process. Figure adapted from Huang et al.[91] and created with biorender.com.

1.3.1.1 Amyloid plaques

Amyloid plaques, also referred to as amyloid fibrils, constitute insoluble extracellular aggregates that are considered a core neuropathological hallmark of AD. Amyloid plaques can further be classified into diffuse and dense-core amyloid plaques based on their morphology and immunostaining with Thioflavin-S or Congo Red[92]. Diffuse amyloid plaques are amorphous amyloid deposits that are negative for both Thioflavin-S and Congo Red and can be found in both demented and non-demented individuals. In contrast, dense-core amyloid plaques are fibrillar amyloid deposits that contain a compact core and stain positive for both Thioflavin-S and Congo Red. Dense-core amyloid plaques are typically surrounded by dystrophic neurites and considered to be the toxic form of amyloid plaques, as their presence is associated with cognitive impairment[92].

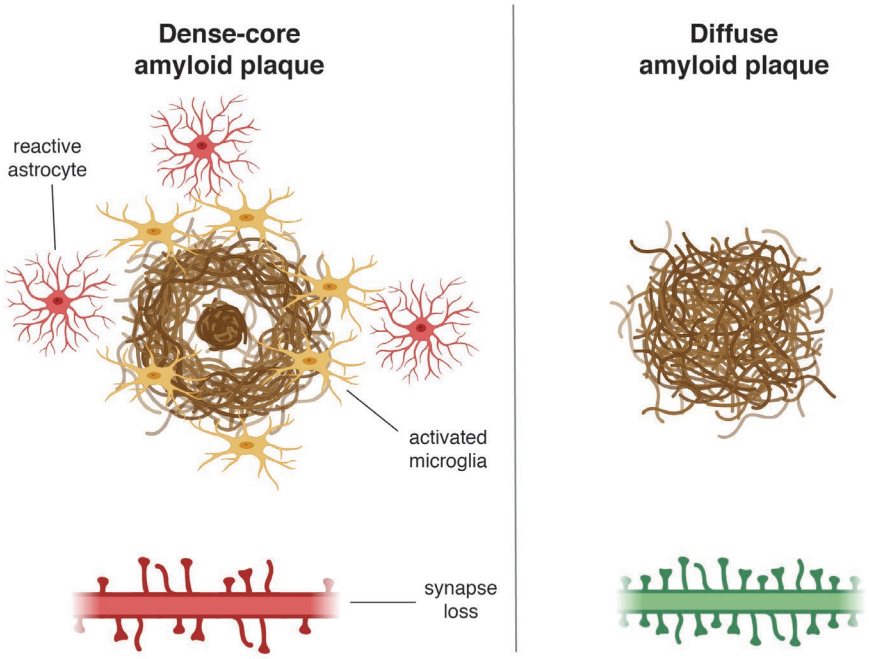

Figure 1.5. Schematic of differences between dense-core amyloid plaques and diffuse amyloid plaques. Dense-core amyloid plaques contain a compact core and are associated with inflammation in the forms of activated microglia within the dense-core amyloid plaque and reactive astrocytes around the periphery of the dense-core amyloid plaque. Moreover, dense-core amyloid plaques are associated with synapse loss. Meanwhile, diffuse amyloid plaques are not associated with inflammatory processes or synapse loss. Figured created with biorender.com.

While there is widespread acceptance that amyloid plaques are the consequence of extracellular seeding of amyloid peptides followed by the cumulative deposition of Aβ at these seeding sites, this "seeding hypothesis" fails to account for the differential morphological features of amyloid plaques[62]. Moreover, while dense-core amyloid plaques are associated with inflammation secondary to activated microglia within amyloid plaques (see section 4.9) and reactive astrocytes outside the perimeter of amyloid plaques, as well as synaptic loss, diffuse amyloid plaques are not associated with glial responses or synaptic loss[92]. Therefore, it is possible that these morphologically distinct amyloid plaques have different origins and should be considered as distinct entities in the context of AD treatment[93].

1.3.1.2 Intracellular Aβ

Although neither the number nor size or amyloid plaques is reliably correlated to cognitive status in AD patients[94], total Aβ load appears to be a better predictive measure[95]. A particular form of Aβ that may have detrimental cognitive effects is iAβ. Research using animal models has demonstrated that synaptic dysfunction, including LTP deficits, manifests prior to amyloid plaque and NFT pathology[96]. Additionally, such animal models have demonstrated that this long-term synaptic plasticity dysfunction correlates with the accumulation of iAβ[96] and is reversed after clearance of iAβ pathology by immunotherapy[97].

Cell biology studies have generally supported the view that Aβ is generated intracellularly[98] in a variety of subcellular compartments, including the endoplasmic reticulum (ER)[99], the trans-Golgi network[100], and the autophagic and endosomal-lysosomal systems[101, 102], as well as in actin inclusions containing APP and its proteolytic processing machinery[103]. However, it is still unknown whether the accumulation of iAβ is due to the retention and subsequent aggregation of intracellularly generated Aβ or represents the re-uptake of extracellular Aβ. While the AD dogma suggests that the accumulation of Aβ occurs extracellularly, leading to the formation of amyloid plaques, there have been several reasons to question this notion. For instance, research has suggested that the gradual intracellular accumulation of Aβ42 may lead to eventual cellular lysis and the deposition of Aβ into amyloid plaques[104]. This idea is supported by research reporting that most of the so-called 'dense cores' of amyloid plaques in the EC and hippocampus exhibit a remarkably consistent, spherical shape, which would likely not be the case if such amyloid plaques were formed extracellularly, as released lysosomal proteases would be expected to facilitate a radial dispersion of released cytoplasmic materials after disrupting the integrity of the cell membrane. Additionally, this research revealed that a cytosolic remnant that frequently resembles the nucleus of Aβ-laden pyramidal cells from the hippocampus and EC can be found at the center of most amyloid plaques[104]. In line with this, it has been shown that patients with DS accumulate iAβ prior to the formation of extracellular amyloid plaques[105], while research using animal models has also shown that iAβ levels decrease as extracellular amyloid plaques begin to accumulate[88].

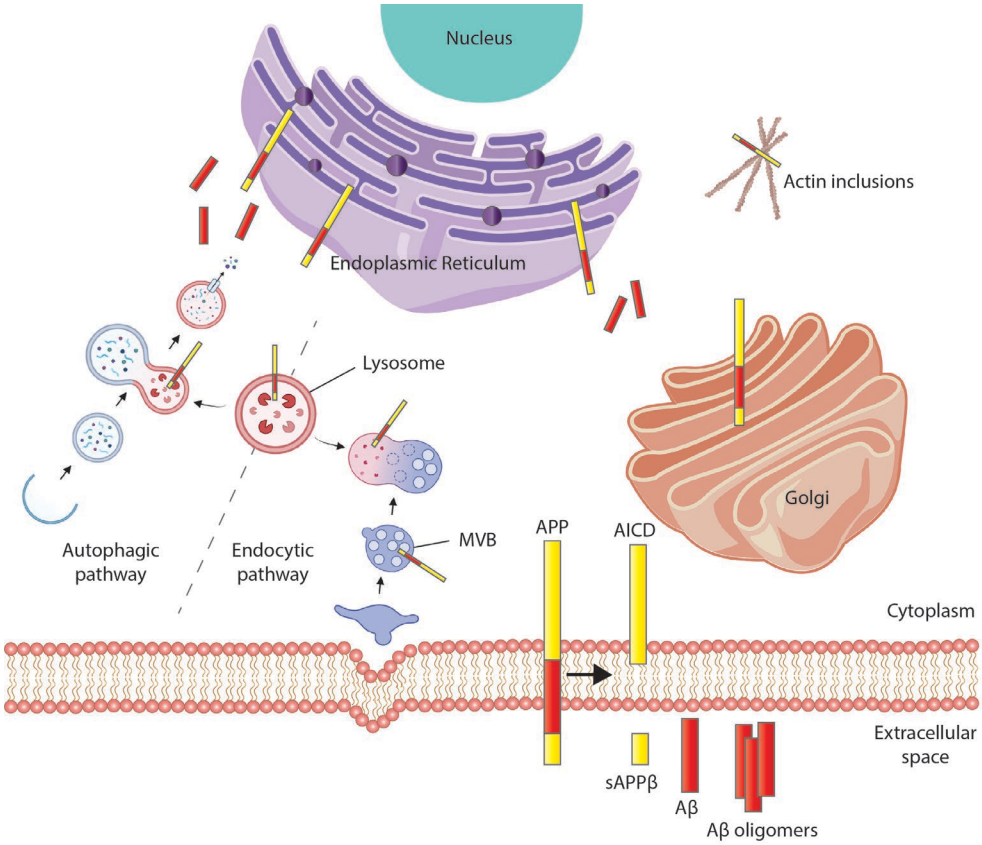

Figure 1.6. Intracellular sites of APP processing and Aβ production. APP is present in the ER, the trans-Golgi network, at actin inclusions, in the autophagic and endocytic pathways (particularly in MVBs and lysosomes), and in the plasma membrane. Figure adapted from Placido et al.[106] and created with biorender.com. Abbreviations; Aβ: amyloid-β; AICD: amyloid precursor protein intracellular domain; APP: amyloid precursor protein; MVB: multivesicular body; sAPPβ: soluble amyloid precursor protein-β.

1.3.1.2.1 Oligomeric Aβ

Mounting evidence suggests that the most pathogenic Aβ species are the intermediate oligomeric assemblies that precede the formation of amyloid fibrils[85, 107-109]. IAβ appears to be more likely to oligomerize than extracellular Aβ, though both extracellular and iAβ can be oligomeric[110]. While it is difficult to assess the structural determinants of protein oligomers responsible for cellular dysfunction, as they are structurally heterogeneous[108], multiple species of oligomeric Aβ are recognized as causative of synaptic damage and memory decline[111]. Low-weight Aβ oligomers, including dimers and trimers, have been shown to decrease dendritic spine density and potently block LTP when injected onto hippocampal slices[112], while higher-weight Aβ oligomers, such as dodecamers, have been shown to impair spatial memory, as evidenced by behavioral deficits in the Morris water maze test[113].

Additional support for the notion that oligomeric, readily diffusible assemblies of Aβ are the principal cytotoxic species comes from research demonstrating that *APP* transgenic mice exhibit electrophysiological, neuroanatomical, and behavioral abnormalities prior to Aβ deposits becoming microscopically visible[114]. In general, small oligomers provide a far greater

surface area for interactions with neurons than the large, non-diffusible amyloid plaques[114]. Additionally, oligomeric Aβ may cause neuronal damage indirectly by stimulating microglia to release neurotoxic mediators that propagate an inflammatory response[115]. Understanding the roles of the various species of Aβ peptides as well as the early molecular events leading to the deposition of amyloid plaques represent major challenges for developing successful AD drug treatment.

1.3.2 Role of the Wnt signaling pathway

Wingless-related integration site (Wnt) signaling plays critical roles in various cellular processes, including cell adhesion, cell fate determination, and synaptic activity[116]. Dysfunctional Wnt signaling induced by Aβ has been reported in AD[117]. As Wnt signaling plays a crucial role in regulating the formation and function of neuronal circuits, it has been hypothesized that the neurodegeneration and synapse impairment observed in AD may be related to Aβ-induced Wnt signaling dysfunction[118]. Aβ has been shown to activate a branch of Wnt signaling known as the Wnt-planar-cell-polarity (Wnt-PCP) pathway through the induction of Dickkopf-1 (Dkk1)[119]. Subsequently, Dkk1 blocks the binding of low-density lipoprotein receptor-related protein 6 (LRP6) to frizzled, preventing canonical Wnt-β catenin activity and activating Wnt-PCP signaling[120]. Research has demonstrated that activation of Wnt-β catenin signaling enhances synapse stability and reduces Aβ production, while activation of Wnt-PCP signaling drives synapse retraction and results in increased Aβ production[121]. Therefore, manipulating the Wnt signaling pathway may be relevant as an early intervention for treatment of AD.

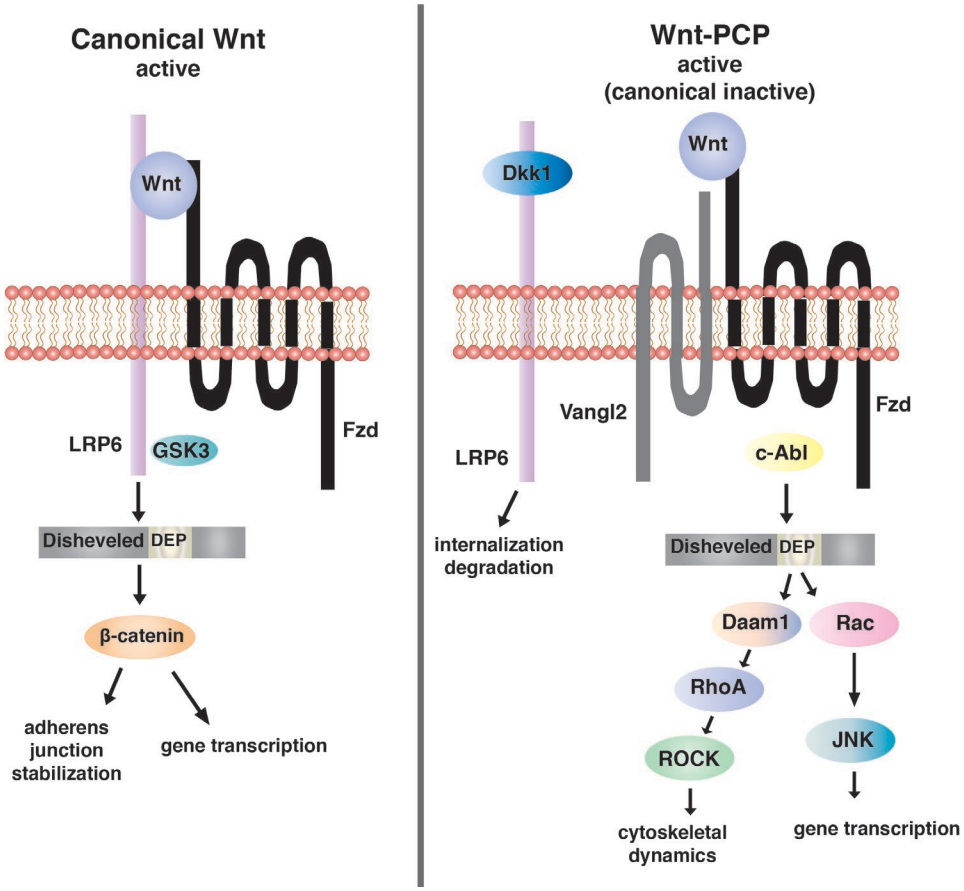

Figure 1.7. Schematic of the canonical Wnt and Wnt-PCP pathways. Aβ has been shown to activate the Wnt-PCP pathway through the ability of Aβ to induce Dkk1. Dkk1 then prevents the binding interaction between LRP6 and frizzled, activating Wnt-PCP signaling and blocking canonical Wnt-β-catenin activity. In the Wnt-PCP pathway, the two arms diverge below disheveled, acting via Daam/RhoA/ROCK to regulate cytoskeletal dynamics and JNK/c-Jun to regulate gene transcription. Figured adapted from Sellers et al.[122]. Abbreviations; Aβ: amyloid-β; DAAM1: disheveled associated activator of morphogenesis 1; DEP: DEP domain of disheveled protein; Dkk1: Dickkopf-1; Dvl: disheveled; Fzd: frizzled; GSK3: glycogen synthase kinase 3; JNK1: c-Jun N-terminal kinase; LRP6: low-density lipoprotein receptor-related protein 6; PCP: planar cell polarity; RhoA: Ras homolog family member A; ROCK: Rho-associated coiled-coil containing protein kinase; Vangl2: Van Gogh-like protein 2; Wnt: Wingless-related integration site.

The Wnt signaling pathway may also provide a potential link between Aβ and subsequent development of tau hyperphosphorylation. A growing body of data provides evidence that misfolded, toxic oligomers of Aβ and tau can spread extracellularly through the brain in a prion-like manner[26, 123, 124]. In line with this, Aβ42 oligomers have been found to increase tau phosphorylation and compromise cell survival through a mechanism mediated by GSK-3β[125]. While the canonical Wnt-β catenin pathway results in the inactivation of GSK-3β, Dkk1 induction has been shown to induce the upregulation of GSK-3β activity and thereby increase tau phosphorylation and ultimately hyperphosphorylation[126]. Therefore, Aβ may induce and exacerbate tau phosphorylation by inhibiting the canonical Wnt pathway.

1.4 The role of tau in AD

1.4.1 Formation of neurofibrillary tangles

As tau pathology propagates in a stereotypical manner in the AD brain and correlates with disease severity and cognitive impairment[24], it is likely that the aggregation of tau plays a major role in AD-related neurodegeneration. While the exact mechanisms behind tau-induced neurodegeneration remain to be elucidated, research points to a probable combination of loss of normal tau function and gains of pathological functions of abnormally phosphorylated tau. Abnormal phosphorylation of tau likely leads to detachment of tau from microtubules, preventing its normal physiological functions of microtubule assembly and microtubule stabilization/labilization[127]. Additionally, while some research suggests that NFTs themselves may alter neuronal firing and ultimately lead to synapse loss and neurodegeneration[128, 129], other research has found that the presence of NFTs alone is insufficient to disrupt neuronal function[130, 131]. Therefore, while tau undoubtedly plays a central role in the pathogenesis of AD, it is likely that the neurodegeneration seen in the disease is the result of a complex interplay of multiple factors.

1.4.2 Autophagy-mediated tau clearance mechanisms

The lysosomal degradation pathway referred to as macroautophagy (hereafter autophagy) is the only known mechanism that eukaryotic cells possess that can dispose of intracellular organelles and protein aggregates too large to be degraded by the proteasome[132]. Autophagy is initiated by the formation of the phagophore, which then elongates and expands to sequester material for degradation, forming a double-membraned autophagosome. The autophagosome then matures through docking and fusion with a lysosome, creating an autolysosome. Finally, the inner membrane and cargo of the autophagosome are broken down through acid hydrolases inside the autolysosome and the resulting macromolecules are recycled through permeases[133]. Previous research suggests that autophagy appears to be a major route for tau clearance in healthy neurons[134].

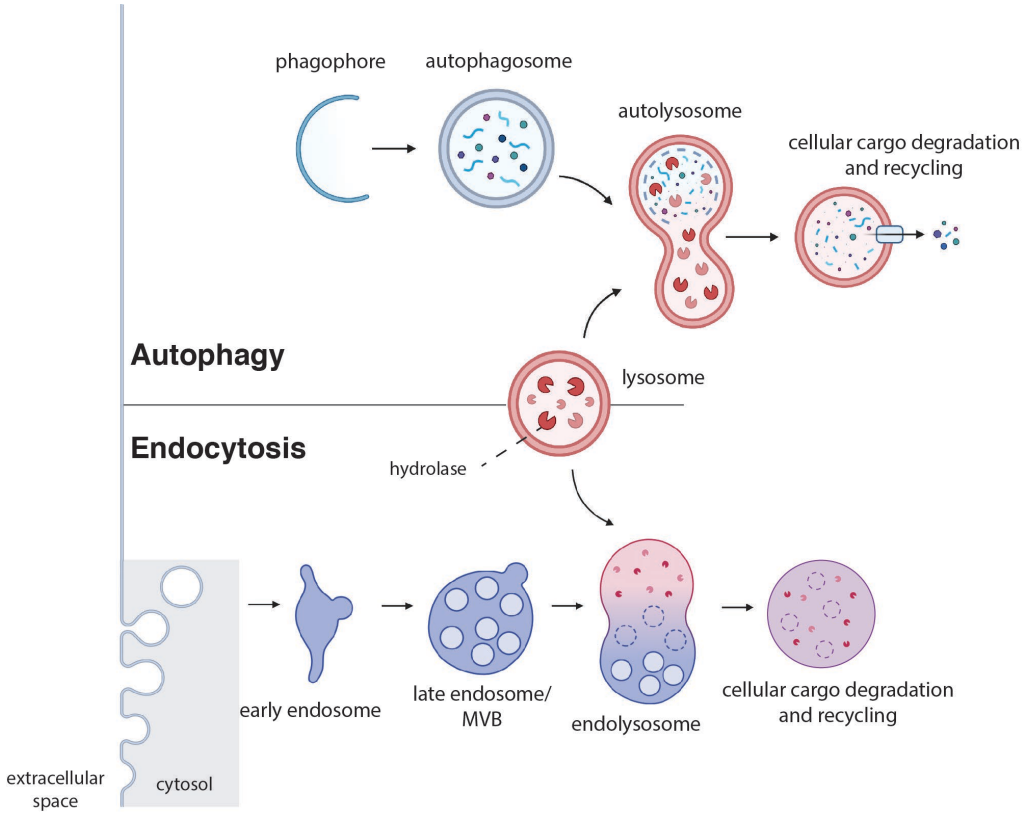

Figure 1.8. Overview of the autophagic and endocytic pathways. In macroautophagy, the phagophore encloses a portion of cytoplasm that contains organelles and large proteins destined for degradation, forming an autophagosome. The autophagosome then fuses with a lysosome, forming an autolysosome. Lysosomal hydrolases then degrade the internalized material and recycle components back to the plasma membrane. Endocytosis first involves internalization of extracellular material and plasma membrane, which are then delivered to the early endosome. After progressive maturation of the early endosome into a late endosome (also referred to as a multivesicular body [MVB]), the late endosome fuses with a lysosome. As in autophagy, cellular cargo in the lysosome is then degraded via acid hydolases. Therefore, both the autophagic and the endocytic pathways converge on the lysosome. Figure adapted from Birgisdottir et al.[135] and created with biorender.com.

While an excess of autophagosomes and other autophagic vacuoles (AV) is frequently observed in neurons in the neocortex of AD brains[136], it is unclear whether autophagy impairment is a contributor or consequence of tauopathy[137, 138]. Regardless of the initial cause, a progressive impairment of AV maturation to lysosomes appears to play a role in the pathogenic accumulation of AVs[139]. Activating autophagy has increasingly been considered as a potential therapeutic treatment for AD, with animal and cellular models showing that autophagy activators can reduce the levels of misfolded and aggregation proteins, prevent the spread of tau, and reduce neuronal loss[140-142]. In particular, the inhibition of mammalian target of rapamycin (mTOR) signaling has been suggested as a potential therapeutic strategy for reducing NFTs[143, 144]. Considered a master regulator of autophagy, mTOR negatively regulates induction of the phagophore[145, 146]. In line with this, administration of the mTOR inhibitor rapamycin has been shown to reduce tau pathology in a pure tauopathy mouse model[147].

Additionally, cell culture studies have revealed that mTOR inhibitors reduce tau levels by activating autophagy[148]. However, the impact of autophagy upregulation on Aβ pathology has been less well-characterized.

1.5 Protein abnormalities in cerebrospinal fluid as an AD biomarker

An AD biomarker can be defined as a measurable indicator within a patient that may be used to test and monitor the progress of pathology[149]. Ideally, a biomarker should be consistent, readily accessible, inexpensive, and easy to implement in the clinic or primary care setting[20, 150, 151]. Measuring protein concentration changes in cerebrospinal fluid (CSF) has gained traction as a biomarker for AD due to its reflection of true biochemical changes in the brain[152, 153]. The CSF is continuously secreted by the four choroid plexuses (CP), located in the two lateral, the third, and the fourth ventricles of the brain[154]. The three core CSF biomarkers that are used for AD diagnosis include Aβ42, total tau (t-tau), and phosphorylated tau (p-tau)[155]. Using a combination of these three biomarkers is better than using them individually, particularly for the differential diagnosis of AD from other neurodegenerative diseases[156].

1.5.1 Classification and temporal course of CSF biomarkers

Due to the long prodromal phase of AD, understanding the temporal course of CSF biomarkers offers valuable insight into the extent of disease progression. In patients, the most widely used method for CSF sampling is by lumbar puncture. Meanwhile in rodents, the most widely used method for CSF sampling is collection from the cisterna magna without repeated sampling. However, collection from the cisterna magna is a terminal procedure; *in vivo* microdialysis offers an alternative CSF sampling technique for the continuous sampling of molecules within the extracellular space[20, 157].

1.5.1.1 Amyloid-β as a biomarker for AD

Although the AD field cannot yet offer answers to how Aβ pathology initiates, it is generally accepted that after production, Aβ42 aggregates and accumulates intracellularly and/or in the extracellular space up to a critical threshold, at which point CSF Aβ42 decreases[158]. This decrease in CSF Aβ42 represents the sequestering of the peptide into plaques in the brain parenchyma[159]. Therefore, a widely used biomarker in AD diagnostic research is CSF measurement of Aβ40 and Aβ42[20]. While Aβ40 is typically present at approximately 10-20 times increased concentration in CSF, Aβ42 tends to aggregate more readily and correlates better with AD neuropathology[20, 160]. Additionally, measurement of the ratio of CSF Aβ42:Aβ40 is more accurate in distinguishing between mild cognitive impairment (MCI; transition phase to AD) patients who progress or not to develop AD dementia[161, 162].

Given that CSF Aβ42 changes occur at an earlier time point in the disease process than changes in CSF t-tau or p-tau, CSF Aβ42 is an appealing early biomarker for AD[163]. However, the temporal course of CSF Aβ42 changes has been difficult to elucidate, as some studies have indicated that Aβ42 levels increase[164], while other studies have indicated levels decrease[165] or exhibit no change[166] over the course of the disease. The conflicting Aβ42 levels observed in AD patients may reflect different time points of the disease, with the initial observed increase reflecting an increase in Aβ generation via the APP processing pathway, followed by a decline in CSF Aβ that represents the deposition of Aβ into amyloid plaques[167]. Mouse models of AD have confirmed an increase in CSF Aβ42 around the time of the appearance of the first amyloid plaques followed by a decrease in CSF Aβ42 throughout the course of amyloid plaque deposition[167, 168]. However, the initial increase in CSF Aβ42 at the time of first amyloid plaque deposition has been difficult to confirm in humans due to the long, asymptomatic prodromal phase of AD. Therefore, low CSF Aβ42 is considered a sensitive marker for AD[169, 170].

1.5.1.2 Tau as a biomarker for AD

Increased CSF t-tau concentrations constitutes a sensitive marker for neurodegeneration, albeit a non-specific one for AD[20]. Although it is still not entirely clear whether the phosphorylation of tau plays a *critical* role in the propensity of the protein to aggregate, animal studies have pointed to a link between tau phosphorylation and the formation of tau aggregates[171]. In line with this, studies have found correlations between levels of CSF p-tau and NFT deposition in the brain[172, 173]. Unlike CSF Aβ42 levels, both CSF t-tau and p-tau levels generally increase throughout the course of AD[174]. High CSF t-tau and p-tau levels have also been shown to better predict the progression of cognitive decline compared to CSF Aβ42[175]. However, the best CSF biomarker of AD is considered the combination of low CSF Aβ42 and high CSF tau (CSF t-tau and p-tau), which is a pattern with high diagnostic accuracy that is referred to as the "AD signature"[176]. However, it is important to note that while increases in CSF tau are indicative of the neurodegeneration observed in AD, not all tauopathies have increased CSF tau. Therefore, more research is needed on the relationship between tau biomarkers, neurodegeneration, and cognitive decline in AD.

1.6 Using microdialysis to infuse disease-modifying drugs

First developed by Ungerstedt and colleagues to continuously measure the dynamic changes of neurotransmitters *in vivo*[177], microdialysis has since proven to be a powerful technique for the real-time measurement of analytes in extracellular tissue fluid[178], as well as for the pharmacokinetic analysis of drug transport to the brain[179]. In traditional microdialysis, animals are typically sampled once or twice prior to sacrifice. However, as push-pull microdialysis

enables serial sampling from a single animal, it is possible to observe the dynamic temporal alterations of target molecules (such as Aβ and tau) without requiring the collection of tissue samples or sacrifice. Additionally, each animal can serve as its own intrinsic control, reducing inter-animal variability and limiting the number of animals used in experiments[20].

1.6.1 Key principles of microdialysis

Microdialysis is performed by placing a probe comprised of a semi-permeable membrane in the tissue of interest. Solutes are driven by passive diffusion into the probe and collected at the end of the outlet tubing (dialysate)[180]. As the perfusion liquid equilibrates with the fluid outside of the tube, *in vivo* intracerebral microdialysis in the lateral ventricle (LV) offers an avenue to simultaneously infuse disease-modifying drugs while collecting CSF[181]. Bjorkli and colleagues recently validated a modified 'push-pull' technique of microdialysis using a syringe pump to perfuse the microdialysis probe (push) and a peristaltic pump (pull) to collect the sample coming from the probe outlet[168]. This technique allows for the collection of two large proteins (Aβ and tau), rendering the method useful for the longitudinal analysis of AD CSF biomarkers.

1.6.1.1 Bypassing the BBB

The strict regulation of the molecular and cellular exchange between the blood and the brain is maintained by two major interactions: the BBB and the BCSFB. Given that all brain cells are within 25 μm of a capillary, drugs that bypass the BBB find short diffusion distances to neurons and glia[182]. However, over 98% of all small-molecule drugs and approximately 100% of all large-molecule drugs do not cross the BBB[183]. Therefore, most AD drug candidates are not capable of crossing the BBB, which has presented a major challenge for clinical therapeutic drug discovery.

The second major interface between the blood and the brain is the blood-cerebrospinal fluid barrier, which is located upstream of CSF flow at the epithelium of the CP and downstream of CSF flow at the arachnoid membrane[154]. The CP, which is a part of the BCSFB, regulates the entry of nutrients from the periphery into the brain and plays a central role in the clearance of toxins and drugs[184]. CSF flows from the ventricles over the surface of the brain and is eventually absorbed into the systemic blood circulation via passage across valves in the arachnoid villi of the superior sagittal sinus[154]. Therefore, as CSF from the ventricles directly reaches both the surface of the brain and the blood circulation of the brain, drug infusion into the LV via microdialysis offers a powerful mechanism to bypass the BBB.

1.7 Aims and hypotheses

The amyloid cascade hypothesis holds that amyloid deposits are the driving force in both EOAD and LOAD. This hypothesis offers straightforward, appealing therapeutic treatment:

clear away amyloid fibrils/oligomers, block neuronal death, and ultimately eliminate dementia[185]. However, despite several decades of research attempting to counteract the effects of Aβ pathogenesis, all but one clinical trial, aducanumab, has failed to prevent or slow down cognitive decline, while clinical trials with other initially promising drugs such as verebecestat and atabecestat have been halted due to adverse side-effects[151, 186-188]. However, even if Aβ aggregation is in fact the causation of AD, the clinical staging of AD typically lasts approximately 9-10 years, while the deposition of Aβ begins 20-30 years prior to the onset of clinical symptoms[189, 190]. Therefore, targeting Aβ earlier in the AD biochemical cascade may be necessary to prevent aggregation and subsequent neurotoxicity.

Given the possibility that clinical trials have been conducted too late in the AD biochemical cascade, the use of preclinical animal models of AD may elucidate the initiation and progression of biomarkers that allow for the evaluation of disease-modifying drugs, as such models allow for the targeting of drugs at much earlier time points than is possible in patients[20]. Additionally, the span of AD is over months in rodents, compared to many years in patients, which allows for the real-time analysis of the impact of disease-modifying drugs on CSF biomarkers and AD neuropathology. This thesis aimed to use a modified push-pull microdialysis methodology, developed in our lab, for the simultaneous infusion of disease-modifying drugs and collection of CSF. By infusing preclinical AD models at various time points in the disease with drugs aimed at halting neuropathology, the impact of these disease-modifying drugs on AD molecular progression could be observed in a way that is not feasible in patients. Two disease-modifying drugs were used: Fasudil, which affects the Wnt signaling pathway, and Lonafarnib, which increases lysosomal activity. The following working hypotheses were in place: 1) Fasudil treatment would reduce iAβ in younger animals and extracellular amyloid plaques in older animals 2) Fasudil treatment would decrease CSF Aβ40 and Aβ42 in younger and older animals, 3) Lonafarnib treatment would reduce AD conformation-specific tau reactivity and CSF p-tau and t-tau in both younger and older animals, 3) dense-core amyloid plaques would display a distinct immunolabeling pattern from diffuse amyloid plaques, and 4) amyloid plaque pathology would be associated with microglial activation in the 3xTg mouse model.

2 Materials and methods

2.1 Animals

As the molecular, cellular, and pathological changes that culminate in cognitive decline in the AD brain remain poorly understood, animal models serve as invaluable tools[97]. Additionally,

given that identifying patients at preclinical AD stages has proven difficult, gene-targeted and transgenic mice modeling various aspects of AD neuropathology hold significant translational value[20, 96, 191]. Fourteen 3xTg mice and two non-transgenic B6129 mice were included in these experiments. The 3xTg mouse model is based on a C57BL/6;129X1/SvJ;129S1/Sv (Jackson Laboratory, Bar Harbor, ME, USA) background and contains three human gene mutations: a knocked-in *PSEN1* gene with the M146V mutation, an *APP* transgene with the Swedish-double mutation (KM670/671NL), and the mutated transgene *MAPT* (P301L). The model exhibits both amyloid plaques and NFTs, and cognitive impairment appears at 4 months of age in these mice, coinciding with the appearance of iAβ in pyramidal neurons of the CA1 region of the hippocampus[96, 97]. However, cognitive impairment appears prior to the development of amyloid plaques and gliosis (11-13 months) or NFTs (17 months) in this model[192] (Bjorkli, unpublished work). In contrast, human sporadic AD patients typically develop toxic amyloid plaques and gliosis at approximately 50 years of age, tau tangles at approximately 60 years of age, and neurodegeneration and cognitive impairment at approximately 70-80 years of age[193] (Fig. 2.1).

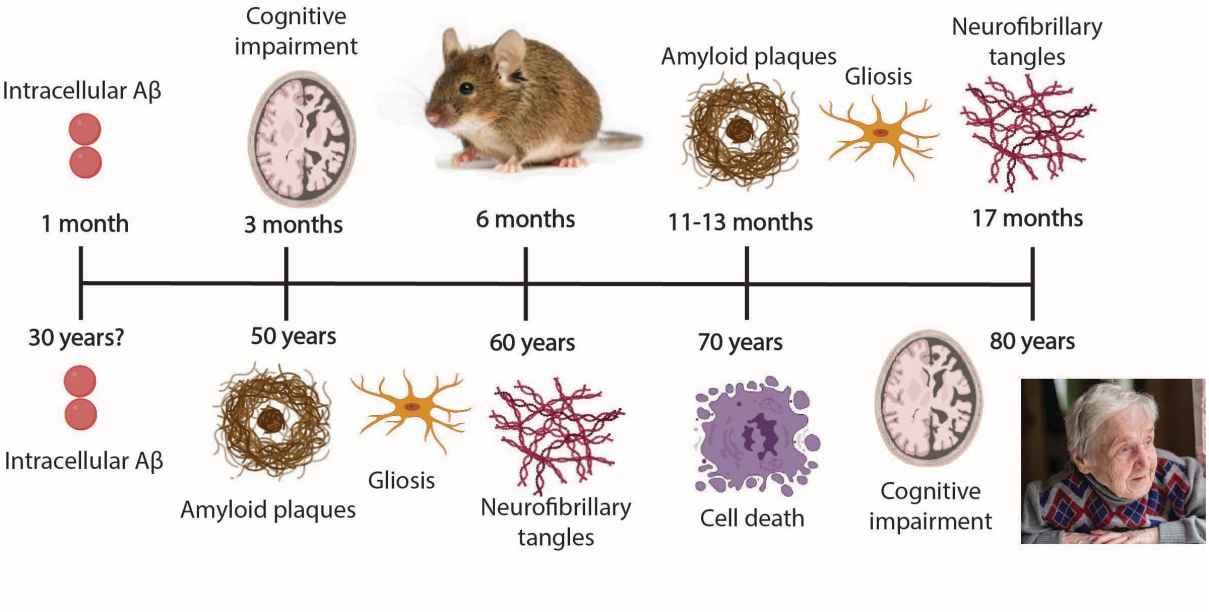

Figure 2.1. A comparison of pathology and subsequent symptoms along the AD biochemical cascade between the preclinical 3xTg model and patients. The 3xTg model develops iAβ by 1 month of age, which is followed by cognitive impairment by 3 months of age then development of amyloid plaques and concomitant gliosis by 11-13 months and NFTs by 17 months of age. The typical sporadic AD patient is hypothesized to accumulate iAβ up to two decades before the appearance of amyloid plaques and gliosis, which are abundant by 50 years of age. In patients, Aβ pathology is followed by the appearance of NFTs by approximately 60 years of age. Finally, between 70 and 80 years of age, neurodegeneration and cognitive impairment become prominent in patients. Figure adapted from Bjorkli et al.[20] and created with biorender.com.

Therefore, while cognitive impairment in human patients likely is a result of NFTs, cognitive impairment in the 3xTg mouse model occurs prior to the development of NFTs and may be the

result of iAβ and synaptic dysfunction[96]. See Appendix A for details on all animals used in this thesis. In 2014, the donating investigators communicated to Jackson Laboratories that male transgenic mice may not exhibit the phenotypic traits as originally described[97]. Therefore, only female mice were included in these experiments. All housing and breeding of animals used in this thesis was approved by the Norwegian Animal Research Authority and was in accordance with the Norwegian Animal Welfare Act §§ 1-28, the Norwegian Regulations of Animal Research §§ 1-26, and the European Convention for the Protection of Vertebrate Animals used for Experimental and Other Scientific Purposes (FOTS ID 21061). All mice used in this thesis were bred at the Avdeling for Komparativ Medisin/Comparative Medicine Core Facility (AKM/CoMed) at the Norwegian University of Science and Technology. The animals were kept on a 12h light/dark cycle under standard laboratory conditions (19-22°C, 50-60% humidity), and had access to food and water ad libitum.

2.2 Microdialysis probe implantation

Implantation surgery was performed to implant microdialysis guide cannulas (CMA 7, CMA Microdialysis AB, Kista, Sweden) into the LV of the mice, where CSF is produced (Fig. 2.2)[168]. Mice were anesthetized with isoflurane gas (4% induction and 1.5-3% maintenance; IsoFlo vet., Abbott Laboratories, Chicago, IL, USA) prior to being fixed in a Kopf stereotaxic frame (Chicago, IL, USA). Anesthesia levels were monitored throughout surgery via respiration and testing toe pinch reflexes. All surgical instruments were autoclaved prior to surgery and disinfected during surgery in 70% ethanol. After being placed into the anesthesia mask, the animal was fixed into the stereotaxic frame using ear bars. The fur of the skull was shaved and the skin was cleaned with saline and chlorhexidine. Prior to making any incisions, Marcain (Aspen Pharma, Ballerup, Denmark) was injected subcutaneously into the scalp (0.03-0.18 mg/kg) and Metacam (0.05-0.15 mg/kg; Boehringer Ingelheim Vetmedia, Copenhagen, Denmark) and Temgesic (0.05-0.09; Invidor UK, Slough, Great Britian) were administered subcutaneously for intraoperative pain relief. After using bregma and lambda to horizontally level the skull with a ±0.1mm tolerance, the stereotaxic coordinates were derived to target LV[194] (A/P -0.1mm, M/L +1.2mm, D/V -2.75mm). The skull was drilled through at these coordinates and the guide cannula was slowly lowered into the drilled hole. The guide cannula was attached to the skull with super glue and dental cement. After surgery, the animal was placed in a heating chamber until awake and moving normally. Post-surgery, Metacam and Temgesic were administered within 24 hours. As research has indicated that a complete recovery of physiological functions does not occur until 5-7 days after surgery, no CSF sampling was conducted until 7 days post-surgery[195]. All experimental surgeries were

performed by my supervisor, Christiana Bjørkli. However, I did accompany Christiana on multiple occasions to observe and successfully performed independent microdialysis probe implantation surgeries on three animals not included in these analyses (see Appendix B for images of probe implantations).

2.3 Viral injection of P301L tau

One limitation of the 3xTg mouse model is its distribution of pathological tau proteins in the brain. In humans, the initial neurons affected are in LEC LII[196]. However, due to the *MAPT* frontotemporal dementia tau mutation in the 3xTg mouse model, tau pathology begins in the frontal cortex. Therefore, P301L tau was injected into LEC LII of four young 3xTg mice to mimic the pathology of AD patients (Fig. 2.2). The viral construct used in this thesis was engineered in-house by Dr. Rajeevkumar Nair Raveendran at the Viral Vector Core Facility with the Kavli Institute for Systems Neuroscience, NTNU. The experimental viral vector used was an adeno-associated virus (AAV8) containing P301L tau separated from green fluorescent protein (GFP) with 2a protein to allow for the monitoring of the temporal sequence and spatial distribution induced by injections of pathological tau into LEC LII *in vivo*. The surgical procedure was identical to implantation surgeries until craniotomy and determining the stereotaxic coordinates for LEC LII[194]; A/P: +0.5mm, ~M/L +4mm (the lateral coordinate depended on the size of the animal; the beginning of the curvature of the skull was targeted), ~D/V -3.6mm (this also depended on the size of the animal, with more ventral placement in bigger animals). The skull was drilled through at these coordinates and the Neurosys Hamilton syringe (32G, Hamilton Company, Reno, NV, USA) was slowly lowered into the skull to the correct depth. Injections were conducted at a speed of 200-250nl/min (total 2000-2500nl) using a microprocessor-based controller (Micro4, WPI, Sarasota, FL, USA). Once lowered, the needle was kept in place for a minimum of 5 minutes before injection and 5 minutes after injection to restrict upward leakage of the viral solution. Subsequently, the skin was sutured and the surgery wound was cleaned with chlorhexidine and 70% ethanol. Post-surgery, Metacam was administered within 24 hours. The virus was allowed to transfect for 2 months in the animals before microdialysis probe implantations. All viral injections were performed by my co-supervisor, Christiana Bjørkli.

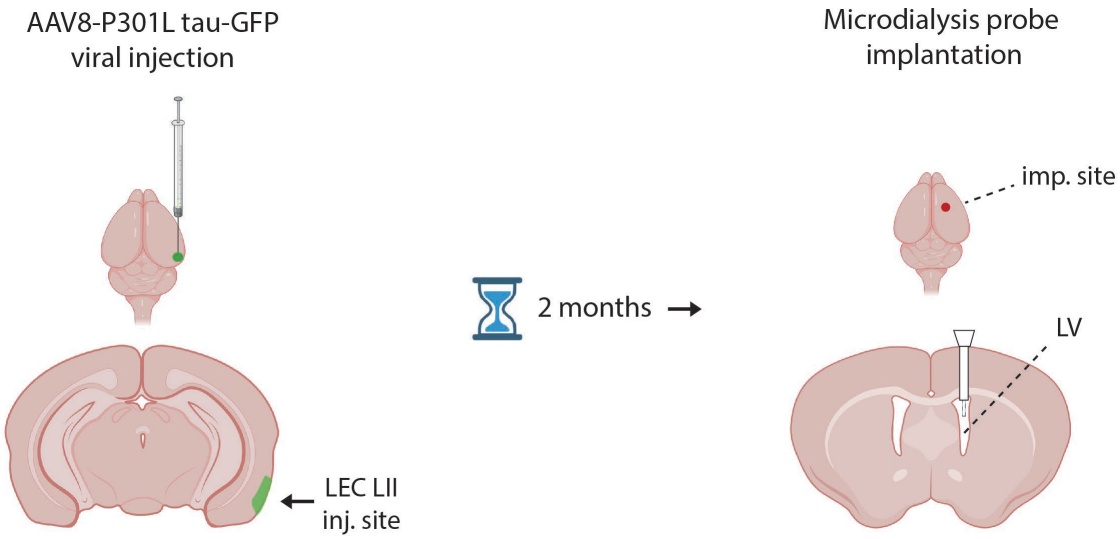

Figure 2.2. Schematic of P301L tau viral injection followed by microdialysis probe implantation. Four experimental animals were virally injected with P301L tau into LEC LII, which was followed by a 2-month transfection period before microdialysis probe implantation into LV (probe depicted in white). All fourteen experimental animals were implanted with microdialysis probes in LV. Abbreviations; AAV8: adeno-associated virus 8; GFP: green fluorescent protein; imp: implantation; inj: injection; LEC LII: layer II of the lateral entorhinal cortex; LV: lateral ventricle. Figure created with biorender.com.

2.4 In vivo microdialysis

Intracerebral microdialysis was performed for the dynamic sampling of CSF Aβ and tau during drug infusions (Fig. 2.3)[168]. The push-pull method was utilized to allow for the measurement of larger endogenous proteins with a high molecular weight. The refrigerated fraction collector (CMA 470, Harvard Apparatus, Cambridge, MA, USA) was set to 6°C for the storage of collected CSF in polypropylene plastic vials. Fluorinated ethylene propylene peristaltic (FEP) tubing was placed inside each plastic vial for collection and connected to the cassette of the peristaltic roller pump (Reglo ICC Digital, Harvard Apparatus, Cambridge, MA, USA). This peristaltic FEP tubing was connected to the outlet side of the microdialysis probes with tubing adapters (CMA Microdialysis AB, Kista, Sweden). FEP tubing (CMA Microdialysis AB, Kista, Sweden) was connected to each microsyringe. The FEP tubing was then connected to the inlet side of the microdialysis probes (CMA 7 2MDa molecular weight cut-off, CMA Microdialysis AB, Kista, Sweden). Cages were prepared with 1.5cm of bedding, filled water bottles, and treats. The disease-modifying drug was loaded inside a gastight microsyringe (0.2mL; CMA Microdialysis AB, Kista, Sweden), which was placed into a syringe pump (CMA 4004, CMA Microdialysis AB, Kista, Sweden). Fasudil (Selleck Chemicals, Houston, TX, USA) and Lonafarnib (Cayman Chemical, Ann Arbor, MI, USA) were administered at a flow rate of 1µl per minute for one hour via reverse microdialysis (see section 2.4.1 for details on disease-modifying drugs). Fasudil was administered at 50 mg/kg daily and Lonafarnib was administered at 80 mg/kg daily. Littermates that were infused with saline (CMA Microdialysis

AB, Kista, Sweden) at the same flow rate were used as controls. Mice were habituated to human handling and restraining for one week prior to microdialysis sampling and restrained to remove the dummy probe of the guide cannula and replace it with the microdialysis probe. After the mice were connected to the sampling apparatus, the room lights were turned off for the duration of drug infusion. At the conclusion of drug infusion, the vials of 60µl of collected CSF were centrifuged and kept at -80°C until the samples were analyzed with multiplex enzyme-linked immunosorbent assay (ELISA; Milliplex HNABTMAG-68K, Merck KGaA, Darmstadt, Germany). The Milliplex is a 4-plex kit that measures Aβ40, Aβ42, t-tau, and p-tau. Microdialysis drug infusions were performed by my co-supervisor, Christiana Bjørkli.

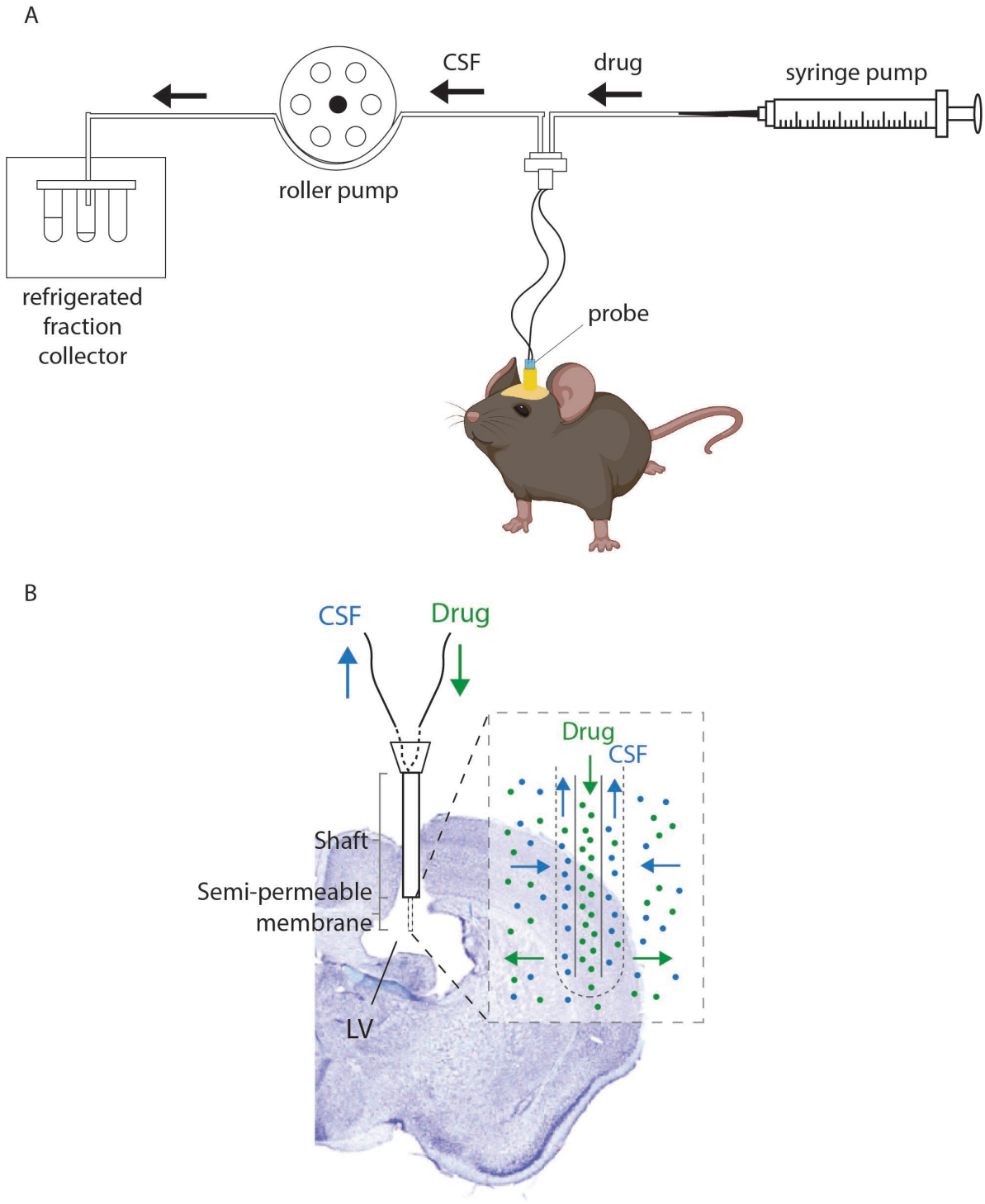

Figure 2.3. (A-B): Push-pull microdialysis system. (A): In the microdialysis setup, the syringe pump is loaded with the disease-modifying drug and then used to perfuse the microdialysis probe (push) while the peristaltic pump is used to collect the CSF sample coming from the probe outlet (pull). The CSF containing microdialyte is collected in a refrigerated fraction collector. Figure adapted from Takeda et al.[157] (B): Schematic of the microdialysis probe inserted into the LV during drug infusion. The disease-modifying drug is slowly and constantly pumped through the probe's semipermeable membrane while the CSF containing microdialyte is collected. Figure adapted from Bjorkli et al.[168]. Abbreviations; CSF: cerebrospinal fluid; LV: lateral ventricle.

2.4.1 Disease-modifying drugs

2.4.1.1 Fasudil

Fasudil is a Rho-associated protein kinase (ROCK) inhibitor that was first reported to reduce cerebral vasospasm[197]. ROCK is an effector of the small guanosine triphosphate (GTP)ase Rho; GTPases are a superfamily of hydrolase enzymes that bind to GTP and hydrolyze it to guanosine diphosphate (GDP)[198]. Rho GTPases regulate the assembly and organization of the actin cytoskeleton in all eukaryotic cells[199]. In neurons, ROCK has been shown to be a key regulator of synapse formation[200]. Previous research has demonstrated that ROCK kinases can induce the processing of APP to the toxic Aβ42 peptide and that this can be prevented by ROCK inhibition[201]. Additionally, the Wnt-PCP-RhoA/ROCK pathway has been shown to mediate Aβ synaptoxicity and increase the production of Aβ via the induction of Dkk1 in animal models of AD. In this research, the ROCK inhibitor Fasudil was shown to have good brain availability and to protect against Aβ-induced synaptotoxicity and cognitive impairment in animal models[122]. In addition to its status as a ROCK inhibitor, Fasudil also is an intracellular Ca^{2+} antagonist[202].

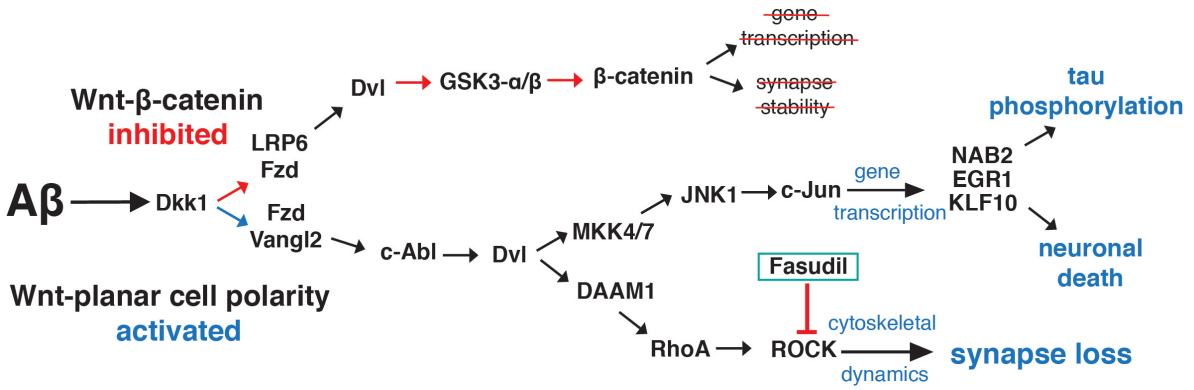

Figure 2.4. Schematic of Wnt-PCP activation via Aβ. The presence of Aβ has been shown to rapidly increase Dkk1 expression. Dkk1 then activates Wnt-PCP signaling by antagonizing the LRP6-Fzd interaction. Previous research has demonstrated that Aβ-driven synaptotoxicity is mediated by the Daam1/RhoA/ROCK arm of the Wnt-PCP pathway and that this synapse loss can be blocked by Fasudil. Figure adapted from Sellers et al.[122]. Abbreviations; Aβ: amyloid-β; DAAM1: disheveled associated activator of morphogenesis 1; Dkk1: Dickkopf-1; Dvl: disheveled; EGR1: early growth response 1; Fzd: frizzled; GSK3α/β: glycogen synthase kinase α/β; JNK1: c-Jun N-terminal kinase; LRP6: low-density lipoprotein receptor-related protein 6; MKK4/7: mitogen-activated protein kinase 4/7; NAB2: NGFI-A binding protein 2; PCP: planar cell polarity; RhoA: Ras homolog family member A; ROCK: Rho-associated coiled-coil containing protein kinase; Vangl2: Van Gogh-like protein 2; Wnt: Wingless-related integration site.

2.4.1.2 Lonafarnib

Originally developed as a treatment for cancer, Lonafarnib has since proven successful as a treatment for chronic hepatitis-D[203]. Lonafarnib is a farnesyltransferase inhibitor that crosses the BBB and is generally well-tolerated in humans[204]. Farnesyltransferase inhibitors were originally designed to prevent the posttranslational modifications of Ras oncoproteins[205]. However, the induction of autophagy appears to be a pharmacological class effect of the

inhibition of farnesyltransferase[206]. Previous research has demonstrated that Lonafarnib effectively reduces tau pathology via the induction of autophagy in animal models[142]. In this research, Lonafarnib had its principal effect on enhancing protein degradation in the lysosome. Cell culture studies have also found that Lonafarnib inhibits mTOR signaling, offering another potential pathway for the drug to upregulate autophagy[207].

2.5 Tissue processing and immunohistochemistry

2.5.1 Transcardial perfusion

Once anesthetized, animals received an intraperitoneal injection of pentobarbital NAF (100 mg/kg; Apotek 1, Lørenskog, Norway). After testing reflexes (i.e. repeated foot pinch), a transverse abdominal incision was performed to expose the animal's heart. The right atrium of the heart was then cut, and a needle connected to a Peri-Star Pro 4-channel low rate pump (World Precision Instruments, Inc., USA) was inserted into the apex of the left ventricle. First, animals were perfused with Ringer's solution (3.35 mM KCl [Merck Millipore, Merck kGaA, Darmstadt, Germany], 145 mM NaCl [VWR International, Radnor, PA, USA], 2.28 mM NaHCO3 [Merck Millipore, Merck kGaA, Darmstadt, Germany, pH ~6.9]) to rinse the circulatory system until blood was cleared. Complete clearance of the circulatory system was determined by the animal's liver and the liquid returning through the right atrium being clear. After the circulatory system was cleared of blood, a 4% solution of freshly depolymerized paraformaldehyde (PFA; Merck Millipore, Merck kGaA, Darmstadt, Germany) in 125 mM phosphate buffer (PB, pH 7.4) was administered for tissue fixation. The fixation was deemed successful based on blanching of the liver and the observation of PFA fixation (as a result of the cross-linking of proteins). PFA administration was continued until the cross-linking reaction had ceased. After the perfusion, brains were dissected from the skull and post-fixed in PFA for 24 hours. Following fixation, each brain was transferred to a solution containing 2% dimethyl sulfoxide (DMSO; VWR International, Radnor, PA, USA) in 125mM PB for cryoprotection and preserved at 4°C for at least 24 hours before sectioning.

2.5.2 Sectioning and storage of brain tissue slices

A freezing-sledge microtome (Microm HM430, Thermo Fisher Scientific, Waltham, MA, USA) set to -40°C was used to section brain slices in the coronal plane. The caudal portion of the cerebellum was cut off with a razorblade to create a flat base, then the back of the brain was then attached to the stage using a 30% sucrose (VWR International, Radnor, PA, USA) solution (sucrose dissolved in 0,4M PB and H_20). Once attached to the stage, the brain was covered in pulverized dry ice to freeze solid. Each brain was cut at 40µm and divided into four equally spaced brain tissue section series. The tissue was stored in section tubes containing

DMSO at -23°C until immunohistochemical processing. Due to the exploratory nature of this thesis, some series were sorted rostro-caudally and further divided into more series to provide tissue for a greater number of analyses.

2.5.3 Cresyl violet-staining (Nissl staining)

To verify probe placement, one tissue section series of each brain was first dehydrated in ethanol (KiiltoClean AS, Asker, Norway), then left in Xylene (VWR International, Radnor, PA, USA) and rehydrated before staining with Cresyl violet (Nissl; Sigma-Aldrich, St. Louis, MO, USA) for 3 minutes on a shaker while protected from light. The sections were then alternatively dipped in ethanol-acetic acid (5 mL acetic acid in 1L 70% ethanol) and rinsed with cold water before re-staining with Cresyl violet for 2 minutes. Then, sections were alternatively dipped in ethanol-acetic acid and rinsed with cold water until the desired contrast was obtained, then dehydrated, cleared in Xylene, and coverslipped with Entellan (VWR International, Radnor, PA, USA) containing Xylene.

2.5.4 Fluorescent immunohistochemistry

To promote epitope availability, heat-induced antigen retrieval (HIAR) was performed on all tissue at 60°C for 2 hours in ~100ml of PB. Sections were then washed 3 times for 10 minutes with PB containing 0.2% Triton X-100 (Merck, Darmstadt, Germany; PBT). Next, sections were blocked with 5% normal goat serum (Abcam, Cambridge, UK) for 1 hour in 2.5mL PBT. After blocking, sections were incubated with the primary antibodies at a 1:1000 concentration for 4 hours at 5°C in PBT with 5% goat serum (see Table 1 for primary antibodies used). The tissue was then left in PB overnight at 5°C. The following day, the sections were washed 3 times for 10 minutes with PBT. Then, in order to visualize the primary antibodies, sections were incubated with Alexa Fluor 488 goat anti-rabbit (Invitrogen, Carlsbad, CA, USA) and Alexa Fluor 546 goat anti-mouse (Invitrogen, Carlsbad, CA, USA) at 1:400 concentrations in PBT with 5% goat serum while protected from light at room temperature. For a complete list of secondary antibodies used in this thesis, see Appendix D. Next, sections were washed for 10 minutes with DAPI (Abcam, Cambridge, UK) at a 1:10,000 concentration in PB while protected from light, then washed 3 times for 10 minutes in PB. Processed tissue was then placed in a solution of 50mM tris(hydroxymethyl)aminomethane (Tris HCl; Merck Millipore, Merck kGaA, Darmstadt, Germany; pH adjusted to 7.6 with hydrochloric acid) and mounted on positively charged cut edge frosted glass slides (VWR International, Radnor, PA, USA). After mounting, the slides were left to dry for a minimum of 4 hours on a 38°C heating plate, protected from light. To remove excess water and de-fat the tissue, mounted tissue was placed in Xylene for a minimum of 5 minutes. The mounted tissue was then coverslipped with Entellan

containing Xylene and left to dry overnight, protected from light. See Appendix A for details on primary antibodies used for each animal.

Table 1
Overview of primary antibodies used in this thesis.

Antibody	Target	Manufacturer	Catalog numbers
Mouse anti-Aβ (McSA1)	Aβ38-42	MediMabs	MM-0015-1P
Rabbit anti-human Aβ	Aβ42	Immuno-biological labs (IBL)	JP28051
Mouse anti-Iba1	Ionized calcium binding adaptor molecule 1 (Iba1); microglial activation	Abcam	ab15690
Rabbit anti-oligomer (A11)	Aβ42 oligomers	Thermo-Fisher	AHB0052
Rabbit anti-amyloid fibrils (OC)	Generic epitopes common to amyloid fibrils and fibrillar oligomers	Merck Millipore	AB2286
Mouse anti-MC1	AD-specific conformational modification of tau	Peter Davies, Department of Pathology, Albert Einstein College of Medicine	N/A
Rabbit anti-TREM2	TREM2 receptor; microglial activation	Invitrogen	MA530971
Rabbit anti-MAP2	Microtubule-associated protein 2; neuronal marker	Abcam	ab183830
Rabbit anti-LAMP1	Lysosomal associated membrane protein 1; Lysosomal activation	Merck Millipore	L1418

2.6 Microscopy

2.6.1 Fluorescent wide-field microscopy and brightfield microscopy

Fluorescently stained tissue was imaged using an AxioScanZ1 automated microscope (objective 20x, NA 0.8), Carl Zeiss Microscopy, Oberkochen, Germany) using either reflected fluorescence (for sections stained with a fluorophore) or transmitted white light (for sections stained with DAB or Cresyl violet) as the light source.

2.6.2 Confocal microscopy

To obtain a high-resolution image of the co-localization of MC1 reactivity around an amyloid plaque, one slide was scanned using confocal microscopy (Axio Imager Z1 confocal microscope; LSM 880, Carl Zeiss, Jena, Germany). An Argon laser was used to excite Aβ labeling (Alexa Fluor 488), a DPS 651-10 laser was used to excite MC1 labeling (Alexa Fluor 546), and an Argon laser was used to excite DAPI.

2.7 Data analyses

2.7.1 CSF protein quantification

In order to graphically visualize data from CSF sample concentrations of Aβ40, Aβ42, t-tau, and p-tau, the mean of duplicates was calculated for each time point of each animal, then the total mean across all animals of a certain treatment group was calculated to represent the CSF concentration. Due to the low number of observations for each treatment group, statistical analyses were not performed.

2.7.1 iAβ quantification

To determine whether Fasudil infusion impacted iAβ reactivity prior to the development of amyloid plaque pathology, McSA1-positive cells were manually quantified in the dSub of two young Fasudil-infused animals and one young saline-infused animal. The dSub was quantified as it is the first area to display amyloid plaques in the 3xTg model and exhibits significant iAβ accumulation prior to the development of amyloid plaques (Bjorkli, unpublished work). Two to three sections containing the dSub of implanted hemispheres at corresponding bregma levels of each animal were chosen and quantified by hand. After quantifying McSA1-positive cells, the Shapiro-Wilk test was employed to test for normality distribution (see Appendix F for QQ plots) before comparing the mean number of cells in the young Fasudil-infused group to the mean number of cells in the young saline-infused group and an unpaired t-test was used. See Appendix E for examples of iAβ quantification.

2.7.2 Amyloid plaque quantification

Amyloid plaques were manually quantified and measured by size (widest part across the amyloid plaque). In the three old Fasudil-infused animals, amyloid plaque size and number were compared between the implanted and the non-implanted hemispheres. However, as quantification did not reveal significant differences in amyloid plaque number or size between implanted and non-implanted hemispheres, only amyloid plaques contained in implanted hemispheres were quantified to compare treatment groups (old Fasudil-infused, Lonafarnib-infused, and saline-infused). All sections containing amyloid plaques in the dSub were identified and sorted rostro-caudally to ensure that each implanted hemisphere was compared to an implanted hemisphere at the corresponding bregma level along the rostrocaudal axis[194]. As initial quantification did not reveal clear differences in amyloid plaque size or number between the McSA1 and OC primary antibodies, amyloid plaques stained by OC were quantified in the final analysis. After amyloid plaques from all treatment groups were quantified by size and number, the Shapiro-Wilk test was employed to test for normality distribution (See Appendix F for Q-Q plots) before comparing the drug-treated groups to the

saline-infused group. If groups were normally distributed, a parametric unpaired t-test was used. If groups were not normally distributed, a non-parametric Mann-Whitney U test was used. See Appendix C for examples of amyloid plaque quantification.

2.7.3 Dense-core amyloid plaque quantification

Previous research has demonstrated that the absence of MAP-2 immunolabeling in small, well-defined areas of the entorhinal cortex and hippocampus is indicative of dense-core amyloid plaque pathology[208]. Based on the presence of McSA1-positive staining with a corresponding absence of MAP-2 immunolabeling, dense-core amyloid plaques were identified then measured and quantified by hand in a similar manner as amyloid plaques, with both the total number of dense-core amyloid plaques and the size (distance across the widest part of the dense-core amyloid plaques) quantified (see Appendix B for dense-core amyloid plaque immunostaining protocol). Due to the limited amount of available tissue, the dSub of one corresponding implanted and non-implanted hemisphere from two Fasudil-infused, one Lonafarnib-infused, and one saline-infused animal were quantified. Given the limited number of observations for the number of amyloid plaques per slice, statistical analyses were only performed to test for differences in the sizes of amyloid plaques between treatment groups. Statistical analyses were performed in a similar manner to amyloid plaque quantification.

All statistical tests and graphs were made in Prism 9 (GraphPad Software Inc., CA, USA). All amyloid plaque quantification was performed using Zen Blue Microscope Software (Carl Zeiss Microscopy, Oberkochen, Germany). IAβ quantification was performed using Stereo Investigator Software (MBF Bioscience, VT, USA).

3 Results

3.1 Intermittent, longitudinal Fasudil infusions reduce iAβ in young 3xTg mice

Three young 3xTg mice were infused with either saline (n = 1) or Fasudil (n = 2) once a day for 7 days, then 30 days without any infusions, then once a day for 5 days. We hypothesized that intermittent, longitudinal Fasudil infusions would reduce iAβ in young mice. IAβ was determined as McSA1-positive cells with McSA1 staining in intracellular compartments, including the cytosol (Fig. 3.1). Manual cell quantification of McSA1-positive cells in the dSub of Fasudil-infused and saline-infused young mice revealed that there were significantly more McSA1-positive cells in the dSub of the saline-infused mouse (M = 254.30, SD = 55.05) compared to the Fasudil-infused mice (M = 129.20, SD = 12.84), $t(7) = 5.64$, $p < 0.01$.

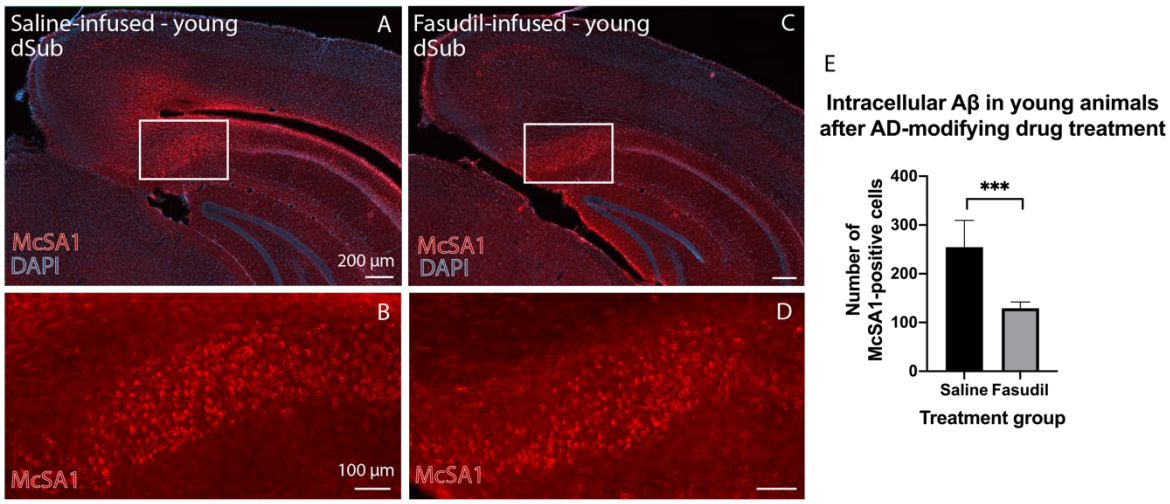

Figure 3.1 (A-D): Immunohistochemistry of brain tissue slices after microdialysis probe implantation into the lateral ventricle with saline (left, *n* = 1) or Fasudil (right; *n* = 2) infused once a day for 7 days, then 30 days without any infusions, then once a day for another 5 days in 6-month-old 3xTg mice. iAβ (red; McSA1) reactivity is shown in the dSub of the saline-infused mouse (A-B) and Fasudil-infused mice (C-D). Manual cell quantification of McSA1-positive cells is shown in (E). Abbreviations; dSub: dorsal subiculum; DAPI: 4′,6-diamidino-2-phenylindole; AD-modifying: Alzheimer's disease-modifying. Error bars = SD.

3.2 CSF biomarkers increase during Fasudil infusion pause in young 3xTg mice

We next examined CSF concentrations of Aβ40, Aβ42, t-tau, and p-tau in the three young 3xTg mice that received longitudinal, intermittent infusions of either Fasudil (*n* = 2) or saline (*n* = 1) to determine whether AD-modifying drug treatment impacted CSF concentrations in young animals (Fig. 3.2). We hypothesized that intermittent, longitudinal Fasudil treatment would decrease CSF Aβ40 and Aβ42 concentrations in young animals. CSF Aβ40 and CSF p-tau concentrations rose during the 30-day infusion pause in both Fasudil-infused and saline-infused animals, then lowered again once treatment was resumed. CSF Aβ42 concentrations rose during the 30-day infusion pause in the saline-infused animal but remained stable after day 4 in the Fasudil-infused animal. CSF t-tau concentrations rose during the 30-day infusion pause in the saline-infused animal but gradually lowered throughout the treatment period in the Fasudil-infused animals.

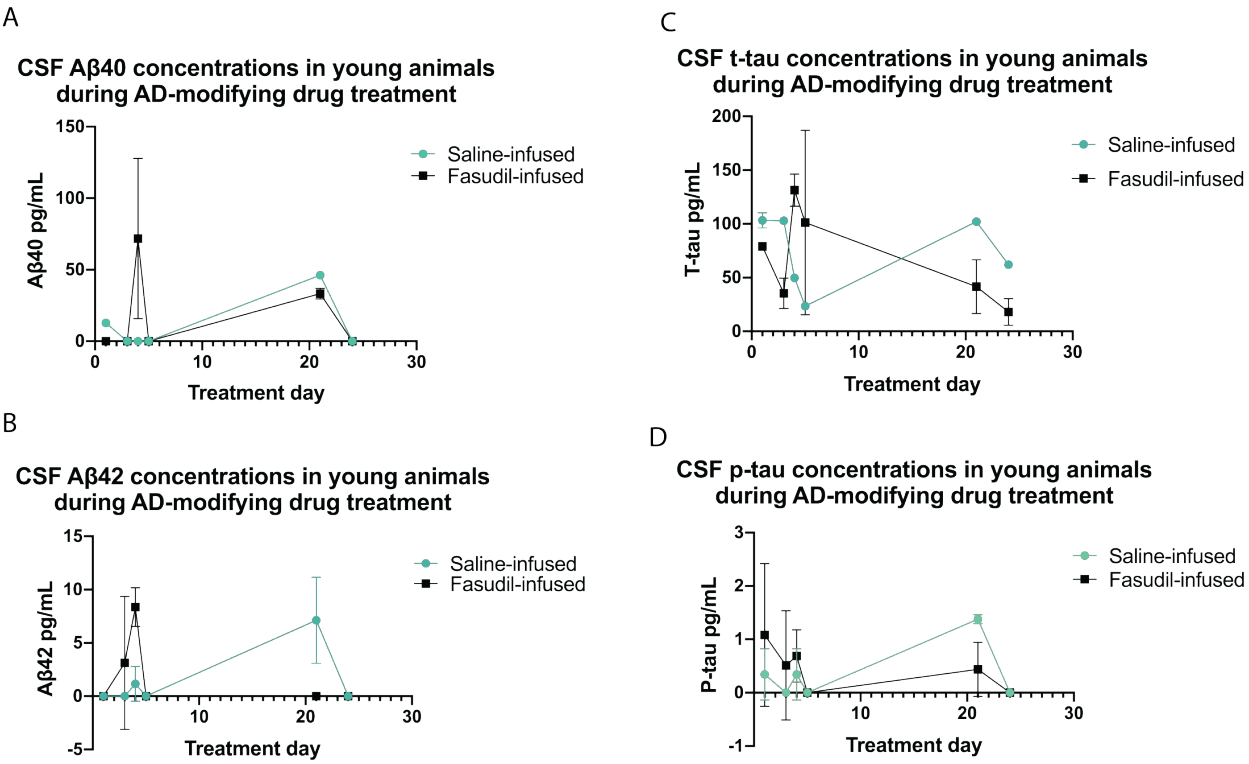

Figure 3.2. (A-D): *In vivo* CSF microdialysis results from three 6-month old 3xTg mice infused with saline (*n* = 1) or Fasudil (*n* = 2) once a day for 7 days, then 30 days without any infusions, then once a day for 5 days. Mean concentrations of duplicates of CSF Aβ40, Aβ42, t-tau, and p-tau on days 1, 3, 4, 5, 21, and 25 of drug infusions or pause shown, as measured by multiplex ELISA. Aβ40 and p-tau concentrations rose during Fasudil infusion pause, while Aβ40, Aβ42, t-tau, and p-tau concentrations rose during saline infusion pause. Abbreviations; CSF: cerebrospinal fluid; Aβ: amyloid-β; t-tau: total-tau; p-tau: phosphorylated-tau; AD-modifying: Alzheimer's disease-modifying. No data points = no recovery of protein in microdialyte. Error bars = SD.

3.3 Chronic Lonafarnib infusions moderately decrease conformation-specific tau reactivity in the LEC of young, tau-injected 3xTg mice

As the 3xTg mouse model does not develop tau pathology first in the LEC, we wanted to observe whether Lonafarnib-infused, tau-injected animals (*n* = 2) displayed less conformation-specific tau reactivity at the P301L tau viral injection site than saline-infused, tau-injected animals (*n* = 2). Based on visual inspection (Fig. 3.3), Lonafarnib-infused, tau-injected animals appeared to display slightly less MC1 immunoreactivity at the P301L tau viral injection site.

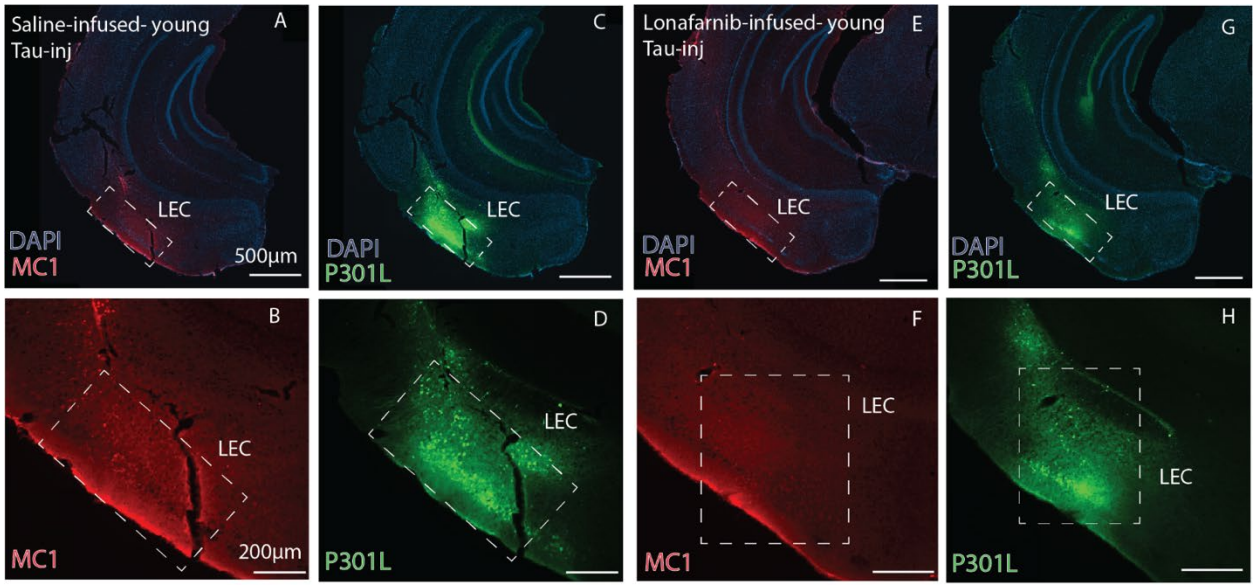

Figure 3.3. (A-H): Immunohistochemistry of brain tissue slices after microdialysis probe implantation into the lateral ventricle with Lonafarnib (*n* = 2) or saline (*n* = 2) infused once a day for 10 days in 5-month-old, tau-injected 3xTg mice. (A-D): One mouse infused with saline for 10 days. P301L tau (C-D; green; GFP) in LEC LII is outlined. Conformation-specific tau immunoreactivity (A-B; red; MC1) appears to be stronger in saline-infused mice compared to Lonafarnib-infused mice. (E-H): One mouse infused with Lonafarnib for 10 days. P301L tau (G-H; green; GFP) injection site in LEC LII is outlined. Conformation-specific tau (E-F; red; MC1) immunoreactivity appears to be weaker in Lonafarnib-infused mice compared to saline-infused mice. Abbreviations; Tau-inj: tau-injected; DAPI: 4′,6-diamidino-2-phenylindole; LEC: lateral entorhinal cortex.

3.4 Chronic Lonafarnib infusions decrease CSF t-tau and p-tau concentrations in young, tau-injected 3xTg mice

We next examined CSF concentrations of Aβ40, Aβ42, t-tau, and p-tau in the four young, tau-injected 3xTg mice that received chronic infusions of either Lonafarnib (*n* = 2) or saline (*n* = 2) (Fig. 3.4). We hypothesized that chronic Lonafarnib infusions would decrease CSF t-tau and p-tau concentrations throughout treatment. In line with our hypotheses, Lonafarnib infusions decreased CSF t-tau and p-tau concentrations over the course of treatment. Additionally, Lonafarnib infusions increased the concentration of CSF Aβ40 on day 3 of treatment, then decreased CSF Aβ40 to undetectable concentrations for the remainder of treatment.

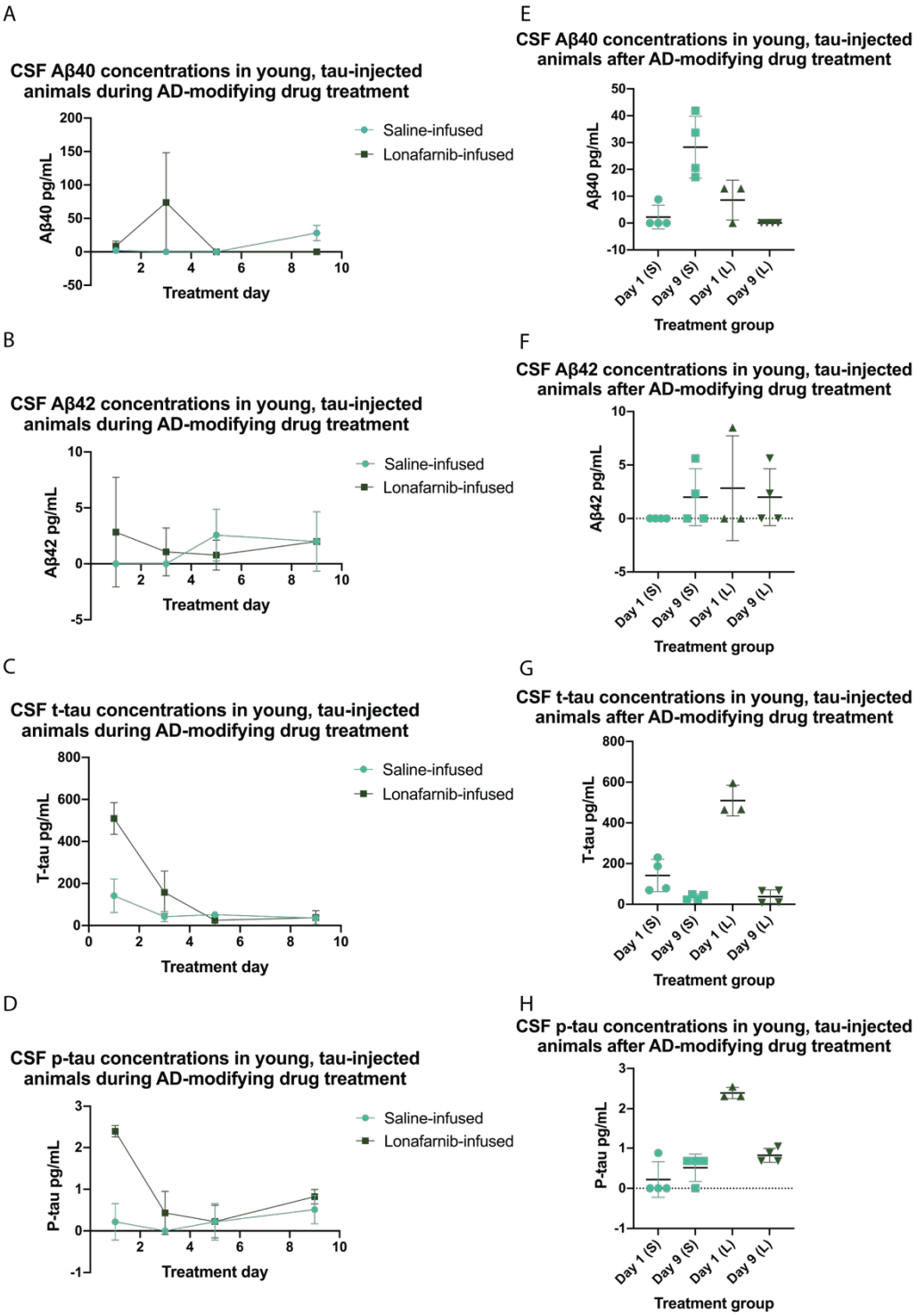

Figure 3.4. (A-H): In vivo CSF microdialysis results from four 5-month old tau-injected 3xTg mice infused with saline (*n* = 2) or Lonafarnib (*n* = 2) once a day for 10 days. Mean concentrations of duplicates of CSF Aβ40, Aβ42, t-tau, and p-tau on days 1, 3, 5, and 9 of drug infusions (A-D) and CSF concentrations of duplicates of Aβ40 (E), Aβ42 (F), t-tau (G), and p-tau (H) CSF samples on day 9 of treatment shown for each animal, as measured by multiplex ELISA. Lonafarnib infusions increased CSF Aβ40 on treatment day 3 (A) but did not alter CSF Aβ42 over time (B; F). Lonafarnib infusions decreased t-tau (C; G) and p-tau (D; H) over time. Abbreviations; CSF: cerebrospinal fluid; Aβ: amyloid-β; t-tau: total-tau; p-tau: phosphorylated-tau; AD-modifying: Alzheimer's disease-modifying. No data points = no recovery of protein in microdialyte. Error bars = SD.

3.5 Chronic Fasudil infusions reduce size and number of amyloid plaques; chronic Lonafarnib infusions increase size but not number of amyloid plaques in old 3xTg mice

We hypothesized that Fasudil treatment would decrease amyloid plaques in old animals. Compared to the saline-infused mouse (n = 1), there appeared to be more OC reactivity in the dSub of the Lonafarnib-infused mouse (n = 1) and less OC reactivity in the dSub of the Fasudil-infused mice (n = 3) (Fig. 3.5). This was confirmed by quantification of the size (average distance across the widest part of each amyloid plaque) and the number of amyloid plaques. Compared to saline infusion (number of amyloid plaques: M = 33.50, SD = 13.80; size of amyloid plaques: M = 59.46μm, SD = 36.75), Fasudil infusion decreased the number of amyloid plaques by 39.61% (M = 23.86, SD = 16.66, $t(26) = 1.28$, $p = 0.21$) and significantly decreased the size of amyloid plaques (M = 40.18μm, SD = 27.08) (Mann-Whitney U = 29544, n_{saline}= 201, $n_{Fasudil}$ = 526, $P < 0.01$ two-tailed) stained by OC in the dSub. Compared to saline infusion, Lonafarnib infusion decreased the number of amyloid plaques by 58.81% (M = 13.80, SD = 5.53), $t(14) = 3.86$, $p < 0.01$, but significantly increased the size of amyloid plaques (M = 73.10μm, SD = 54.93) (Mann-Whitney U = 11763, n_{saline}= 201, $n_{Lonafarnib}$ = 138, $P < 0.05$ two-tailed). However, it is important to note that amyloid plaques became too large to individually distinguish in the Lonafarnib-infused group (see Fig. 3.5F).

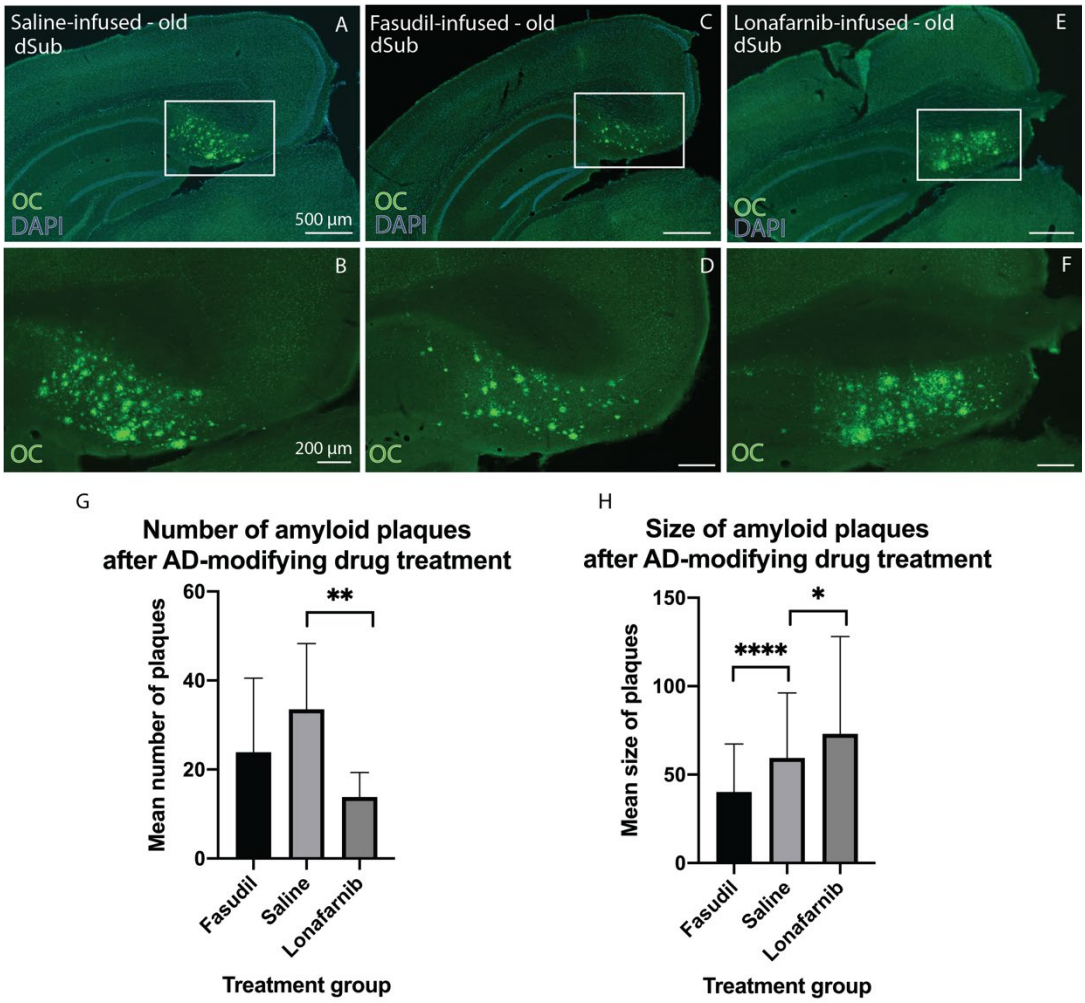

Figure 3.5. (A-F): Immunohistochemistry of brain tissue slices after microdialysis probe implantation into the lateral ventricle with saline (left; *n* = 1) infused once a day for 10 days, Fasudil (middle; *n* = 3) infused once a day for 14 days, or Lonafarnib (right; *n* = 1) infused once a day for 10 days in 14-month-old 3xTg mice. (G-H): Amyloid plaque quantification after 14 days of Fasudil infusions (*n* = 3), 10 days of saline infusions (*n* = 1), or 10 days of Lonafarnib infusions (*n* = 1) in 14-month-old 3xTg mice. Fibrillar Aβ42 (green; OC) reactivity is shown in the dSub. There is more OC reactivity in the dSub of saline-infused mice (A-B) than in Fasudil-infused mice (C-D) and more OC reactivity in the dSub of Lonafarnib-infused mice (E-F) than in saline-infused mice. Quantification of the number and size of amyloid plaques after AD-modifying drug treatment is shown in (G) and (H), respectively. Abbreviations; dSub: dorsal subiculum; DAPI: 4′,6-diamidino-2-phenylindole; AD-modifying: Alzheimer's disease-modifying. Error bars = SD.

3.6 Chronic Fasudil infusions decrease size and number of dense-core amyloid plaques in old 3xTg mice; chronic Lonafarnib infusions increase number but decrease size of dense-core amyloid plaques in old 3xTg mice

Dense-core amyloid plaques were also quantified by number and size after co-staining with MAP2 and McSA1 in two of the Fasudil-infused old animals, the saline-infused old animal, and the Lonafarnib-infused old animal (Fig. 3.6). Compared to saline infusions (M = 11.00, SD = 2.82), Fasudil infusions (M = 7.00, SD = 5.94) decreased the number of dense-core amyloid plaques by 36.36% and significantly decreased the size of dense-core amyloid plaques (saline:

$M = 59.01\mu m$, $SD = 28.04$; Fasudil: $M = 34.99\mu m$, $SD = 4.62$) (Mann-Whitney $U = 10$, $n_{saline} = 22$, $n_{Fasudil} = 10$, $P < 0.01$ two-tailed) in the dSub. Lonafarnib increased the number of dense-core amyloid plaques ($M = 14.00$, $SD = 1.41$) by 18.19% and did not significantly alter the size of dense-core plaques ($M = 51.40\mu m$, $SD = 24.55$) (Mann-Whitney $U = 93$, $n_{saline} = 22$, $n_{Lonafarnib} = 13$, $P = 0.09$ two-tailed) in the dSub.

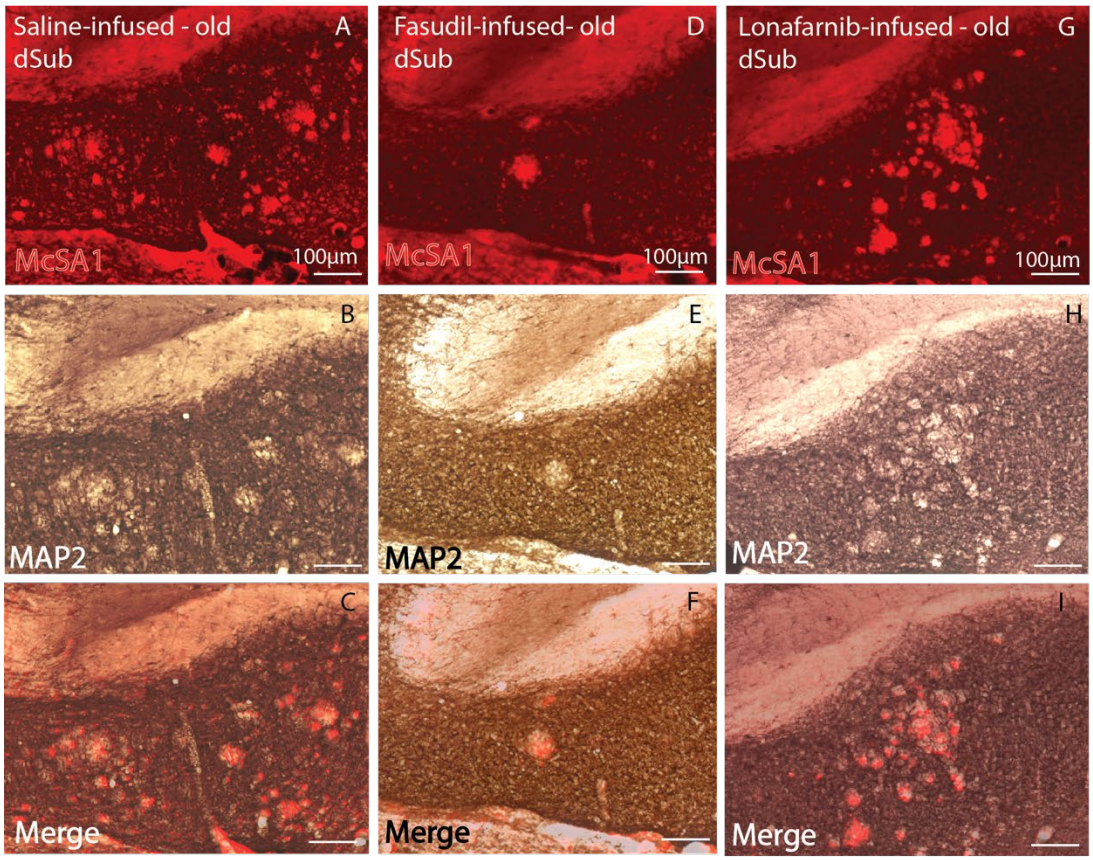

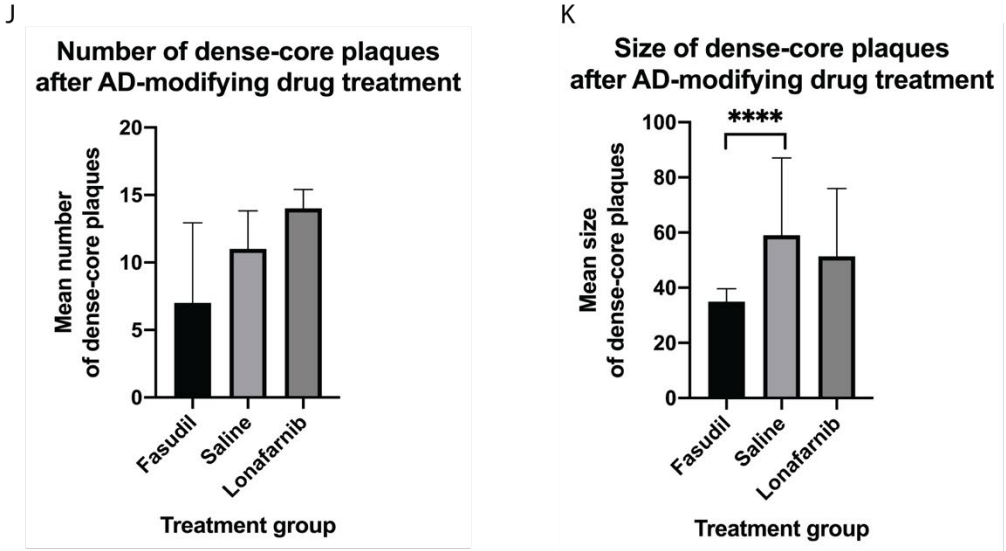

Figure 3.6. (A-I): Immunohistochemistry of brain tissue slices after microdialysis probe implantation into the lateral ventricle with Fasudil (left; *n* = 2) infused once a day for 14 days, saline (middle; *n* = 1) infused once a day for 10 days, or Lonafarnib (right; *n* = 1) infused once a day for 10 days in 14-month-old 3xTg mice. (J-K): Dense-core amyloid plaque quantification after 14 days of Fasudil infusions (*n* = 3), 10 days of saline infusions (*n* = 1), or 10 days of Lonafarnib infusions (*n* = 1) in 14-month-old 3xTg mice. Aβ38-42 (red;

McSA1) staining for amyloid plaques (A, D, G) and microtubule-associated protein 2 (B, E, H; brown; MAP2). McSA1 and the absence of MAP2 staining colocalized (C, F, I), confirming previous research indicating that MAP2 processes are absent within dense-core amyloid plaques. Quantification of the number and size of dense-core amyloid plaques after AD-modifying drug treatment is shown in (J) and (K), respectively. Abbreviations; dSub: dorsal subiculum; AD-modifying: Alzheimer's disease-modifying. Error bars = SD.

3.7 Chronic Lonafarnib infusions increase lysosomal production in old 3xTg mice

As Lonafarnib has previously been shown to increase the activation of lysosomes, we hypothesized that Lonafarnib infusions would increase lysosomal associated membrane protein 1 (LAMP1) immunoreactivity[142]. LAMP1 immunoreactivity was more prominent in the dSub of the Lonafarnib-infused mouse than the saline-infused mouse, particularly in well-defined spots that appeared to correspond to amyloid plaques in the dSub (Fig. 3.7).

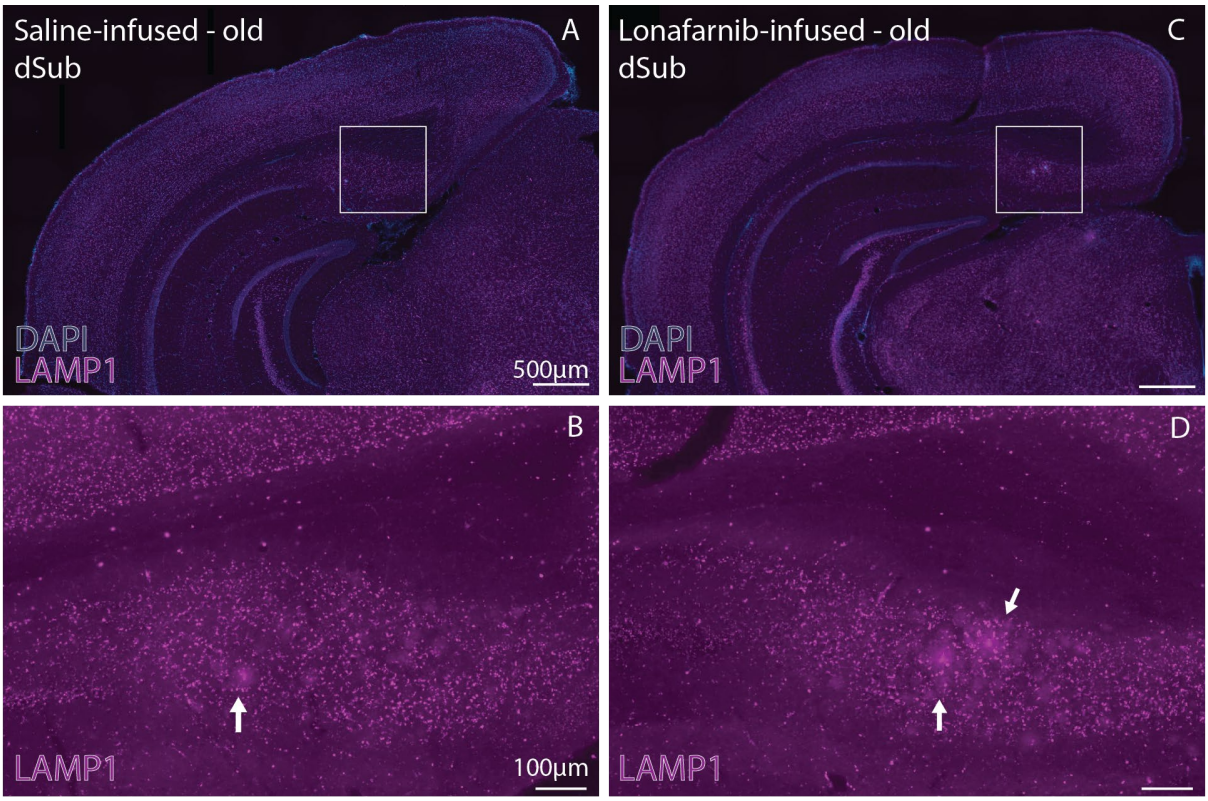

Figure 3.7. (A-F): Immunohistochemistry of brain tissue slices after microdialysis probe implantation into the lateral ventricle with Lonafarnib (*n* = 1) or saline (*n* = 1) infused once a day for 10 days in 14-month-old 3xTg mice. Lysosomal associated membrane protein 1 immunoreactivity (purple; LAMP1) appears to be stronger in the dSub of the Lonafarnib-infused mouse (D-F) compared to the saline-infused mouse (A-C). White arrows in (C) and (D) indicate spots of prominent LAMP1 reactivity in the dSub of both mice. Abbreviations; dSub: dorsal subiculum; DAPI: 4′,6-diamidino-2-phenylindole.

3.8 Chronic Fasudil infusions decrease CSF amyloid-β 42 and CSF p-tau in old 3xTg mice; chronic Lonafarnib infusions increase CSF amyloid-β 40 and amyloid-β 42 in old 3xTg mice

We next examined CSF concentrations of Aβ40, Aβ42, t-tau, and p-tau in the five old 3xTg mice that received chronic infusions of either Fasudil (n = 3), Lonafarnib (n = 1), or saline (n = 1) (Fig. 3.8). We hypothesized that Fasudil infusions would decrease CSF Aβ40 and CSF Aβ42 over the course of treatment while Lonafarnib infusions would decrease CSF t-tau and p-tau concentrations over the course of treatment. Over the course of treatment, Lonafarnib infusions increased CSF Aβ40 and Aβ42 concentrations, while Fasudil infusions decreased CSF Aβ42 and p-tau concentrations. Saline and Lonafarnib infusions decreased CSF t-tau throughout treatment. Additionally, CSF p-tau concentrations remained undetectable throughout treatment in saline- and Lonafarnib-infused animals.

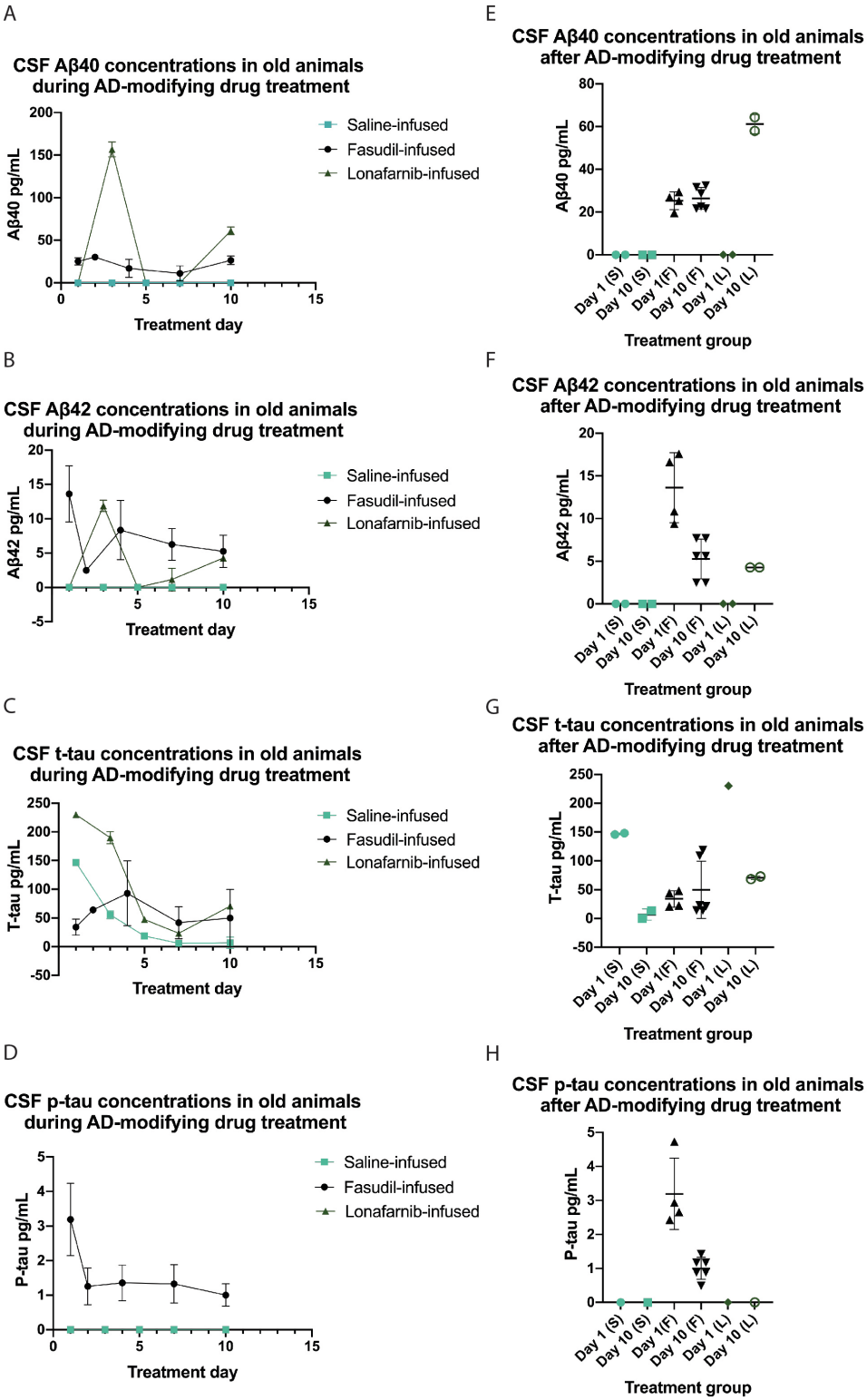

Figure 3.8. (A-H): In vivo CSF microdialysis results from five 14-month old 3xTg mice infused with saline (*n* = 1), Lonafarnib (*n* = 1), or Fasudil (*n* = 3) once a day for 10 days (saline and Lonafarnib) or 14 days (Fasudil). Mean concentrations of duplicates of Aβ40, Aβ42, t-tau, and p-tau CSF samples on days 1, 3, 5, 7, and 10 (saline and Lonafarnib) and days 1, 2, 4, 7, and 10 (Fasudil) of drug infusions (A-D) and CSF concentrations of duplicates of Aβ40 (E), Aβ42 (F), t-tau (G), and p-tau (H) CSF samples on day 10 of treatment for each animal shown, as measured by multiplex ELISA. Lonafarnib infusions increased CSF Aβ40 (A; B) and CSF Aβ42 (B; D) over time while Fasudil infusions decreased CSF Aβ42 (B; D) over time. Lonafarnib and saline infusions decreased CSF t-tau (C; F) over time, while Fasudil infusions decreased CSF p-tau over time (G; H). Abbreviations; CSF: cerebrospinal fluid; Aβ: amyloid-β; t-tau: total-tau; p-tau:

phosphorylated-tau; AD-modifying: Alzheimer's disease-modifying. No data points = no recovery of protein in microdialyte. Error bars = SD.

3.9 Chronic Lonafarnib infusions reduce conformation-specific tau reactivity in old 3xTg mice

The old, Lonafarnib-infused 3xTg mouse and the old, saline-infused 3xTg mouse were also visually compared for MC1 immunoreactivity (Fig. 3.9). Unlike the young cohort, this cohort was not injected with the P301L tau virus. Therefore, MC1 reactivity was visualized around the implantation site and in the hippocampus. In line with our hypotheses, there appeared to be more MC1 reactivity around the implantation site and in the HPC of the saline-infused mouse than the Lonafarnib-infused mouse.

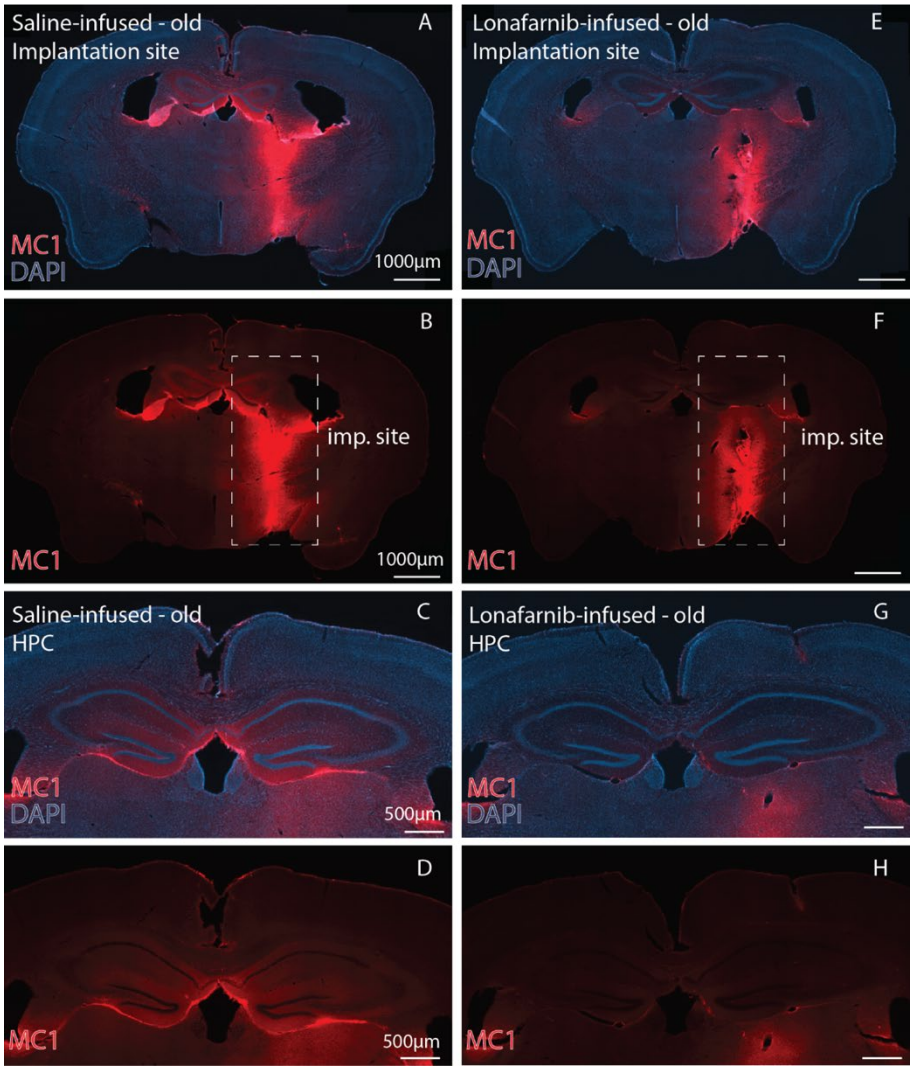

Figure 3.9. (A-H): Immunohistochemistry of brain tissue slices after microdialysis probe implantation into the lateral ventricle with Lonafarnib (*n* = 1) or saline (*n* = 1) infused once a day for 10 days in 14-month-old 3xTg mice. (A-B; E-F): Implantation sites of the mouse infused with saline for 10 days (A-B) and the mouse infused with Lonafarnib for 10 days (E-F). Conformation-specific tau immunoreactivity (red; MC1) appears to be stronger around the implantation site of the saline-infused mouse (B) compared to Lonafarnib-infused mouse (F). (E-F; G-H): Hippocampi (HPC) of the mouse infused with saline for 10 days (C-D) and the mouse infused with Lonafarnib for 10 days (G-H). Conformation-specific tau immunoreactivity (red; MC1) appears to be stronger in the HPC of the saline-infused mouse (D) compared to the Lonafarnib-infused mouse (H). Abbreviations; HPC: hippocampi; DAPI: 4′,6-diamidino-2-phenylindole.

3.10 TREM2 clusters around amyloid plaques in the 3xTg mouse model

We co-stained for triggering receptor expressed on microglia 2 (TREM2; marker of microglial activation) and McSA1 and found that TREM2 and McSA1 colocalized, indicating the presence of TREM2 receptors within amyloid plaques in the 3xTg mouse model. TREM2 was found to colocalize with amyloid plaques in all three treatment groups (saline-infused, Fasudil-infused, and Lonafarnib-infused), and the intensity of TREM2 staining appeared to be proportionate to the intensity of amyloid plaque (McSA1) immunoreactivity (Fig. 3.10).

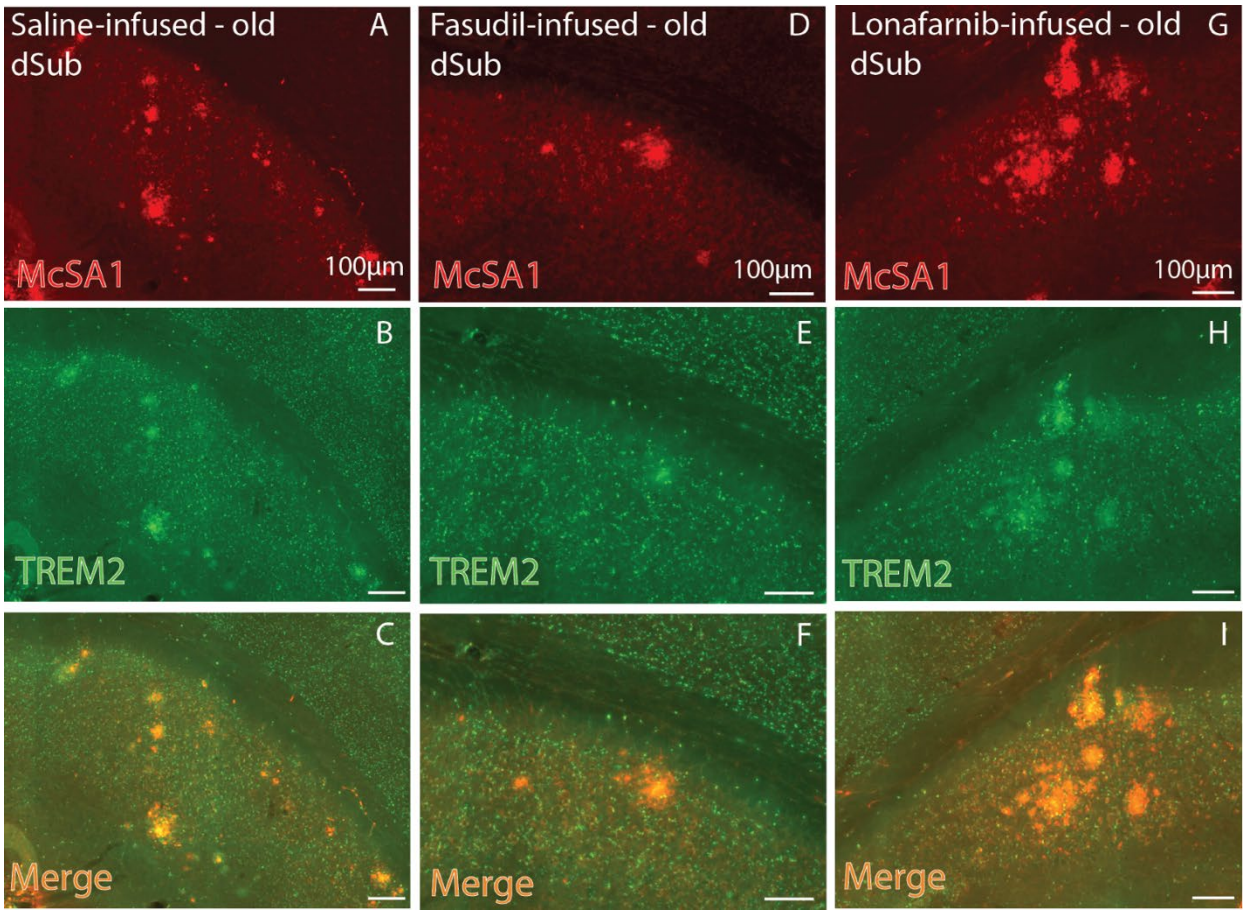

Figure 3.10. (A-I): Immunohistochemistry of brain tissue slices after microdialysis probe implantation into the lateral ventricle with saline (A-C; *n* = 1) infused once a day for 10 days, Fasudil (D-F; *n* = 3) infused once a day for 14 days, or Lonafarnib (G-I; *n* = 1) infused once a day for 10 days in 14-month-old 3xTg mice. Aβ38-42 (red; McSA1) staining for amyloid plaques (top) and microglial activation (green; TREM2) in dSub. Amyloid plaques and TREM2 reactivity colocalized, indicating the presence of TREM2 receptors within amyloid plaques. Abbreviations; dSub: dorsal subiculum; TREM2: triggering receptor expressed on myeloid cells 2.

3.11 Conformation-specific tau reactivity is present within amyloid plaques of the 3xTg model

Conformation-specific tau was found to co-localize around amyloid plaques in the 3xTg mouse model. (Fig. 3.11). Further analysis using confocal microscopy revealed that conformation-specific tau was localized to the central core of the amyloid plaque (Fig. 3.12).

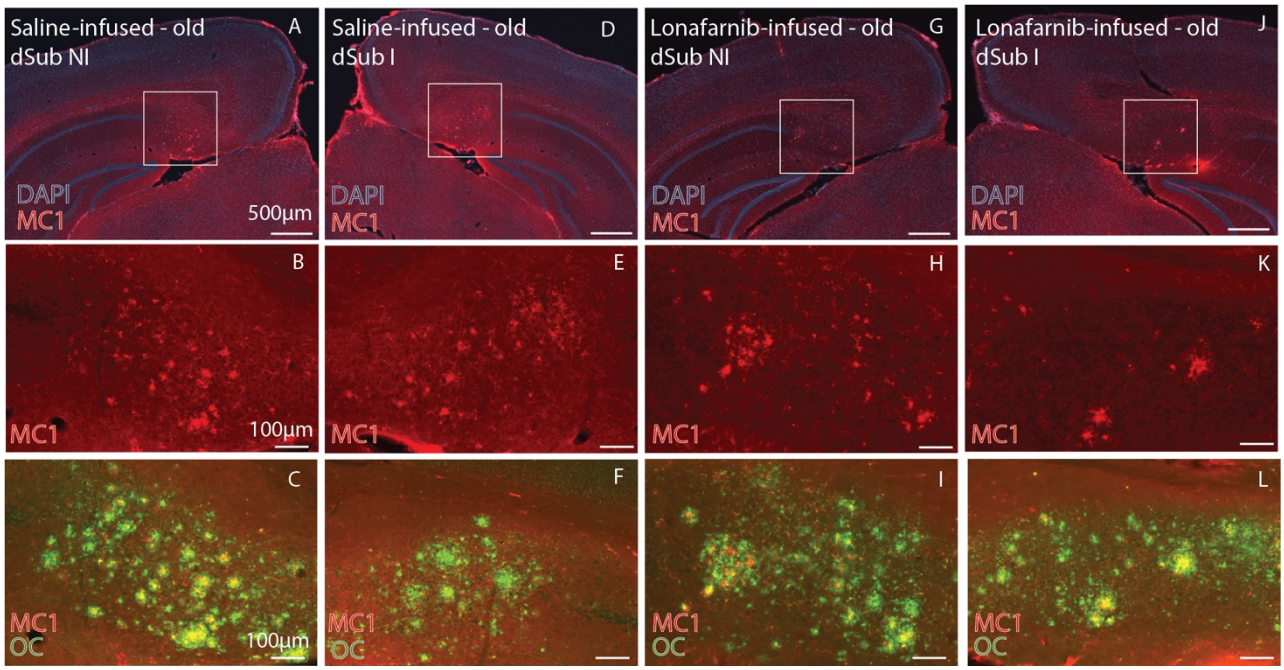

Figure 3.11. (A-L): Immunohistochemistry of brain tissue slices after microdialysis probe implantation into the lateral ventricle with saline (A-F, *n* = 1) or Lonafarnib (G-L; *n* = 1) infused once a day for 10 days in 14-month-old 3xTg mice. Conformation-specific tau reactivity (red; MC1) and fibrillar Aβ42 reactivity (green; OC) are shown in the implanted (I) and non-implanted (NI) hemispheres of the dSub of saline-infused and Lonafarnib-infused mice. MC1 and OC exhibit cross-labeling, indicating the presence of conformation-specific tau reactivity within amyloid plaques. Abbreviation list; dSub: dorsal subiculum; I: implanted; NI: non-implanted; DAPI: 4′,6-diamidino-2-phenylindole.

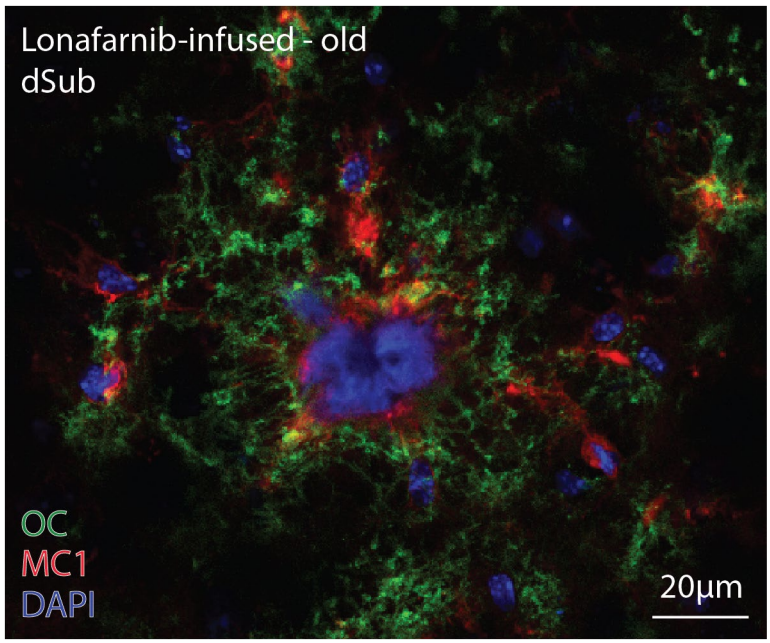

Figure 3.12. Immunohistochemistry of a brain tissue slice after microdialysis probe implantation into the lateral ventricle with Lonafarnib infused once a day for 10 days in a 14-month-old mouse. Confocal microscopy image displays an amyloid plaque (green; OC) in the dSub with a burst nuclear core (blue; DAPI) surrounded by conformation-specific tau (red; MC1). Abbreviation list; dSub: dorsal subiculum; DAPI: 4′,6-diamidino-2-phenylindole.

4 Discussion

4.1 Summary of main findings

The primary aim of this thesis was to elucidate time points when pharmaceutical treatment may reduce AD-associated iAβ, amyloid plaques, and conformation-specific tau. By using a modified push-pull microdialysis method for simultaneous drug infusion and collection of CSF, the number of amyloid plaques and iAβ-positive neurons in dSub were reduced after treatment with Fasudil in old and young mice, respectively. Additionally, Fasudil treatment decreased CSF Aβ42 and CSF p-tau in old mice. Conversely, chronic Lonafarnib treatment increased the size of amyloid plaques in dSub and increased CSF Aβ40 and CSF Aβ42 in old mice. The impact of chronic Lonafarnib infusions on conformation-specific tau reactivity was less explicit, although there appeared to be a moderate reduction after treatment in young, tau-injected animals and older animals. Taken together, these results suggest that successful pharmaceutical treatment of AD may drastically depend on the timing of administration. Additionally, targeting molecular systems that reduce either amyloid plaque or NFT pathology may have inadvertent consequences by increasing the pathology of the other.

4.2 Intermittent, longitudinal Fasudil infusions reduce iAβ in young mice

In line with our hypotheses, the young mice infused with Fasudil contained significantly fewer McSA1-positive cells in the dSub compared to the young saline-infused mouse. In addition to its status as a ROCK inhibitor, Fasudil also is an intracellular Ca^{2+} antagonist, with previous research indicating that Fasudil-treated rats display improved diastolic intracellular Ca^{2+} removal[202, 209]. As elevated cytoplasmic Ca^{2+} has been shown to increase iAβ42 production[210], it is possible that Fasudil has reduced iAβ42 by reducing cytoplasmic Ca^{2+}. Additionally, one can speculate that the inhibition by Fasudil of ROCK also inhibits actin reorganization, thereby reducing the availability of actin in the surrounding cellular environment[211]. As BACE1-cleaved APP has been shown to accumulate at actin inclusions in neurons, it is possible that inhibiting the ROCK pathway with Fasudil has reduced the availability of actin inclusions and thus reduced the amount of BACE1-cleaved APP and iAβ[103].

4.3 CSF biomarkers rise during Fasudil infusion pause in young mice

Over the course of the 30-day treatment pause, CSF Aβ40, t-tau, and p-tau levels increased in the young saline-treated animal, while CSF Aβ40 and p-tau levels increased and CSF Aβ42 levels remained undetectable in young Fasudil-treated animals. The fact that CSF Aβ42 levels remained undetectable in Fasudil-treated animals during the period of no drug infusions may indicate that initial treatment with Fasudil continued to reduce iAβ42 production during the treatment pause, as the Fasudil-treated mice displayed both reduced CSF Aβ42

levels and less iAβ in the dSub than the saline-treated mouse. In line with previous research demonstrating that inhibition of the Wnt-PCP-RhoA/ROCK pathway preferentially reduces Aβ42 concentrations both *in vivo* and *in vitro*, Fasudil shows promise as a potential Aβ-targeted disease-modifying drug[212].

4.4 Chronic Fasudil infusions reduce size and number of amyloid plaques in old mice

In each old Fasudil-infused mouse, the number of amyloid plaques in dSub was reduced compared to the saline-infused mouse, with a total average reduction of 39.61% in Fasudil-infused mice compared to the saline-infused mouse. All three old Fasudil-infused mice displayed significant reductions in mean amyloid plaque size in dSub compared to the old saline-infused mouse. Therefore, in line with our hypotheses, it appears that Fasudil significantly reduces amyloid plaque pathology present in the HPC of old 3xTg mice.

4.4.1 Dense-core amyloid plaques

Although Thioflavin-S and Congo Red are considered the gold standard for the immunolabeling of dense-core amyloid plaques, the Faculty of Medicine at NTNU does not approve these stains due to HSE regulations[92]. Therefore, an alternate protocol developed by D'Andrea and Nagele (2002) was used in which dense-core amyloid plaques appear as spots devoid of MAP2 immunolabeling, while diffuse amyloid plaques do not display a different labeling pattern than the surrounding tissue[208]. Although the origin of dense-core amyloid plaques remains unknown, the 'inside-out hypothesis' postulates that iAβ gradually accumulates inside a cell until a lysis event occurs, dispelling the cellular contents of the neuron into the extracellular space in a radial-like manner[104, 213]. As MAP2 is known to be sensitive to proteolytic digestion, it is possible that the dispersion of intracellular proteolytic enzymes during the cellular lysis event results in the degradation of MAP2[208]. This notion is supported by research demonstrating that cathepsin-D, a lysosome-derived protease, can both degrade MAP2 and retain enzymatic activity for prolonged periods of time in dense-core amyloid plaques[214]. The current study validated D'Andrea and Nagele's (2002) protocol, providing further support for the inside-out hypothesis. While the McSA1 antibody reportedly stains both diffuse and dense-core amyloid plaques, most amyloid plaques in the brains of 14-month-old 3xTg mice can be categorized as dense-core. This observation may be due to the aggressive AD phenotype that the 3xTg mouse model displays, which is more representative of EOAD than LOAD. As the 3xTg model contains two transgenes that both increase the production of Aβ, the *APP* transgene and the *PSEN1* transgene, it is possible that the high proportion of

dense-core amyloid plaques observed in the model is a result of the dramatic overproduction of Aβ and subsequent overloading of cells with Aβ42-positive material.

Overall, the decrease in dense-core amyloid plaque pathology in dSub after treatment with Fasudil is in line with the reduction of iAβ in dSub observed in young animals after chronic Fasudil infusion. This indicates that chronic Fasudil infusion not only decreases iAβ accumulation in young mice, but also may prevent cellular lysis events and subsequent dense-core amyloid plaque formation in older mice. Therefore, Fasudil may be a useful treatment option prior to the development of amyloid plaque pathology to target iAβ and prevent the subsequent formation of neurotoxic dense-core amyloid plaques.

4.5 Chronic Fasudil infusions decrease CSF amyloid-β and CSF p-tau in old mice

Interestingly, chronic Fasudil infusions reduced both amyloid plaque load in dSub and CSF Aβ42, which would be unexpected if the drug were clearing out Aβ via the CSF. The current research diagnostic criteria for patients with AD consists of either low levels of CSF Aβ40 and Aβ42, low Aβ40:42 ratio, or high brain amyloid load (as measured by Aβ positron emission tomography [PET] tracers) as equivalent measures of Aβ pathology[215, 216]. Both CSF and PET measures usually provide highly concordant information[217]. However, multiple studies have reported that a significant proportion of cases display discordant CSF and PET results (i.e., low CSF Aβ and low brain amyloid load, or high CSF Aβ and high brain amyloid load), raising the possibility that brain amyloid load and CSF Aβ levels convey partially independent information[218, 219]. One reason to suspect this is that amyloid plaque load is indicative of fibrillar, insoluble Aβ accumulation, while CSF Aβ is a marker of soluble Aβ species and only indirectly related to fibrillar Aβ. Therefore, CSF Aβ may be affected by variations in APP processing and Aβ production, while amyloid plaque load is reflective of the aggregation of Aβ. As previously mentioned, Fasudil has been reported to act as an intracellular Ca^{2+} antagonist[209] and may therefore be decreasing iAβ42 production while simultaneously inhibiting actin reorganization, ultimately reducing soluble Aβ42 in the CSF and amyloid plaque formation in the brain[210, 211]. It is worth noting that a similar increase in CSF Aβ40 was not observed in old Fasudil-infused animals, potentially indicating that Fasudil treatment results in the selective inhibition of Aβ42 production.

4.6 Chronic Lonafarnib infusions increase size of amyloid plaques in old mice

Based on visual inspection, chronic Lonafarnib infusion increased the total surface area covered by amyloid plaques, although the individual amyloid plaques appeared to be less

numerous. Therefore, it appears that the drug has either increased the overall production of amyloid plaques or caused existing amyloid plaques to sequester other amyloid plaques or Aβ fragments. Previous research has demonstrated that Lonafarnib up-regulates macroautophagy, particularly through the activation of lysosomes[142]. The present study confirmed increased activation of lysosomes after Lonafarnib administration. While upregulating macroautophagy through either Lonafarnib administration or the inhibition of mTOR signaling has been shown to reduce tau pathology in both animal[142] and cell culture studies[148], the impact of upregulating macroautophagy on Aβ pathology has not been elucidated. As multiple lines of evidence support that the lysosomal system is associated with Aβ generation and toxicity, it is possible that activating lysosomes via Lonafarnib infusion may have the unintended consequence of increasing Aβ generation and/or Aβ secretion in the extracellular space[139, 220]. Although lysosomes are responsible for the degradation of proteins, lysosomal proteolysis is impaired by AD-associated *PSEN1* mutations[221]. Therefore, increasing Aβ production after activating lysosomes with Lonafarnib may stress an endosomal/lysosomal system that is already overloaded with insoluble proteins, leading to further spillage of lysosomal hydrolases and proteases into the cytoplasm and eventual cell death and formation of dense-core amyloid plaques. While chronic Lonafarnib infusions seem to reduce conformation-specific tau-reactivity (see section 4.8), confirming previous results indicating that this drug treatment offers promise in reducing NFT pathology, stimulating autophagy may have unintended consequences on iAβ and amyloid plaque pathology[142].

4.7 Chronic Lonafarnib infusions increase CSF amyloid-β 40 and amyloid-β 42 in old mice

The increase in CSF Aβ40 and Aβ42 observed in the old, Lonafarnib-treated mouse is in line with the hypothesis that Lonafarnib is up-regulating autophagy, thereby increasing Aβ production in the process. Although increased levels of CSF Aβ40 and Aβ42 would typically indicate increased clearance of Aβ from the brain, we observed increases in CSF Aβ40 and Aβ42 as well as increased amyloid plaque load in the dSub of the Lonafarnib-infused mouse. One potential explanation for the observed increase in both CSF Aβ and amyloid plaques is that stimulating the autophagic pathway can result in both the increased production and increased fibrillization of Aβ. As similar increases in CSF Aβ40 and Aβ42 were not observed in young, tau-injected mice after Lonafarnib administration, the increases observed in the older mouse may be reflective of reduced clearance of Aβ as a consequence of aging[29, 33]. Therefore, increased levels of CSF Aβ40 and Aβ42 at early stages in the AD biochemical cascade may represent increased clearance of Aβ, while increased CSF Aβ levels

after Lonafarnib administration later in the AD biochemical cascade may represent increased Aβ production without sufficient clearance due to BBB dysfunction[222].

Multiple components of the endocytic-autophagic pathways have been identified as sites of Aβ production, including multivesicular bodies (MVBs), AVs, and lysosomes, and upregulating autophagy in cell lines has been shown to accelerate Aβ generation[139, 223]. As treating cells *in vitro* with Lonafarnib has been shown to significantly increase AV abundance, it is reasonable to assume that Lonafarnib infusions have resulted in an increase in Aβ production in the current study, which may be reflected as an increase in CSF Aβ concentrations in older animals[142]. As Lonafarnib infusions also resulted in an increase in amyloid plaque size, it is possible that stimulating autophagy with Lonafarnib, particularly through the activation of lysosomes, has inadvertently resulted in increased fibrillization of Aβ. Given that the current study found an increase in lysosomal immunoreactivity particularly in the vicinity of amyloid plaques in the Lonafarnib-infused old mouse, it raises the question of whether overburdening lysosomes with insoluble Aβ aggregates can culminate in a cellular lysis event. Lysosomes have been found to be the final destination for Aβ42 oligomers in both the endocytic and the autophagic pathways, with lysosomal hydrolases functioning optimally at a low pH of about 5[224]. However, research has demonstrated that Aβ42 peptides form large and complex fibrils much more efficiently at acidic rather than neutral pH, with Aβ aggregates at a pH of 5.8 inducing significant apoptotic death in cell cultures[225]. Additionally, previous research has found that iAβ42 is particularly resistant to degradation within lysosomes. Consistent with the inside-out hypothesis, it is possible that stimulating autophagy with Lonafarnib has led to the increased production and fibrillization of Aβ in the autophagic pathway. Previous research has demonstrated that compromised lysosomes can leak cathepsins into the cytoplasm, leading to the activation of cellular death programs that are mediated by caspases, calpains and lysosomal hydrolases[226]. Therefore, activating autophagy via Lonafarnib may have the unintended consequences of cell death and the increased formation of dense-core amyloid plaques[227].

4.8 Chronic Lonafarnib infusions reduce tau reactivity in young, tau-injected mice and old mice

Previous research has found that the MC1 antibody demonstrates reactivity with pre-tangle neurons, thereby labeling one of the earliest known pathological changes of tau observed in AD[228]. Identifying neurons that are in the process of undergoing AD-specific pathological changes is important to elucidate the earliest time points for intervention. The pathogenic P301L tau mutation has been found to inhibit degradation of tau by all three autophagic

pathways[229]. Therefore, Lonafarnib may have decreased this pathogenic tau by inducing autophagy through either the suppression of Rhes, a GTPase in the Ras family, or the inhibition of mTOR signaling, a central regulator of autophagy[142, 207].

4.9 TREM2 clusters around amyloid plaques in the 3xTg model

Our results suggest that TREM2 clusters around amyloid plaques in dSub in 3xTg mice, further validating the use of this model in the representation of the AD biochemical cascade. Previous studies have shown that TREM2 expression affects the clustering of microglia around amyloid plaques, in particular sustaining the microglial response to Aβ accumulation[230]. Additionally, TREM2 appears to play an important role in phagocytosis, which may be particularly germane in AD as a mechanism for clearance of pathogenic proteins, such as Aβ, or apoptotic cells[231]. However, although TREM2 clustering around amyloid plaques has been observed in the APP23[232], APP/PS1[233], and the 5xFAD[230] mouse models of AD, to our knowledge the TREM2 clustering response has not previously been studied in the 3xTg mouse model of AD.

4.10 Conformational tau reactivity is present in amyloid plaques in the 3xTg model

MC1 reactivity was shown to colocalize with dense-core amyloid plaques in old 3xTg mice, indicating the association of an early conformation-specific change in tau within amyloid plaques. A central tenet of the amyloid cascade hypothesis holds that tau pathology is a downstream consequence of APP misprocessing[63]. However, the mechanistic links between amyloid pathology and NFT formation have remained elusive. Previous research has suggested that the Aβ-dependent formation of dense-core amyloid plaques provides the molecular environment to facilitate the AD-associated biochemical modification of tau[234]. Given that nearly all Aβ-targeted disease-modifying therapies have failed to slow or prevent cognitive decline, understanding the early molecular events and temporal windows linking Aβ and tau pathology may prove pivotal in the successful pharmaceutical treatment of AD[151]. As confocal microscopy revealed the presence of MC1 reactivity within the burst nucleic core of an amyloid plaque, this raises the question of the involvement of the cellular lysis event with the AD-associated conformational modification of tau. Interestingly, abnormal tau phosphorylation has been shown to occur as a result of apoptosis, particularly in the presence of Aβ[235, 236]. However, it is important to note that the confocal microscopy image was only performed on one amyloid plaque, limiting the conclusions that can be drawn.

4.11 Saline reduces CSF biomarkers as effectively as Fasudil and Lonafarnib

As observed particularly in the young, chronically infused Fasudil cohort and the old, Lonafarnib-infused cohort, saline infusion appeared to reduce AD-associated CSF biomarkers at least as effectively as the disease-modifying drugs. However, it is worth noting that this effect was only found in CSF, and not in the brain, which may imply that CSF turnover is more effective in reducing soluble, pre-fibrillar species of Aβ and tau than insoluble, fibrillar species of Aβ and tau. Impairments in CSF turnover are highly suspected in the etiology of AD, with impaired CSF clearance observed in AD mouse models[32, 237]. While ventricular CSF clearance reductions have been found to be associated with increased amyloid deposition in patients[238], it is worth noting that surgical CSF drainage therapy fails to show cognitive benefit in an AD population[239], highlighting both the complexity of these relationships and the potential importance of the timing of administration.

4.12 Methodological considerations

4.12.1 The use of push-pull microdialysis

While intracerebral push-pull microdialysis offers a powerful method for the simultaneous collection of CSF and infusion of disease-modifying drugs, there are several limitations associated with the methodology that should be considered. Recovery rates for all four CSF biomarkers (Aβ40, Aβ42, t-tau, p-tau) were relatively low compared to our lab's previous analyses of longitudinal CSF biomarkers in the 3xTg mouse model, which was likely a result of a relatively fast sampling rate (1 microL/minute). Given that the relative recovery of an analyte is inversely proportional to the perfusate flow rate[240, 241], our lab previously found that a sampling rate of 0.2 microL/minute was ideal for the recovery of CSF Aβ and tau[168]. However, due to the repeated infusions of drugs in animals in the current study, a faster sampling rate was used to reduce infusion time per animal as well as to administer the drugs as one dose, rather than as a slow diffusion process over many hours. Additionally, as CSF t-tau levels generally increased in the first few days of sampling, it is likely that the removal and insertion of the microdialysis dummy and sampling probe resulted in minor tissue damage at the start of sampling. This is consistent with the fact that in response to acute brain injury, CSF t-tau concentrations increase in the first few days following injury, then reduce over time[242].

4.12.2 Tau pathology in the 3xTg model

The old animals used in the current study were 14 months old and were thus too young to display significant tau pathology. Although the 3xTg mice purchased from Jackson Laboratory are reported to develop tau pathology between 12 and 15 months of age, tau pathology emerges

around 18 months of age in the 3xTg mice bred at CoMed (Bjorkli, unpublished findings), likely due to genetic drift in the colony. The current study attempted to circumnavigate this shortcoming of the 3xTg model by injecting *P301L* tau virally into the LEC, where NFT pathology begins in patients[24, 196]. However, these viral injections contained pathological tau associated with frontotemporal dementia, not AD, as no tau mutations associated with AD have been identified[243]. Therefore, although *P301L* mutated tau is a more favorable substrate for hyperphosphorylation than the wild-type protein and has pro-aggregate properties[244, 245], it is unknown whether reducing *P301L* tau in the 3xTg model would translate to a reduction in NFT load in AD patients. As AD is a very complex disease to model, understanding snapshots of how disease-modifying drugs may impact various aspects of the biochemical cascade as seen in animal models is important, but should not be mistaken for understanding the grand scheme of the disease.

4.12.3 Aβ antibodies

Throughout the course of AD, Aβ accumulates in multiple different states, including insoluble plaque deposits, iAβ, and soluble oligomers[85]. Such distinct assembly states of Aβ can be recognized by specific, conformation-dependent antibodies[246]. The current study used the primary antibodies IBL Aβ42, OC, A11, and McSA1 to recognize various conformations of Aβ. We first used IBL Aβ42 to stain for the specific Aβ42 isoform. We also used the antibody OC, which preferentially binds an epitope found in Aβ fibrils and some soluble oligomers ("fibrillar oligomers"), but not random coil monomers or prefibrillar oligomers[247]. Therefore, OC was used to indicate amyloid plaques in the current study. A11 recognizes a mutually exclusive epitope from OC, found on other soluble oligomers ("non-fibrillar oligomers")[247]. We first stained for iAβ with A11, but A11 appeared to stain various intracellular bodies rather than the cytosol itself (see Appendix C for images of A11 staining). To assess iAβ, we utilized the monoclonal antibody McSA1, which also stained for amyloid plaques. McSA1-positive neurons were only counted as iAβ if the stained McSA1 remained within the cellular membrane. McSA1 is a non-conformation-specific antibody that recognizes the N-terminal amino acids 1-12 of human Aβ. As Aβ aggregation is a complicated process that likely involves more than a simple conversion of soluble monomer to fibril[248], understanding how disease-modifying drugs impact antibody staining of different conformations of Aβ (i.e., monomers, oligomers, or fibrils) may offer insight into to the biochemical pathways involved in the formation of different conformation states. Given the exploratory nature of this thesis, the impact of disease-modifying drugs on non-fibrillar conformation states of Aβ was not explored in depth. However, as it is currently unknown whether therapeutic

interventions that reduce Aβ fibrils at the cost of augmenting nonfibrillar Aβ species (such as monomers or non-fibrillar oligomers) would be helpful or harmful[90], elucidating the impact of disease-modifying drugs on various conformational states of Aβ through the utilization of different antibodies may elicit time points at which pharmaceutical intervention is most likely to prevent downstream neurodegeneration and cognitive decline.

4.12.4 Translational value

Developing successful pharmaceutical treatments for AD requires precision in many facets, including the correct target, correct biomarker, correct participant, and correct timing of administration[249]. The correct target involves identifying the appropriate biologic process for AD therapeutic intervention, while correct biomarkers include those of target engagement and those supportive of disease modification. The correct participant and correct timing are contingent on the identification of the phase of AD (i.e., preclinical, prodromal, or dementia). Animal models of AD allow for the elucidation of biologic processes at various time points in the AD disease course in a way that is not possible in patients. Additionally, understanding the effect of disease-modifying drugs at time points corresponding to the preclinical, prodromal, and dementia stages of AD in models provides valuable information on when treatment may be most successful in patients. Finally, drug administration using push-pull microdialysis circumvents the need for the drug to cross the BBB and allows for the observation of the disease-modifying drugs' impact on CSF biomarkers in real-time, ultimately deepening insight into the biochemical cascades occurring at various time points during the progression of AD.

4.13 Future directions

Activating autophagy has been increasingly considered as a potential therapeutic strategy for the amelioration of tau pathology. Although previous research has found that pharmaceutically inhibiting mTOR activity and activating autophagy reduced iAβ reactivity in 8-month-old 3xTg mice[250], to our knowledge mTOR inhibition (and concomitant autophagy induction) has not been studied in the context of amyloid plaques or in older mice. The results of the current study suggest that activating autophagy may increase Aβ pathology in older animals, potentially due to an 'already-stressed' endosomal-lysosomal pathway. Therefore, future research should examine the impact of autophagy stimulation on both Aβ and tau pathology at different time points in the AD biochemical cascade, with particular focus on the impact of autophagy stimulation on Aβ production and fibrillization in animal models. Additionally, as the current study found that AD-associated conformational changes in tau reactivity were localized around dense-core amyloid plaques, future studies should assess possible

relationships between AD-associated posttranslational modifications of tau and Aβ-induced cellular lysis events.

While previous research has demonstrated that Fasudil protects against synaptotoxicity and rescues Aβ-driven cognitive impairment in animal models[122], no studies to date have examined Fasudil in the context of reducing iAβ or amyloid plaque pathology, and the present study found a reduction in both. However, the impact of these reductions on cognitive performance was not assessed. Therefore, future studies should combine pharmaceutical treatment with cognitive behavioral testing to assess the impact of treatment on memory impairment, as memory is dependent on the integrity of the EC and HPC, which are the earliest areas affected by iAβ in AD[23]. Additionally, although intracerebral push-pull microdialysis offers a powerful method for the simultaneous infusion of disease-modifying drugs and collection of CSF while bypassing the BBB, it is an invasive treatment approach for patients. Therefore, future studies should be conducted to assess the impact of Fasudil treatment via intraperitoneal, oral, or intranasal administration on AD biomarkers in the 3xTg mouse model as well as probe the intracellular pathways involved in the present observations of the reductions of iAβ and amyloid plaque pathology in the HPC following Fasudil administration. Additionally, although the current study found that the A11 antibody stained for various intracellular bodies rather than the cytosol itself, we did not have the time nor resolution to quantify such intracellular accumulation. Therefore, future studies should employ microscopy methods with higher resolution to further assess the impact of Fasudil administration on iAβ accumulation. As the present study found that infusing saline at a relatively fast sampling rate of 0.1 microL/minute reduced CSF biomarkers over time, more research should be conducted on the impact of increased CSF turnover on the pathogenesis of AD. Finally, the primary limitation of this thesis was the small sample size in each treatment group, as the thesis was exploratory in nature. Therefore, future studies should include more animals to increase the translational value of findings.

4.14 Conclusions

Treating AD pharmaceutically in patients has proven to be an immense challenge. The complex biochemical cascade of AD over a long time-course, with a paucity of consistent biomarkers signaling the prodromal stage, has made it difficult to grasp when and how to intervene effectively. While it has previously been suggested that targeting iAβ42 may be a viable treatment strategy for Alzheimer's disease[104], intervening early enough without consistent biomarkers of dysfunction would prove challenging. Additionally, understanding the underlying molecular biology and time progression of different conformations of Aβ

throughout particular brain regions may have an impact on the pharmaceutical treatment of AD. Meanwhile, attempting to clear tau through the induction of autophagy may inadvertently increase the production or deposition of Aβ into the extracellular space. Finally, as amyloid plaques were shown to colocalize with a very early conformation-specific change of tau, administering disease-modifying drug treatment before the appearance of amyloid plaques may be necessary to halt the AD biochemical cascade. Ultimately, the findings of this thesis offer support for using repurposed drugs in AD animal models to probe potential timing windows for successful treatment and further understanding of the biochemical events that should be targeted to halt the AD disease cascade.

5 References

1. Dementia in Norway [Internet]. Norwegian Institute of Public Health. 2019.
2. Association. As. 2019 Alzheimer's disease facts and figures. Alzheimers Dement. 2019;15(3):321-87.
3. De Strooper B, Karran E. The Cellular Phase of Alzheimer's Disease. Cell. 2016;164(4):603-15.
4. Lopez-Gonzalez I, Schluter A, Aso E, Garcia-Esparcia P, Ansoleaga B, F LL, et al. Neuroinflammatory signals in Alzheimer disease and APP/PS1 transgenic mice: correlations with plaques, tangles, and oligomeric species. J Neuropathol Exp Neurol. 2015;74(4):319-44.
5. Khan TK. An Algorithm for Preclinical Diagnosis of Alzheimer's Disease. Front Neurosci. 2018;12:275.
6. Morris JC, Price JL. Pathologic correlates of nondemented aging, mild cognitive impairment, and early-stage Alzheimer's disease. J Mol Neurosci. 2001;17(2):101-18.
7. Braak H, Del Tredici K. Amyloid-beta may be released from non-junctional varicosities of axons generated from abnormal tau-containing brainstem nuclei in sporadic Alzheimer's disease: a hypothesis. Acta Neuropathol. 2013;126(2):303-6.
8. Villemagne VL, Burnham S, Bourgeat P, Brown B, Ellis KA, Salvado O, et al. Amyloid beta deposition, neurodegeneration, and cognitive decline in sporadic Alzheimer's disease: a prospective cohort study. Lancet Neurol. 2013;12(4):357-67.
9. Sperling RA, Karlawish J, Johnson KA. Preclinical Alzheimer disease-the challenges ahead. Nat Rev Neurol. 2013;9(1):54-8.
10. Sasaguri H, Nilsson P, Hashimoto S, Nagata K, Saito T, De Strooper B, et al. APP mouse models for Alzheimer's disease preclinical studies. EMBO J. 2017;36(17):2473-87.
11. Selkoe DJ, Hardy J. The amyloid hypothesis of Alzheimer's disease at 25 years. EMBO Mol Med. 2016;8(6):595-608.
12. Knopman DS, Parisi JE, Salviati A, Floriach-Robert M, Boeve BF, Ivnik RJ, et al. Neuropathology of cognitively normal elderly. J Neuropathol Exp Neurol. 2003;62(11):1087-95.
13. Holland D, McEvoy LK, Dale AM, Alzheimer's Disease Neuroimaging I. Unbiased comparison of sample size estimates from longitudinal structural measures in ADNI. Hum Brain Mapp. 2012;33(11):2586-602.
14. Uylings HB, de Brabander JM. Neuronal changes in normal human aging and Alzheimer's disease. Brain Cogn. 2002;49(3):268-76.
15. Nestor SM, Rupsingh R, Borrie M, Smith M, Accomazzi V, Wells JL, et al. Ventricular enlargement as a possible measure of Alzheimer's disease progression validated using the Alzheimer's disease neuroimaging initiative database. Brain. 2008;131(Pt 9):2443-54.
16. Akiyama H, Barger S, Barnum S, Bradt B, Bauer J, Cole GM, et al. Inflammation and Alzheimer's disease. Neurobiol Aging. 2000;21(3):383-421.
17. Gomez-Nicola D, Boche D. Post-mortem analysis of neuroinflammatory changes in human Alzheimer's disease. Alzheimers Res Ther. 2015;7(1):42.
18. Kitazawa M, Yamasaki TR, LaFerla FM. Microglia as a potential bridge between the amyloid beta-peptide and tau. Ann N Y Acad Sci. 2004;1035:85-103.
19. Kinney JW, Bemiller SM, Murtishaw AS, Leisgang AM, Salazar AM, Lamb BT. Inflammation as a central mechanism in Alzheimer's disease. Alzheimers Dement (N Y). 2018;4:575-90.
20. Bjorkli C, Sandvig A, Sandvig I. Bridging the Gap Between Fluid Biomarkers for Alzheimer's Disease, Model Systems, and Patients. Front Aging Neurosci. 2020;12:272.

21. Thal DR, Rub U, Orantes M, Braak H. Phases of A beta-deposition in the human brain and its relevance for the development of AD. Neurology. 2002;58(12):1791-800.
22. Pensalfini A, Albay R, 3rd, Rasool S, Wu JW, Hatami A, Arai H, et al. Intracellular amyloid and the neuronal origin of Alzheimer neuritic plaques. Neurobiol Dis. 2014;71:53-61.
23. Kobro-Flatmoen A, Nagelhus A, Witter MP. Reelin-immunoreactive neurons in entorhinal cortex layer II selectively express intracellular amyloid in early Alzheimer's disease. Neurobiol Dis. 2016;93:172-83.
24. Braak H, Braak E. Neuropathological stageing of Alzheimer-related changes. Acta Neuropathol. 1991;82(4):239-59.
25. Wu JW, Hussaini SA, Bastille IM, Rodriguez GA, Mrejeru A, Rilett K, et al. Neuronal activity enhances tau propagation and tau pathology in vivo. Nat Neurosci. 2016;19(8):1085-92.
26. Liu L, Drouet V, Wu JW, Witter MP, Small SA, Clelland C, et al. Trans-synaptic spread of tau pathology in vivo. PLoS One. 2012;7(2):e31302.
27. Apostolova LG, Green AE, Babakchanian S, Hwang KS, Chou YY, Toga AW, et al. Hippocampal atrophy and ventricular enlargement in normal aging, mild cognitive impairment (MCI), and Alzheimer Disease. Alzheimer Dis Assoc Disord. 2012;26(1):17-27.
28. Schott JM FN, Frost C, Scahill RI, Janssen JC, et al. Assessing the onset of structural change in familial Alzheimer's disease. Ann Neurol. 2002;53(2):181-8.
29. Erickson MA, Banks WA. Blood-brain barrier dysfunction as a cause and consequence of Alzheimer's disease. J Cereb Blood Flow Metab. 2013;33(10):1500-13.
30. Zenaro E, Piacentino G, Constantin G. The blood-brain barrier in Alzheimer's disease. Neurobiol Dis. 2017;107:41-56.
31. Deane R, Du Yan S, Submamaryan RK, LaRue B, Jovanovic S, Hogg E, et al. RAGE mediates amyloid-beta peptide transport across the blood-brain barrier and accumulation in brain. Nat Med. 2003;9(7):907-13.
32. Tarasoff-Conway JM, Carare RO, Osorio RS, Glodzik L, Butler T, Fieremans E, et al. Clearance systems in the brain-implications for Alzheimer disease. Nat Rev Neurol. 2015;11(8):457-70.
33. Montagne A, Barnes SR, Sweeney MD, Halliday MR, Sagare AP, Zhao Z, et al. Blood-brain barrier breakdown in the aging human hippocampus. Neuron. 2015;85(2):296-302.
34. Carrano A, Hoozemans JJ, van der Vies SM, Rozemuller AJ, van Horssen J, de Vries HE. Amyloid Beta induces oxidative stress-mediated blood-brain barrier changes in capillary amyloid angiopathy. Antioxid Redox Signal. 2011;15(5):1167-78.
35. Blair LJ, Frauen HD, Zhang B, Nordhues BA, Bijan S, Lin YC, et al. Tau depletion prevents progressive blood-brain barrier damage in a mouse model of tauopathy. Acta Neuropathol Commun. 2015;3:8.
36. Kang J, Lemaire HG, Unterbeck A, Salbaum JM, Masters CL, Grzeschik KH, et al. The precursor of Alzheimer's disease amyloid A4 protein resembles a cell-surface receptor. Nature. 1987;325(6106):733-6.
37. Dyrks T, Weidemann A, Multhaup G, Salbaum JM, Lemaire HG, Kang J, et al. Identification, transmembrane orientation and biogenesis of the amyloid A4 precursor of Alzheimer's disease. EMBO J. 1988;7(4):949-57.
38. Haass C, Kaether C, Thinakaran G, Sisodia S. Trafficking and proteolytic processing of APP. Cold Spring Harb Perspect Med. 2012;2(5):a006270.
39. Jarrett JT, Berger EP, Lansbury PT, Jr. The C-terminus of the beta protein is critical in amyloidogenesis. Ann N Y Acad Sci. 1993;695:144-8.
40. Kamenetz F, Tomita T, Hsieh H, Seabrook G, Borchelt D, Iwatsubo T, et al. APP processing and synaptic function. Neuron. 2003;37(6):925-37.

41. Chow VW, Mattson MP, Wong PC, Gleichmann M. An overview of APP processing enzymes and products. Neuromolecular Med. 2010;12(1):1-12.
42. Dawkins E, Small DH. Insights into the physiological function of the beta-amyloid precursor protein: beyond Alzheimer's disease. J Neurochem. 2014;129(5):756-69.
43. Morley JE, Farr SA. The role of amyloid-beta in the regulation of memory. Biochem Pharmacol. 2014;88(4):479-85.
44. Bourgade K, Garneau H, Giroux G, Le Page AY, Bocti C, Dupuis G, et al. beta-Amyloid peptides display protective activity against the human Alzheimer's disease-associated herpes simplex virus-1. Biogerontology. 2015;16(1):85-98.
45. Kumar A, Rotter S, Aertsen A. Spiking activity propagation in neuronal networks: reconciling different perspectives on neural coding. Nature reviews neuroscience. 2010;11(9):615-27.
46. Wilson CA, Doms RW, Lee VM. Intracellular APP processing and A beta production in Alzheimer disease. J Neuropathol Exp Neurol. 1999;58(8):787-94.
47. Strang KH, Golde TE, Giasson BI. MAPT mutations, tauopathy, and mechanisms of neurodegeneration. Lab Invest. 2019;99(7):912-28.
48. Goedert M, Spillantini MG, Jakes R, Rutherford D, Crowther RA. Multiple isoforms of human microtubule-associated protein tau: sequences and localization in neurofibrillary tangles of Alzheimer's disease. Neuron. 1989;3(4):519-26.
49. Kametani F, Hasegawa M. Reconsideration of Amyloid Hypothesis and Tau Hypothesis in Alzheimer's Disease. Front Neurosci. 2018;12:25.
50. Hernandez F, Merchan-Rubira J, Valles-Saiz L, Rodriguez-Matellan A, Avila J. Differences Between Human and Murine Tau at the N-terminal End. Front Aging Neurosci. 2020;12:11.
51. Li C, Gotz J. Tau-based therapies in neurodegeneration: opportunities and challenges. Nat Rev Drug Discov. 2017;16(12):863-83.
52. Drubin DG, Kirschner MW. Tau protein function in living cells. J Cell Biol. 1986;103(6 Pt 2):2739-46.
53. Lee G, Rook SL. Expression of tau protein in non-neuronal cells: microtubule binding and stabilization. J Cell Sci. 1992;102 (Pt 2):227-37.
54. Kadavath H, Hofele RV, Biernat J, Kumar S, Tepper K, Urlaub H, et al. Tau stabilizes microtubules by binding at the interface between tubulin heterodimers. Proc Natl Acad Sci U S A. 2015;112(24):7501-6.
55. Qiang L, Sun X, Austin TO, Muralidharan H, Jean DC, Liu M, et al. Tau Does Not Stabilize Axonal Microtubules but Rather Enables Them to Have Long Labile Domains. Curr Biol. 2018;28(13):2181-9 e4.
56. Martin L, Latypova X, Terro F. Post-translational modifications of tau protein: implications for Alzheimer's disease. Neurochem Int. 2011;58(4):458-71.
57. Andorfer C, Kress Y, Espinoza M, de Silva R, Tucker KL, Barde YA, et al. Hyperphosphorylation and aggregation of tau in mice expressing normal human tau isoforms. J Neurochem. 2003;86(3):582-90.
58. Tai HC, Serrano-Pozo A, Hashimoto T, Frosch MP, Spires-Jones TL, Hyman BT. The synaptic accumulation of hyperphosphorylated tau oligomers in Alzheimer disease is associated with dysfunction of the ubiquitin-proteasome system. Am J Pathol. 2012;181(4):1426-35.
59. Plattner F, Angelo M, Giese KP. The roles of cyclin-dependent kinase 5 and glycogen synthase kinase 3 in tau hyperphosphorylation. J Biol Chem. 2006;281(35):25457-65.
60. Hardy J, Allsop D. Amyloid deposition as the central event in the aetiology of Alzheimer's disease. Trends Pharmacol Sci. 1991;12(10):383-8.

61. Selkoe DJ. Amyloid protein and Alzheimer's disease. Sci Am. 1991;265(5):68-71, 4-6, 8.
62. Hardy JA, Higgins GA. Alzheimer's disease: the amyloid cascade hypothesis. Science. 1992;256(5054):184-5.
63. Hardy J, Selkoe DJ. The amyloid hypothesis of Alzheimer's disease: progress and problems on the road to therapeutics. Science. 2002;297(5580):353-6.
64. Goate A, Chartier-Harlin MC, Mullan M, Brown J, Crawford F, Fidani L, et al. Segregation of a missense mutation in the amyloid precursor protein gene with familial Alzheimer's disease. Nature. 1991;349(6311):704-6.
65. Hardy J. Alzheimer's disease: the amyloid cascade hypothesis: an update and reappraisal. J Alzheimers Dis. 2006;9(3 Suppl):151-3.
66. Seltzer B, Sherwin I. A comparison of clinical features in early- and late-onset primary degenerative dementia. One entity or two? Arch Neurol. 1983;40(3):143-6.
67. Glenner GG, Wong CW. Alzheimer's disease and Down's syndrome: sharing of a unique cerebrovascular amyloid fibril protein. Biochem Biophys Res Commun. 1984;122(3):1131-5.
68. McCarron M, McCallion P, Reilly E, Mulryan N. A prospective 14-year longitudinal follow-up of dementia in persons with Down syndrome. J Intellect Disabil Res. 2014;58(1):61-70.
69. Wiseman FK, Al-Janabi T, Hardy J, Karmiloff-Smith A, Nizetic D, Tybulewicz VL, et al. A genetic cause of Alzheimer disease: mechanistic insights from Down syndrome. Nat Rev Neurosci. 2015;16(9):564-74.
70. Hardy J. Amyloid, the presenilins and Alzheimer's disease. Trends Neurosci. 1997;20(4):154-9.
71. Tanzi RE, Bertram L. Twenty years of the Alzheimer's disease amyloid hypothesis: a genetic perspective. Cell. 2005;120(4):545-55.
72. Mawuenyega KG, Sigurdson W, Ovod V, Munsell L, Kasten T, Morris JC, et al. Decreased clearance of CNS beta-amyloid in Alzheimer's disease. Science. 2010;330(6012):1774.
73. Koga H, Kaushik S, Cuervo AM. Protein homeostasis and aging: The importance of exquisite quality control. Ageing Res Rev. 2011;10(2):205-15.
74. Lopez-Otin C, Blasco MA, Partridge L, Serrano M, Kroemer G. The hallmarks of aging. Cell. 2013;153(6):1194-217.
75. Lindsay J, Laurin D, Verreault R, Hebert R, Helliwell B, Hill GB, et al. Risk factors for Alzheimer's disease: a prospective analysis from the Canadian Study of Health and Aging. Am J Epidemiol. 2002;156(5):445-53.
76. Farrer LA, Cupples LA, Haines JL, Hyman B, Kukull WA, Mayeux R, et al. Effects of age, sex, and ethnicity on the association between apolipoprotein E genotype and Alzheimer disease. A meta-analysis. APOE and Alzheimer Disease Meta Analysis Consortium. JAMA. 1997;278(16):1349-56.
77. Khachaturian AS, Corcoran CD, Mayer LS, Zandi PP, Breitner JC, Cache County Study I. Apolipoprotein E epsilon4 count affects age at onset of Alzheimer disease, but not lifetime susceptibility: The Cache County Study. Arch Gen Psychiatry. 2004;61(5):518-24.
78. Bales KR LF, Wu S, Lin S, Koger D, et al. Human APOE isoform-dependent effects on brain β-amyloid levels in PDAPP transgenic mice. J Neurosci. 2009;29(21):6771-9.
79. Mann DM, Iwatsubo T, Pickering-Brown SM, Owen F, Saido TC, Perry RH. Preferential deposition of amyloid beta protein (Abeta) in the form Abeta40 in Alzheimer's disease is associated with a gene dosage effect of the apolipoprotein E E4 allele. Neurosci Lett. 1997;221(2-3):81-4.

80. Verghese PB, Castellano JM, Garai K, Wang Y, Jiang H, Shah A, et al. ApoE influences amyloid-beta (Abeta) clearance despite minimal apoE/Abeta association in physiological conditions. Proc Natl Acad Sci U S A. 2013;110(19):E1807-16.
81. Deane R, Sagare A, Hamm K, Parisi M, Lane S, Finn MB, et al. apoE isoform-specific disruption of amyloid beta peptide clearance from mouse brain. J Clin Invest. 2008;118(12):4002-13.
82. Herrup K. The case for rejecting the amyloid cascade hypothesis. Nat Neurosci. 2015;18(6):794-9.
83. Karran E, De Strooper B. The amyloid cascade hypothesis: are we poised for success or failure? J Neurochem. 2016;139 Suppl 2:237-52.
84. Ricciarelli R, Fedele E. The Amyloid Cascade Hypothesis in Alzheimer's Disease: It's Time to Change Our Mind. Curr Neuropharmacol. 2017;15(6):926-35.
85. Kayed R, Head E, Thompson JL, McIntire TM, Milton SC, Cotman CW, et al. Common structure of soluble amyloid oligomers implies common mechanism of pathogenesis. Science. 2003;300(5618):486-9.
86. Bitan G, Kirkitadze MD, Lomakin A, Vollers SS, Benedek GB, Teplow DB. Amyloid beta -protein (Abeta) assembly: Abeta 40 and Abeta 42 oligomerize through distinct pathways. Proc Natl Acad Sci U S A. 2003;100(1):330-5.
87. Ha C, Park CB. Ex situ atomic force microscopy analysis of beta-amyloid self-assembly and deposition on a synthetic template. Langmuir. 2006;22(16):6977-85.
88. Oddo S, Caccamo A, Tran L, Lambert MP, Glabe CG, Klein WL, et al. Temporal profile of amyloid-beta (Abeta) oligomerization in an in vivo model of Alzheimer disease. A link between Abeta and tau pathology. J Biol Chem. 2006;281(3):1599-604.
89. Barghorn S NV, Striebinger A, Krantz C, Keller P, et al. . Globular amyloid β-peptide oligomer -- a homogenous and stable neuropathological protein in Alzheimer's disease. J Neurochem. 2005;95:834-47.
90. Cheng IH, Scearce-Levie K, Legleiter J, Palop JJ, Gerstein H, Bien-Ly N, et al. Accelerating amyloid-beta fibrillization reduces oligomer levels and functional deficits in Alzheimer disease mouse models. J Biol Chem. 2007;282(33):23818-28.
91. Huang YR, Liu RT. The Toxicity and Polymorphism of beta-Amyloid Oligomers. Int J Mol Sci. 2020;21(12).
92. Serrano-Pozo A, Frosch MP, Masliah E, Hyman BT. Neuropathological alterations in Alzheimer disease. Cold Spring Harb Perspect Med. 2011;1(1):a006189.
93. D'Andrea MR, Nagele RG. Morphologically distinct types of amyloid plaques point the way to a better understanding of Alzheimer's disease pathogenesis. Biotech Histochem. 2010;85(2):133-47.
94. Terry RD, Masliah E, Salmon DP, Butters N, DeTeresa R, Hill R, et al. Physical basis of cognitive alterations in Alzheimer's disease: synapse loss is the major correlate of cognitive impairment. Ann Neurol. 1991;30(4):572-80.
95. Cummings BJ, Cotman CW. Image analysis of beta-amyloid load in Alzheimer's disease and relation to dementia severity. Lancet. 1995;346(8989):1524-8.
96. Oddo S, Caccamo A, Shepherd JD, Murphy MP, Golde TE, Kayed R, et al. Triple-transgenic model of Alzheimer's disease with plaques and tangles: intracellular Abeta and synaptic dysfunction. Neuron. 2003;39(3):409-21.
97. Billings LM, Oddo S, Green KN, McGaugh JL, LaFerla FM. Intraneuronal Abeta causes the onset of early Alzheimer's disease-related cognitive deficits in transgenic mice. Neuron. 2005;45(5):675-88.
98. Selkoe DJ. The cell biology of beta-amyloid precursor protein and presenilin in Alzheimer's disease. Trends Cell Biol. 1998;8(11):447-53.

99. Hartmann T, Bieger SC, Bruhl B, Tienari PJ, Ida N, Allsop D, et al. Distinct sites of intracellular production for Alzheimer's disease A beta40/42 amyloid peptides. Nat Med. 1997;3(9):1016-20.
100. Xu H, Sweeney D, Wang R, Thinakaran G, Lo AC, Sisodia SS, et al. Generation of Alzheimer beta-amyloid protein in the trans-Golgi network in the apparent absence of vesicle formation. Proc Natl Acad Sci U S A. 1997;94(8):3748-52.
101. Koo EH, Squazzo SL. Evidence that production and release of amyloid beta-protein involves the endocytic pathway. J Biol Chem. 1994;269(26):17386-9.
102. Yu WH, Kumar A, Peterhoff C, Shapiro Kulnane L, Uchiyama Y, Lamb BT, et al. Autophagic vacuoles are enriched in amyloid precursor protein-secretase activities: implications for beta-amyloid peptide over-production and localization in Alzheimer's disease. Int J Biochem Cell Biol. 2004;36(12):2531-40.
103. Maloney MT, Minamide LS, Kinley AW, Boyle JA, Bamburg JR. Beta-secretase-cleaved amyloid precursor protein accumulates at actin inclusions induced in neurons by stress or amyloid beta: a feedforward mechanism for Alzheimer's disease. J Neurosci. 2005;25(49):11313-21.
104. D'Andrea MR, Nagele RG, Wang HY, Peterson PA, Lee DH. Evidence that neurones accumulating amyloid can undergo lysis to form amyloid plaques in Alzheimer's disease. Histopathology. 2001;38(2):120-34.
105. Mori C, Spooner ET, Wisniewsk KE, Wisniewski TM, Yamaguch H, Saido TC, et al. Intraneuronal Abeta42 accumulation in Down syndrome brain. Amyloid. 2002;9(2):88-102.
106. Placido AI, Pereira CM, Duarte AI, Candeias E, Correia SC, Santos RX, et al. The role of endoplasmic reticulum in amyloid precursor protein processing and trafficking: implications for Alzheimer's disease. Biochim Biophys Acta. 2014;1842(9):1444-53.
107. Silveira JR, Raymond GJ, Hughson AG, Race RE, Sim VL, Hayes SF, et al. The most infectious prion protein particles. Nature. 2005;437(7056):257-61.
108. Campioni S, Mannini B, Zampagni M, Pensalfini A, Parrini C, Evangelisti E, et al. A causative link between the structure of aberrant protein oligomers and their toxicity. Nat Chem Biol. 2010;6(2):140-7.
109. Rahimi F, Shanmugam A, Bitan G. Structure-function relationships of pre-fibrillar protein assemblies in Alzheimer's disease and related disorders. Curr Alzheimer Res. 2008;5(3):319-41.
110. Meli G, Lecci A, Manca A, Krako N, Albertini V, Benussi L, et al. Conformational targeting of intracellular Abeta oligomers demonstrates their pathological oligomerization inside the endoplasmic reticulum. Nat Commun. 2014;5:3867.
111. Walsh DM, Selkoe DJ. A beta oligomers - a decade of discovery. J Neurochem. 2007;101(5):1172-84.
112. Shankar GM, Li S, Mehta TH, Garcia-Munoz A, Shepardson NE, Smith I, et al. Amyloid-beta protein dimers isolated directly from Alzheimer's brains impair synaptic plasticity and memory. Nat Med. 2008;14(8):837-42.
113. Lesne S, Koh MT, Kotilinek L, Kayed R, Glabe CG, Yang A, et al. A specific amyloid-beta protein assembly in the brain impairs memory. Nature. 2006;440(7082):352-7.
114. Mucke L, Selkoe DJ. Neurotoxicity of amyloid beta-protein: synaptic and network dysfunction. Cold Spring Harb Perspect Med. 2012;2(7):a006338.
115. Sondag CM, Dhawan G, Combs CK. Beta amyloid oligomers and fibrils stimulate differential activation of primary microglia. J Neuroinflammation. 2009;6:1.
116. Nusse R, Varmus H. Three decades of Wnts: a personal perspective on how a scientific field developed. EMBO J. 2012;31(12):2670-84.

117. Silva-Alvarez C, Arrazola MS, Godoy JA, Ordenes D, Inestrosa NC. Canonical Wnt signaling protects hippocampal neurons from Abeta oligomers: role of non-canonical Wnt-5a/Ca(2+) in mitochondrial dynamics. Front Cell Neurosci. 2013;7:97.
118. Ciani L, Salinas PC. WNTs in the vertebrate nervous system: from patterning to neuronal connectivity. Nat Rev Neurosci. 2005;6(5):351-62.
119. Caricasole A, Copani A, Caraci F, Aronica E, Rozemuller AJ, Caruso A, et al. Induction of Dickkopf-1, a negative modulator of the Wnt pathway, is associated with neuronal degeneration in Alzheimer's brain. J Neurosci. 2004;24(26):6021-7.
120. Bafico A, Liu G, Yaniv A, Gazit A, Aaronson SA. Novel mechanism of Wnt signalling inhibition mediated by Dickkopf-1 interaction with LRP6/Arrow. Nat Cell Biol. 2001;3(7):683-6.
121. Elliott C, Rojo AI, Ribe E, Broadstock M, Xia W, Morin P, et al. A role for APP in Wnt signalling links synapse loss with beta-amyloid production. Transl Psychiatry. 2018;8(1):179.
122. Sellers KJ, Elliott C, Jackson J, Ghosh A, Ribe E, Rojo AI, et al. Amyloid beta synaptotoxicity is Wnt-PCP dependent and blocked by fasudil. Alzheimers Dement. 2018;14(3):306-17.
123. Nath S, Agholme L, Kurudenkandy FR, Granseth B, Marcusson J, Hallbeck M. Spreading of neurodegenerative pathology via neuron-to-neuron transmission of beta-amyloid. J Neurosci. 2012;32(26):8767-77.
124. Harris JA, Devidze N, Verret L, Ho K, Halabisky B, Thwin MT, et al. Transsynaptic progression of amyloid-beta-induced neuronal dysfunction within the entorhinal-hippocampal network. Neuron. 2010;68(3):428-41.
125. Resende R, Ferreiro E, Pereira C, Oliveira CR. ER stress is involved in Abeta-induced GSK-3beta activation and tau phosphorylation. J Neurosci Res. 2008;86(9):2091-9.
126. Scali C, Caraci F, Gianfriddo M, Diodato E, Roncarati R, Pollio G, et al. Inhibition of Wnt signaling, modulation of Tau phosphorylation and induction of neuronal cell death by DKK1. Neurobiol Dis. 2006;24(2):254-65.
127. Mandelkow EM, Mandelkow E. Tau in Alzheimer's disease. Trends Cell Biol. 1998;8(11):425-7.
128. Callahan LM, Coleman PD. Neurons bearing neurofibrillary tangles are responsible for selected synaptic deficits in Alzheimer's disease. Neurobiol Aging. 1995;16(3):311-4.
129. Jackson JS, Witton J, Johnson JD, Ahmed Z, Ward M, Randall AD, et al. Altered Synapse Stability in the Early Stages of Tauopathy. Cell Rep. 2017;18(13):3063-8.
130. Wittmann CW, Wszolek MF, Shulman JM, Salvaterra PM, Lewis J, Hutton M, et al. Tauopathy in Drosophila: neurodegeneration without neurofibrillary tangles. Science. 2001;293(5530):711-4.
131. Kuchibhotla KV, Wegmann S, Kopeikina KJ, Hawkes J, Rudinskiy N, Andermann ML, et al. Neurofibrillary tangle-bearing neurons are functionally integrated in cortical circuits in vivo. Proc Natl Acad Sci U S A. 2014;111(1):510-4.
132. Deretic V, Delgado M, Vergne I, Master S, De Haro S, Ponpuak M, et al. Autophagy in immunity against mycobacterium tuberculosis: a model system to dissect immunological roles of autophagy. Curr Top Microbiol Immunol. 2009;335:169-88.
133. Yang Z, Klionsky DJ. Eaten alive: a history of macroautophagy. Nat Cell Biol. 2010;12(9):814-22.
134. Wang Y, Kruger U, Mandelkow E, Mandelkow EM. Generation of tau aggregates and clearance by autophagy in an inducible cell model of tauopathy. Neurodegener Dis. 2010;7(1-3):103-7.
135. Birgisdottir AB, Johansen T. Autophagy and endocytosis - interconnections and interdependencies. J Cell Sci. 2020;133(10).

136. Nixon RA, Wegiel J, Kumar A, Yu WH, Peterhoff C, Cataldo A, et al. Extensive involvement of autophagy in Alzheimer disease: an immuno-electron microscopy study. J Neuropathol Exp Neurol. 2005;64(2):113-22.
137. Wang Y, Mandelkow E. Degradation of tau protein by autophagy and proteasomal pathways. Biochem Soc Trans. 2012;40(4):644-52.
138. Lim F, Hernandez F, Lucas JJ, Gomez-Ramos P, Moran MA, Avila J. FTDP-17 mutations in tau transgenic mice provoke lysosomal abnormalities and Tau filaments in forebrain. Mol Cell Neurosci. 2001;18(6):702-14.
139. Yu WH, Cuervo AM, Kumar A, Peterhoff CM, Schmidt SD, Lee JH, et al. Macroautophagy--a novel Beta-amyloid peptide-generating pathway activated in Alzheimer's disease. J Cell Biol. 2005;171(1):87-98.
140. Schaeffer V, Lavenir I, Ozcelik S, Tolnay M, Winkler DT, Goedert M. Stimulation of autophagy reduces neurodegeneration in a mouse model of human tauopathy. Brain. 2012;135(Pt 7):2169-77.
141. Siman R, Cocca R, Dong Y. The mTOR Inhibitor Rapamycin Mitigates Perforant Pathway Neurodegeneration and Synapse Loss in a Mouse Model of Early-Stage Alzheimer-Type Tauopathy. PLoS One. 2015;10(11):e0142340.
142. Hernandez I, Luna G, Rauch JN, Reis SA, Giroux M, Karch CM, et al. A farnesyltransferase inhibitor activates lysosomes and reduces tau pathology in mice with tauopathy. Sci Transl Med. 2019;11(485).
143. Caccamo A, Majumder S, Richardson A, Strong R, Oddo S. Molecular interplay between mammalian target of rapamycin (mTOR), amyloid-beta, and Tau: effects on cognitive impairments. J Biol Chem. 2010;285(17):13107-20.
144. Caccamo A, Magri A, Medina DX, Wisely EV, Lopez-Aranda MF, Silva AJ, et al. mTOR regulates tau phosphorylation and degradation: implications for Alzheimer's disease and other tauopathies. Aging Cell. 2013;12(3):370-80.
145. Jung CH, Ro SH, Cao J, Otto NM, Kim DH. mTOR regulation of autophagy. FEBS Lett. 2010;584(7):1287-95.
146. Diaz-Troya S, Perez-Perez ME, Florencio FJ, Crespo JL. The role of TOR in autophagy regulation from yeast to plants and mammals. Autophagy. 2008;4(7):851-65.
147. Ozcelik S, Fraser G, Castets P, Schaeffer V, Skachokova Z, Breu K, et al. Rapamycin attenuates the progression of tau pathology in P301S tau transgenic mice. PLoS One. 2013;8(5):e62459.
148. Silva MC, Nandi GA, Tentarelli S, Gurrell IK, Jamier T, Lucente D, et al. Prolonged tau clearance and stress vulnerability rescue by pharmacological activation of autophagy in tauopathy neurons. Nat Commun. 2020;11(1):3258.
149. Hane FT, Robinson M, Lee BY, Bai O, Leonenko Z, Albert MS. Recent Progress in Alzheimer's Disease Research, Part 3: Diagnosis and Treatment. J Alzheimers Dis. 2017;57(3):645-65.
150. Davies P RJ, Resnick B, Gilman S, Growdown JH, et al. . Consensus report of the working group on: “molecular and biochemical markers of Alzheimer’s disease.” Neurobiol Aging. 1998;19:109-16.
151. Bjerke M, Engelborghs S. Cerebrospinal Fluid Biomarkers for Early and Differential Alzheimer's Disease Diagnosis. J Alzheimers Dis. 2018;62(3):1199-209.
152. Fishman R. Cerebrospinal fluid in diseases of the nervous system. 2nd ed. Philadelphia, PA: WB Saunders; 1992.
153. Peskind ER, Riekse R, Quinn JF, Kaye J, Clark CM, Farlow MR, et al. Safety and acceptability of the research lumbar puncture. Alzheimer Dis Assoc Disord. 2005;19(4):220-5.

154. Strazielle N, Ghersi-Egea JF. Physiology of blood-brain interfaces in relation to brain disposition of small compounds and macromolecules. Mol Pharm. 2013;10(5):1473-91.
155. Mattsson N, Insel PS, Donohue M, Landau S, Jagust WJ, Shaw LM, et al. Independent information from cerebrospinal fluid amyloid-beta and florbetapir imaging in Alzheimer's disease. Brain. 2015;138(Pt 3):772-83.
156. Engelborghs S, De Vreese K, Van de Casteele T, Vanderstichele H, Van Everbroeck B, Cras P, et al. Diagnostic performance of a CSF-biomarker panel in autopsy-confirmed dementia. Neurobiol Aging. 2008;29(8):1143-59.
157. Takeda S, Sato N, Ikimura K, Nishino H, Rakugi H, Morishita R. Novel microdialysis method to assess neuropeptides and large molecules in free-moving mouse. Neuroscience. 2011;186:110-9.
158. Cirrito JR, May PC, O'Dell MA, Taylor JW, Parsadanian M, Cramer JW, et al. In vivo assessment of brain interstitial fluid with microdialysis reveals plaque-associated changes in amyloid-beta metabolism and half-life. J Neurosci. 2003;23(26):8844-53.
159. Hong S, Quintero-Monzon O, Ostaszewski BL, Podlisny DR, Cavanaugh WT, Yang T, et al. Dynamic analysis of amyloid beta-protein in behaving mice reveals opposing changes in ISF versus parenchymal Abeta during age-related plaque formation. J Neurosci. 2011;31(44):15861-9.
160. Savage MJ, Kalinina J, Wolfe A, Tugusheva K, Korn R, Cash-Mason T, et al. A sensitive abeta oligomer assay discriminates Alzheimer's and aged control cerebrospinal fluid. J Neurosci. 2014;34(8):2884-97.
161. Gauthier S, Reisberg B, Zaudig M, Petersen RC, Ritchie K, Broich K, et al. Mild cognitive impairment. Lancet. 2006;367(9518):1262-70.
162. Hansson O, Zetterberg H, Buchhave P, Andreasson U, Londos E, Minthon L, et al. Prediction of Alzheimer's disease using the CSF Abeta42/Abeta40 ratio in patients with mild cognitive impairment. Dement Geriatr Cogn Disord. 2007;23(5):316-20.
163. Buchhave P, Minthon L, Zetterberg H, Wallin AK, Blennow K, Hansson O. Cerebrospinal fluid levels of beta-amyloid 1-42, but not of tau, are fully changed already 5 to 10 years before the onset of Alzheimer dementia. Arch Gen Psychiatry. 2012;69(1):98-106.
164. Bouwman FH, van der Flier WM, Schoonenboom NS, van Elk EJ, Kok A, Rijmen F, et al. Longitudinal changes of CSF biomarkers in memory clinic patients. Neurology. 2007;69(10):1006-11.
165. de Leon MJ, DeSanti S, Zinkowski R, Mehta PD, Pratico D, Segal S, et al. Longitudinal CSF and MRI biomarkers improve the diagnosis of mild cognitive impairment. Neurobiol Aging. 2006;27(3):394-401.
166. Stomrud E, Hansson O, Zetterberg H, Blennow K, Minthon L, Londos E. Correlation of longitudinal cerebrospinal fluid biomarkers with cognitive decline in healthy older adults. Arch Neurol. 2010;67(2):217-23.
167. Maia LF, Kaeser SA, Reichwald J, Lambert M, Obermuller U, Schelle J, et al. Increased CSF Abeta during the very early phase of cerebral Abeta deposition in mouse models. EMBO Mol Med. 2015;7(7):895-903.
168. C Bjorkli CL, TH Flo, M Hemler, A Sandvig, I Sandvig. Tapping into the aging brain: In vivo microdialysis reveals mirroring pathology between preclinical models and patients with Alzheimer's disease. bioRxiv. 2021.
169. Blennow K, Vanmechelen E. CSF markers for pathogenic processes in Alzheimer's disease: diagnostic implications and use in clinical neurochemistry. Brain Res Bull. 2003;61(3):235-42.
170. Galasko D. Cerebrospinal fluid levels of A beta 42 and tau: potential markers of Alzheimer's disease. J Neural Transm Suppl. 1998;53:209-21.

171. Perez M, Hernandez F, Lim F, Diaz-Nido J, Avila J. Chronic lithium treatment decreases mutant tau protein aggregation in a transgenic mouse model. J Alzheimers Dis. 2003;5(4):301-8.
172. Tapiola T, Alafuzoff I, Herukka SK, Parkkinen L, Hartikainen P, Soininen H, et al. Cerebrospinal fluid {beta}-amyloid 42 and tau proteins as biomarkers of Alzheimer-type pathologic changes in the brain. Arch Neurol. 2009;66(3):382-9.
173. de Souza LC, Chupin M, Lamari F, Jardel C, Leclercq D, Colliot O, et al. CSF tau markers are correlated with hippocampal volume in Alzheimer's disease. Neurobiol Aging. 2012;33(7):1253-7.
174. Olsson B, Lautner R, Andreasson U, Ohrfelt A, Portelius E, Bjerke M, et al. CSF and blood biomarkers for the diagnosis of Alzheimer's disease: a systematic review and meta-analysis. Lancet Neurol. 2016;15(7):673-84.
175. El Kadmiri N, Said N, Slassi I, El Moutawakil B, Nadifi S. Biomarkers for Alzheimer Disease: Classical and Novel Candidates' Review. Neuroscience. 2018;370:181-90.
176. Blennow K, Dubois B, Fagan AM, Lewczuk P, de Leon MJ, Hampel H. Clinical utility of cerebrospinal fluid biomarkers in the diagnosis of early Alzheimer's disease. Alzheimers Dement. 2015;11(1):58-69.
177. Ungerstedt U, Pycock C. Functional correlates of dopamine neurotransmission. Bull Schweiz Akad Med Wiss. 1974;30(1-3):44-55.
178. Nandi P, Lunte SM. Recent trends in microdialysis sampling integrated with conventional and microanalytical systems for monitoring biological events: a review. Anal Chim Acta. 2009;651(1):1-14.
179. Deguchi Y. Application of in vivo brain microdialysis to the study of blood-brain barrier transport of drugs. Drug Metab Pharmacokinet. 2002;17(5):395-407.
180. Hammarlund-Udenaes M. Microdialysis as an Important Technique in Systems Pharmacology-a Historical and Methodological Review. AAPS J. 2017;19(5):1294-303.
181. Ungerstedt U. Microdialysis--principles and applications for studies in animals and man. J Intern Med. 1991;230(4):365-73.
182. Abbott NJ PA, Dolman DE, Yusof SR, Begley DJ. Structure and function of the blood-brain barrier. Neurobiol Dis. 2010;37(1):13-25.
183. Pardridge WM. Alzheimer's disease drug development and the problem of the blood-brain barrier. Alzheimers Dement. 2009;5(5):427-32.
184. Redzic ZB, Preston JE, Duncan JA, Chodobski A, Szmydynger-Chodobska J. The choroid plexus-cerebrospinal fluid system: from development to aging. Curr Top Dev Biol. 2005;71:1-52.
185. Ferreira ST, Klein WL. The Abeta oligomer hypothesis for synapse failure and memory loss in Alzheimer's disease. Neurobiol Learn Mem. 2011;96(4):529-43.
186. Sevigny J, Chiao P, Bussiere T, Weinreb PH, Williams L, Maier M, et al. The antibody aducanumab reduces Abeta plaques in Alzheimer's disease. Nature. 2016;537(7618):50-6.
187. Egan MF, Mukai Y, Voss T, Kost J, Stone J, Furtek C, et al. Further analyses of the safety of verubecestat in the phase 3 EPOCH trial of mild-to-moderate Alzheimer's disease. Alzheimers Res Ther. 2019;11(1):68.
188. Novak G, Streffer JR, Timmers M, Henley D, Brashear HR, Bogert J, et al. Long-term safety and tolerability of atabecestat (JNJ-54861911), an oral BACE1 inhibitor, in early Alzheimer's disease spectrum patients: a randomized, double-blind, placebo-controlled study and a two-period extension study. Alzheimers Res Ther. 2020;12(1):58.
189. Heyman A, Peterson B, Fillenbaum G, Pieper C. The consortium to establish a registry for Alzheimer's disease (CERAD). Part XIV: Demographic and clinical predictors of survival in patients with Alzheimer's disease. Neurology. 1996;46(3):656-60.

190. Sperling RA, Aisen PS, Beckett LA, Bennett DA, Craft S, Fagan AM, et al. Toward defining the preclinical stages of Alzheimer's disease: recommendations from the National Institute on Aging-Alzheimer's Association workgroups on diagnostic guidelines for Alzheimer's disease. Alzheimers Dement. 2011;7(3):280-92.
191. Barten DM, Cadelina GW, Hoque N, DeCarr LB, Guss VL, Yang L, et al. Tau transgenic mice as models for cerebrospinal fluid tau biomarkers. J Alzheimers Dis. 2011;24 Suppl 2:127-41.
192. Research models 3xTg. https://www.alzforum.org/research-models/3xtg [Internet].
193. Braak H, Del Trecidi K. Neuroanatomy and pathology of sporadic Alzheimer's disease. Adv Anat Embryol Cell Biol. 2015;215:1-162.
194. Paxinos G FK. The Mouse Brain in Stereotaxic Coordinates. London: Academic Press; 2019.
195. Drijfhout WJ KR, Meerlo P, Koolhaas JM, Grol CJ, Westerink BH. A telemetry study on the chronic effects of microdialysis probe implantation on the activity pattern and temperature rhythm of the rat. J Neurosci Methods. 1995;61(1-2):191-6.
196. Gomez-Isla T, Price JL, McKeel DW, Jr., Morris JC, Growdon JH, Hyman BT. Profound loss of layer II entorhinal cortex neurons occurs in very mild Alzheimer's disease. J Neurosci. 1996;16(14):4491-500.
197. Shibuya M, Suzuki Y, Sugita K, Saito I, Sasaki T, Takakura K, et al. Effect of AT877 on cerebral vasospasm after aneurysmal subarachnoid hemorrhage. Results of a prospective placebo-controlled double-blind trial. J Neurosurg. 1992;76(4):571-7.
198. Bourne HR, Sanders DA, McCormick F. The GTPase superfamily: conserved structure and molecular mechanism. Nature. 1991;349(6305):117-27.
199. Schlessinger K, Hall A, Tolwinski N. Wnt signaling pathways meet Rho GTPases. Genes Dev. 2009;23(3):265-77.
200. Ethell IM, Pasquale EB. Molecular mechanisms of dendritic spine development and remodeling. Prog Neurobiol. 2005;75(3):161-205.
201. Tang BL, Liou YC. Novel modulators of amyloid-beta precursor protein processing. J Neurochem. 2007;100(2):314-23.
202. Kondoh Y, Mizusawa S, Murakami M, Nakamichi H, Nagata K. Fasudil (HA1077), an intracellular calcium antagonist, improves neurological deficits and tissue potassium loss in focal cerebral ischemia in gerbils. Neurol Res. 1997;19(2):211-5.
203. Rizzetto M, Ciancio A. The prenylation inhibitor, lonafarnib: a new therapeutic strategy against hepatitis delta. Lancet Infect Dis. 2015;15(10):1119-20.
204. Kieran MW, Packer RJ, Onar A, Blaney SM, Phillips P, Pollack IF, et al. Phase I and pharmacokinetic study of the oral farnesyltransferase inhibitor lonafarnib administered twice daily to pediatric patients with advanced central nervous system tumors using a modified continuous reassessment method: a Pediatric Brain Tumor Consortium Study. J Clin Oncol. 2007;25(21):3137-43.
205. Pan J, Yeung SC. Recent advances in understanding the antineoplastic mechanisms of farnesyltransferase inhibitors. Cancer Res. 2005;65(20):9109-12.
206. Pan J, Song E, Cheng C, Lee MH, Yeung SC. Farnesyltransferase inhibitors-induced autophagy: alternative mechanisms? Autophagy. 2009;5(1):129-31.
207. Niessner H, Beck D, Sinnberg T, Lasithiotakis K, Maczey E, Gogel J, et al. The farnesyl transferase inhibitor lonafarnib inhibits mTOR signaling and enforces sorafenib-induced apoptosis in melanoma cells. J Invest Dermatol. 2011;131(2):468-79.
208. D'Andrea MR, Nagele RG. MAP-2 immunolabeling can distinguish diffuse from dense-core amyloid plaques in brains with Alzheimer's disease. Biotech Histochem. 2002;77(2):95-103.

209. Lai D, Gao J, Bi X, He H, Shi X, Weng S, et al. The Rho kinase inhibitor, fasudil, ameliorates diabetes-induced cardiac dysfunction by improving calcium clearance and actin remodeling. J Mol Med (Berl). 2017;95(2):155-65.
210. Pierrot N, Ghisdal P, Caumont AS, Octave JN. Intraneuronal amyloid-beta1-42 production triggered by sustained increase of cytosolic calcium concentration induces neuronal death. J Neurochem. 2004;88(5):1140-50.
211. Papadopoulou N, Charalampopoulos I, Anagnostopoulou V, Konstantinidis G, Foller M, Gravanis A, et al. Membrane androgen receptor activation triggers down-regulation of PI-3K/Akt/NF-kappaB activity and induces apoptotic responses via Bad, FasL and caspase-3 in DU145 prostate cancer cells. Mol Cancer. 2008;7:88.
212. Zhou Y, Su Y, Li B, Liu F, Ryder JW, Wu X, et al. Nonsteroidal anti-inflammatory drugs can lower amyloidogenic Abeta42 by inhibiting Rho. Science. 2003;302(5648):1215-7.
213. Gouras GK, Willen K, Faideau M. The inside-out amyloid hypothesis and synapse pathology in Alzheimer's disease. Neurodegener Dis. 2014;13(2-3):142-6.
214. Cataldo AM, Nixon RA. Enzymatically active lysosomal proteases are associated with amyloid deposits in Alzheimer brain. Proc Natl Acad Sci U S A. 1990;87(10):3861-5.
215. Dubois B, Feldman HH, Jacova C, Hampel H, Molinuevo JL, Blennow K, et al. Advancing research diagnostic criteria for Alzheimer's disease: the IWG-2 criteria. Lancet Neurol. 2014;13(6):614-29.
216. McKhann GM, Knopman DS, Chertkow H, Hyman BT, Jack CR, Jr., Kawas CH, et al. The diagnosis of dementia due to Alzheimer's disease: recommendations from the National Institute on Aging-Alzheimer's Association workgroups on diagnostic guidelines for Alzheimer's disease. Alzheimers Dement. 2011;7(3):263-9.
217. Jack CR, Jr., Bennett DA, Blennow K, Carrillo MC, Dunn B, Haeberlein SB, et al. NIA-AA Research Framework: Toward a biological definition of Alzheimer's disease. Alzheimers Dement. 2018;14(4):535-62.
218. Scholl M, Wall A, Thordardottir S, Ferreira D, Bogdanovic N, Langstrom B, et al. Low PiB PET retention in presence of pathologic CSF biomarkers in Arctic APP mutation carriers. Neurology. 2012;79(3):229-36.
219. Sala A, Nordberg A, Rodriguez-Vieitez E, Alzheimer's Disease Neuroimaging I. Longitudinal pathways of cerebrospinal fluid and positron emission tomography biomarkers of amyloid-beta positivity. Mol Psychiatry. 2020.
220. Adamec E, Mohan PS, Cataldo AM, Vonsattel JP, Nixon RA. Up-regulation of the lysosomal system in experimental models of neuronal injury: implications for Alzheimer's disease. Neuroscience. 2000;100(3):663-75.
221. Lee JH, Yu WH, Kumar A, Lee S, Mohan PS, Peterhoff CM, et al. Lysosomal proteolysis and autophagy require presenilin 1 and are disrupted by Alzheimer-related PS1 mutations. Cell. 2010;141(7):1146-58.
222. Silverberg GD, Messier AA, Miller MC, Machan JT, Majmudar SS, Stopa EG, et al. Amyloid efflux transporter expression at the blood-brain barrier declines in normal aging. J Neuropathol Exp Neurol. 2010;69(10):1034-43.
223. Pasternak SH, Callahan JW, Mahuran DJ. The role of the endosomal/lysosomal system in amyloid-beta production and the pathophysiology of Alzheimer's disease: reexamining the spatial paradox from a lysosomal perspective. J Alzheimers Dis. 2004;6(1):53-65.
224. Mellman I, Fuchs R, Helenius A. Acidification of the endocytic and exocytic pathways. Annu Rev Biochem. 1986;55:663-700.
225. Su Y, Chang PT. Acidic pH promotes the formation of toxic fibrils from beta-amyloid peptide. Brain Res. 2001;893(1-2):287-91.

226. Nixon RA. Amyloid precursor protein and endosomal-lysosomal dysfunction in Alzheimer's disease: inseparable partners in a multifactorial disease. FASEB J. 2017;31(7):2729-43.
227. Burdick D KJ, Knauer MF, Glabe CG. Preferential adsorption, internalization and resistance to degradation of the major isoform of the Alzheimer's amyloid peptide, A-beta 1-42, in differentiated PC12 cells. Brain Res. 1997;746(1-2):245-84.
228. Weaver CL, Espinoza M, Kress Y, Davies P. Conformational change as one of the earliest alterations of tau in Alzheimer's disease. Neurobiol Aging. 2000;21(5):719-27.
229. Caballero B, Wang Y, Diaz A, Tasset I, Juste YR, Stiller B, et al. Interplay of pathogenic forms of human tau with different autophagic pathways. Aging Cell. 2018;17(1).
230. Wang Y, Cella M, Mallinson K, Ulrich JD, Young KL, Robinette ML, et al. TREM2 lipid sensing sustains the microglial response in an Alzheimer's disease model. Cell. 2015;160(6):1061-71.
231. Ulrich JD, Ulland TK, Colonna M, Holtzman DM. Elucidating the Role of TREM2 in Alzheimer's Disease. Neuron. 2017;94(2):237-48.
232. Frank S, Burbach GJ, Bonin M, Walter M, Streit W, Bechmann I, et al. TREM2 is upregulated in amyloid plaque-associated microglia in aged APP23 transgenic mice. Glia. 2008;56(13):1438-47.
233. Wang Y, Ulland TK, Ulrich JD, Song W, Tzaferis JA, Hole JT, et al. TREM2-mediated early microglial response limits diffusion and toxicity of amyloid plaques. J Exp Med. 2016;213(5):667-75.
234. Li T, Braunstein KE, Zhang J, Lau A, Sibener L, Deeble C, et al. The neuritic plaque facilitates pathological conversion of tau in an Alzheimer's disease mouse model. Nat Commun. 2016;7:12082.
235. Guise S, Braguer D, Carles G, Delacourte A, Briand C. Hyperphosphorylation of tau is mediated by ERK activation during anticancer drug-induced apoptosis in neuroblastoma cells. J Neurosci Res. 2001;63(3):257-67.
236. Xu J, Zhang R, Zuo P, Yang N, Ji C, Liu W, et al. Aggravation effect of isoflurane on Abeta(25-35)-induced apoptosis and tau hyperphosphorylation in PC12 cells. Cell Mol Neurobiol. 2012;32(8):1343-51.
237. Peng W, Achariyar TM, Li B, Liao Y, Mestre H, Hitomi E, et al. Suppression of glymphatic fluid transport in a mouse model of Alzheimer's disease. Neurobiol Dis. 2016;93:215-25.
238. de Leon MJ, Li Y, Okamura N, Tsui WH, Saint-Louis LA, Glodzik L, et al. Cerebrospinal Fluid Clearance in Alzheimer Disease Measured with Dynamic PET. J Nucl Med. 2017;58(9):1471-6.
239. Silverberg GD, Mayo M, Saul T, Fellmann J, Carvalho J, McGuire D. Continuous CSF drainage in AD: results of a double-blind, randomized, placebo-controlled study. Neurology. 2008;71(3):202-9.
240. Alexander GM, Grothusen JR, Schwartzman RJ. Flow dependent changes in the effective surface area of microdialysis probes. Life Sci. 1988;43(7):595-601.
241. Benveniste H. Brain microdialysis. J Neurochem. 1989;52(6):1667-79.
242. Neselius S, Brisby H, Theodorsson A, Blennow K, Zetterberg H, Marcusson J. CSF-biomarkers in Olympic boxing: diagnosis and effects of repetitive head trauma. PLoS One. 2012;7(4):e33606.
243. Iqbal K, Liu F, Gong CX. Tau and neurodegenerative disease: the story so far. Nat Rev Neurol. 2016;12(1):15-27.
244. Alonso Adel C, Mederlyova A, Novak M, Grundke-Iqbal I, Iqbal K. Promotion of hyperphosphorylation by frontotemporal dementia tau mutations. J Biol Chem. 2004;279(33):34873-81.

245. Wegmann S, Bennett RE, Delorme L, Robbins AB, Hu M, McKenzie D, et al. Experimental evidence for the age dependence of tau protein spread in the brain. Sci Adv. 2019;5(6):eaaw6404.
246. Liu P, Reed MN, Kotilinek LA, Grant MK, Forster CL, Qiang W, et al. Quaternary Structure Defines a Large Class of Amyloid-beta Oligomers Neutralized by Sequestration. Cell Rep. 2015;11(11):1760-71.
247. Kayed R, Head E, Sarsoza F, Saing T, Cotman CW, Necula M, et al. Fibril specific, conformation dependent antibodies recognize a generic epitope common to amyloid fibrils and fibrillar oligomers that is absent in prefibrillar oligomers. Mol Neurodegener. 2007;2:18.
248. Necula M, Kayed R, Milton S, Glabe CG. Small molecule inhibitors of aggregation indicate that amyloid beta oligomerization and fibrillization pathways are independent and distinct. J Biol Chem. 2007;282(14):10311-24.
249. Cummings J, Feldman HH, Scheltens P. The "rights" of precision drug development for Alzheimer's disease. Alzheimers Res Ther. 2019;11(1):76.
250. Spilman P, Podlutskaya N, Hart MJ, Debnath J, Gorostiza O, Bredesen D, et al. Inhibition of mTOR by rapamycin abolishes cognitive deficits and reduces amyloid-beta levels in a mouse model of Alzheimer's disease. PLoS One. 2010;5(4):e9979.

6 Appendices

6.1 Appendix A – Details on all animals

6.1.1 Cohort 1

Animal ID	Strain	Age	Drug	Length drug testing	Age when perfused	Primary antibodies used	Notes
90200	3xTg	13 months	Fasudil	14 days	14 months		Tissue damaged. Excluded from analysis
90555	3xTg	13 months	Fasudil	14 days	14 months	MC1, OC, McSA1, TREM2	OC plaques quantified
90556	3xTg	13 months	Fasudil	14 days	14 months	MC1, OC, McSA1, TREM2	OC plaques quantified
90557	3xTg	13 months	Fasudil	14 days	14 months	MC1, OC, McSA1, TREM2	OC plaques quantified

6.1.2 Cohort 2

Animal ID	Strain	Age	Drug	Length drug testing	Age when perfused	Primary antibodies used	Notes
64 (tau-injected)	3xTg	5 months	Lonafarnib	10 days	6 months	OC, MC1, A11, McSA1, TREM2	
65 (tau-injected)	3xTg	5 months	Saline	10 days	6 months	OC, MC1, A11, McSA1, TREM2	
66 (tau-injected)	3xTg	5 months	Lonafarnib	10 days	6 months	OC, MC1, A11, McSA1, TREM2	
67 (tau-injected)	3xTg	5 months	Saline	10 days	6 months	OC, MC1, A11, McSA1, TREM2	

6.1.3 Cohort 3

Animal ID	Strain	Age	Drug	Length drug testing	Age when perfused	Primary antibodies used	Notes
34	3xTg	6 months	Saline	2 months (1 week + 5 days)	7 months	McSA1, OC, A11, TREM2	iAβ quantified
35	3xTg	6 months	Fasudil	2 months (1 week + 5 days)	7 months	McSA1, OC, A11, TREM2	iAβ quantified
37	3xTg	6 months	Fasudil	2 months (1 week + 5 days)	7 months	McSA1, OC, A11, TREM2	iAβ quantified

6.1.4 Cohort 4

Animal ID	Strain	Age	Drug	Length drug tresting	Age when perfused	Primary antibodies used	Notes
154	B6129	5 months	Saline	10 days	6 months	MC1, OC, McSA1, TREM2, LAMP1	
155	B6129	5 months	Lonafarnib	10 days	6 months	MC1, OC, McSA1, TREM2, LAMP1	
91902	3xTg	13 months	Saline	10 days	14 months	MC1, OC, McSA1, TREM2, LAMP1	OC plaques quantified
91903	3xTg	13 months	Lonafarnib	10 days	14 months	MC1, OC, McSA1, TREM2, LAMP1	OC plaques quantified

6.1.5 Non-experimental animals (surgery practice)

Animal ID	Strain	Age	Surgery	Notes
53	B6129	7 months	Microdialysis probe implantation	Not successful
55	B6129	7 months	Microdialysis probe implantation	Successful
58	B6129	8 months	Microdialysis probe implantation	Successful
59	B6129	8 months	Microdialysis probe implantation	Successful

6.2 Appendix B – Implantation surgeries

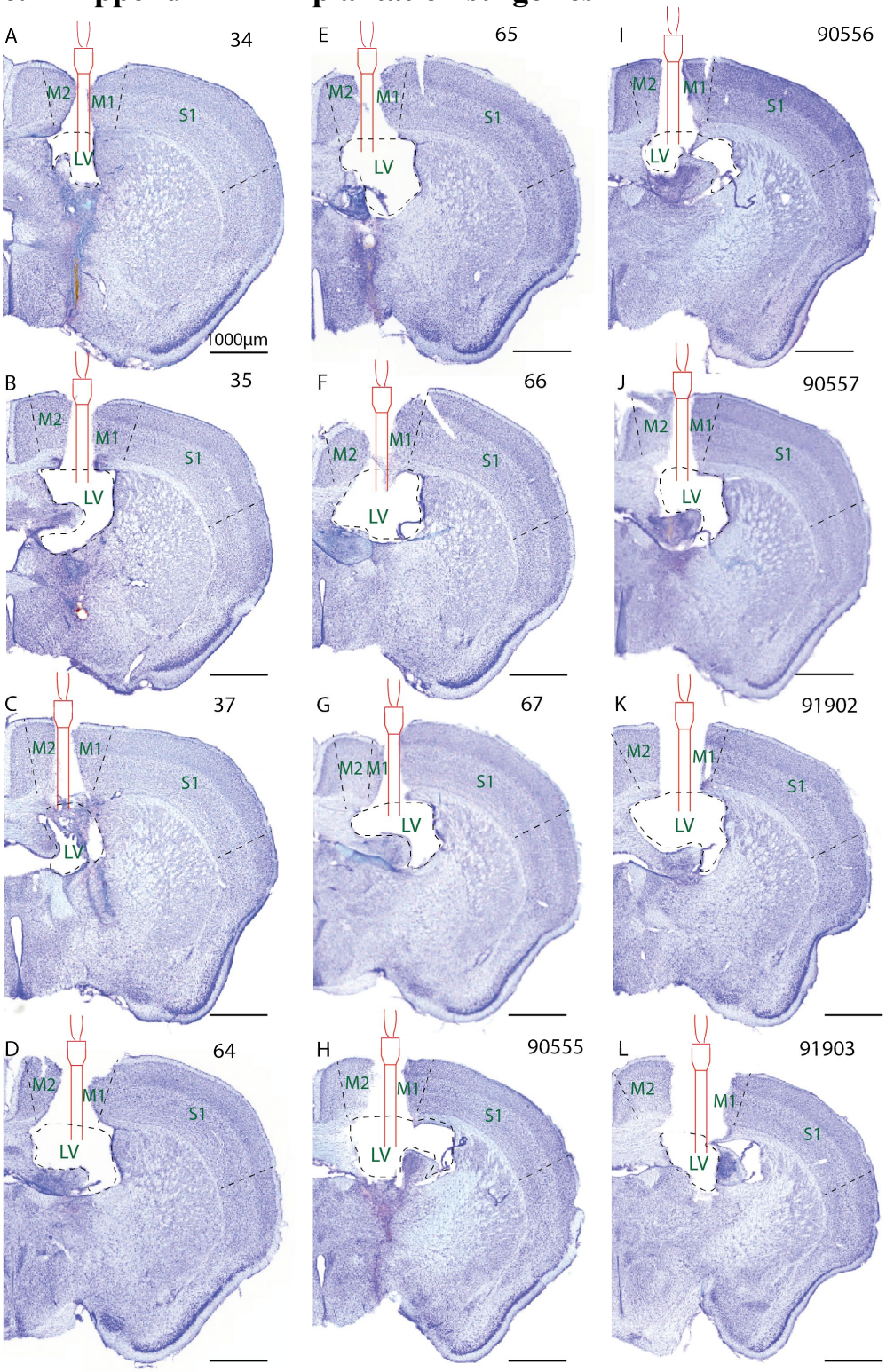

Figure 6.1. (A-L): Microdialysis probe implantation as verified by Cresyl violet (Nissl) staining in 12 3xTg mice. The microdialysis probe was successfully implanted in LV along the rostrocaudal axis in all 12 experimental 3xTg animals. Stereotaxic coordinates: A/P: -0.1mm, M/L: +1.2mm, D/V: -2.75mm. Delineations based on Paxinos and Franklin[194]. Abbreviations; LV: lateral ventricle; M1: primary motor cortex; M2: secondary motor cortex; S1: primary somatosensory cortex.

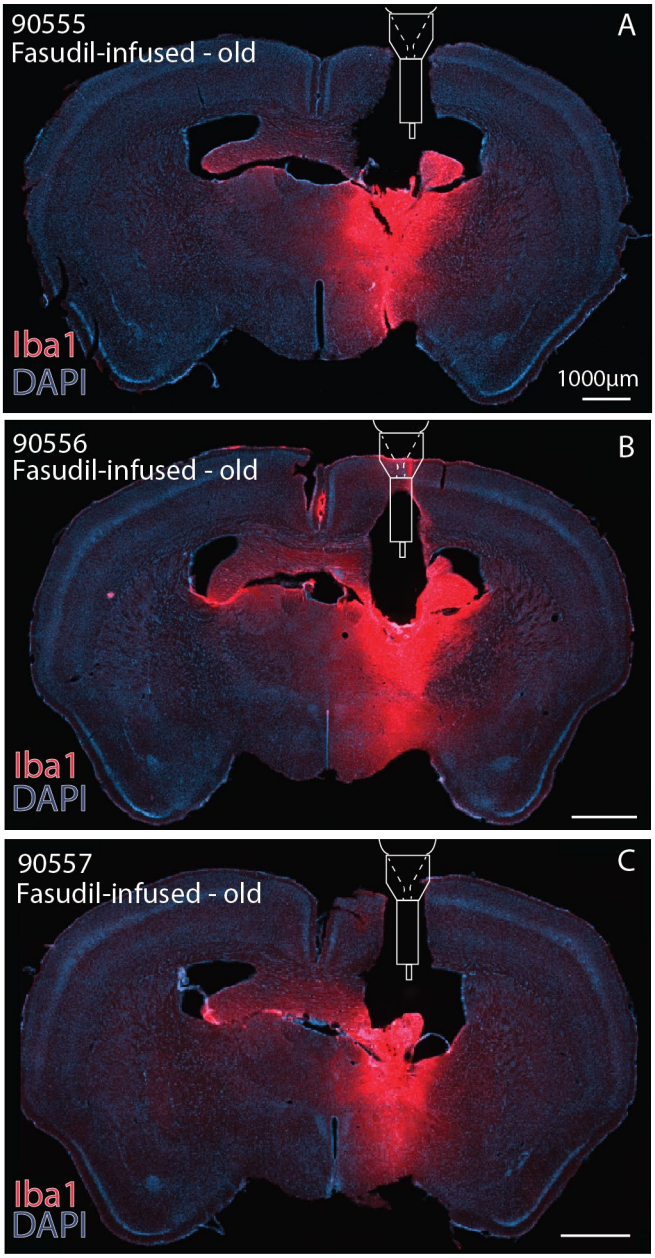

Figure 6.2. (A-C): Immunohistochemistry of brain tissue slices after microdialysis probe implantation into the lateral ventricle with Fasudil (*n* = 3) infused infused once a day for 14 days in 14-month-old 3xTg mice. Iba1 (red; microglial activation) immunoreactivity around the implantation track revealed moderate inflammation. Abbreviations; DAPI: 4′,6-diamidino-2-phenylindole.

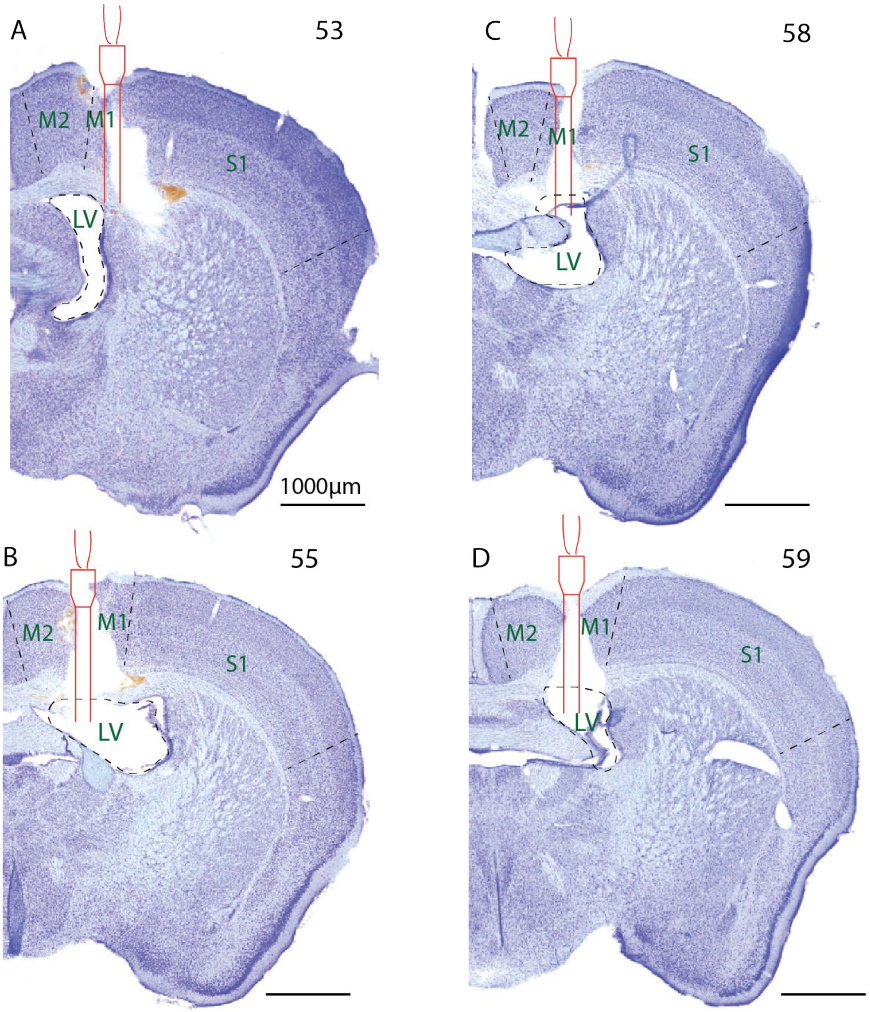

Figure 6.3. (A-D): Practice microdialysis probe implantation as verified by Cresyl violet (Nissl) staining in four B6129 mice, performed by me. (A): The microdialysis probe was implanted laterally in the mediolateral axis to the LV. (B-D): The microdialysis probe was successfully implanted in LV along the rostrocaudal axis. Stereotaxic coordinates: A/P: -0.1mm, M/L: +1.2mm, D/V: -2.75mm. Delineations based on Paxinos and Franklin[194]. Abbreviations; LV: lateral ventricle; M1: primary motor cortex; M2: secondary motor cortex; S1: primary somatosensory cortex.

6.3 Appendix C – Additional immunohistochemistry images

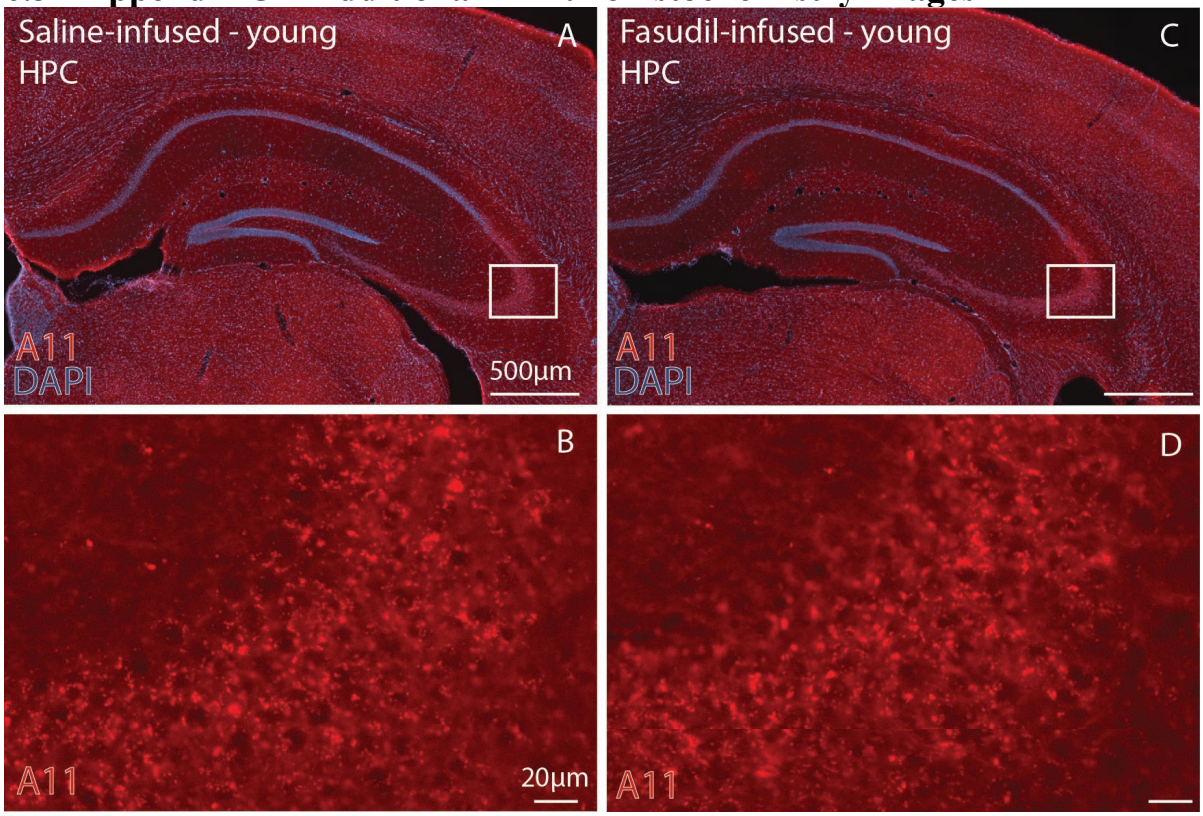

Figure 6.4. (A-D): Immunohistochemistry of brain tissue slices after microdialysis probe implantation into the lateral ventricle with saline (left, *n* = 1) or Fasudil (right; *n* = 2) infused once a day for 7 days, then 30 days without any infusions, then once a day for another 5 days in 6-month-old 3xTg mice. Oligomeric iAβ (red; A11) reactivity is shown in the CA3 region of the HPC of the saline-infused mouse (A-B) and a Fasudil-infused mouse (C-D). A11 appeared to stain various intracellular bodies rather than the cytosol itself. As this was not easily quantifiable, McSA1 staining was used for iAβ quantification in the current study. Abbreviations; DAPI: 4′,6-diamidino-2-phenylindole; HPC: hippocampus.

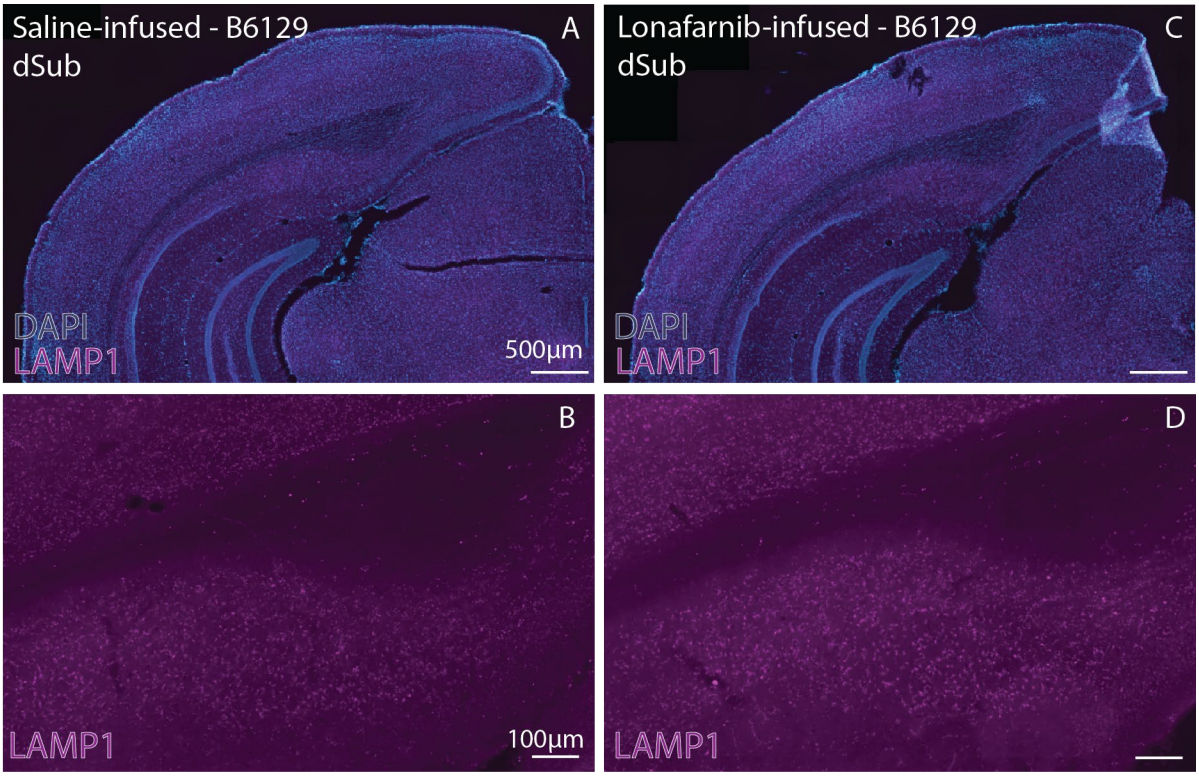

Figure 6.5. (A-D): Immunohistochemistry of brain tissue slices after microdialysis probe implantation into the lateral ventricle with Lonafarnib (*n* = 1) or saline (*n* = 1) infused once a day for 10 days in 5-month-old B6129 mice. Lysosomal associated membrane protein 1 immunoreactivity (purple; LAMP1) appears to be stronger in the dSub of the Lonafarnib-infused mouse (C-D) compared to the saline-infused mouse (A-B). Abbreviations; dSub: dorsal subiculum; DAPI: 4′,6-diamidino-2-phenylindole.

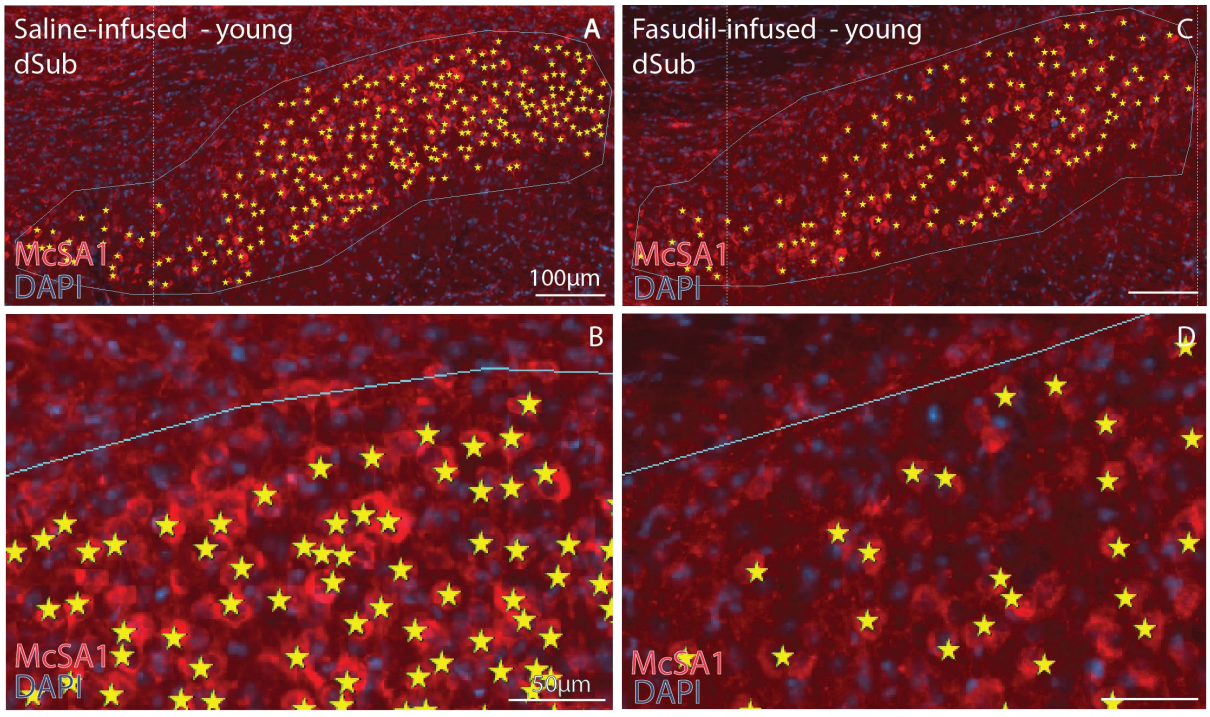

Figure 6.6. (A-D): Immunohistochemistry of brain tissue slices after microdialysis probe implantation into the lateral ventricle with saline (*n* = 1) or Fasudil (*n* = 2) infused once a day for 7 days, then 30 days without any infusions, then once a day for another 5 days in 7-month-old 3xTg mice. Examples of manual iAβ quantification of McSA1-positive cells in the dSub of one brain section of a saline-infused mouse (A-B) and a

Fasudil-infused mouse (C-D). Manual quantification was performed using Stereo Investigator Software. Abbreviations; dSub: dorsal subiculum; DAPI: 4′,6-diamidino-2-phenylindole.

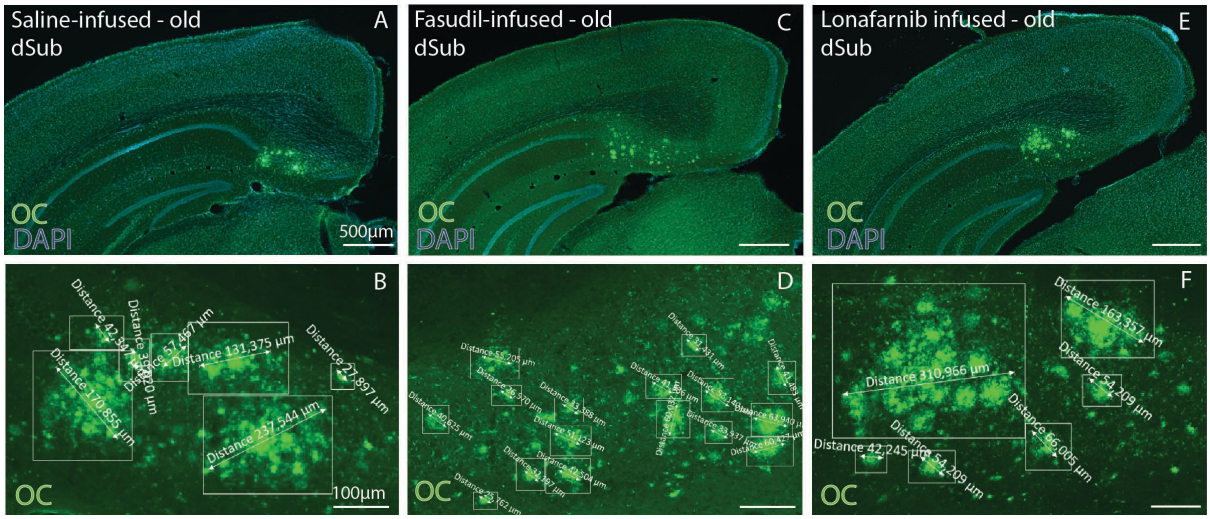

Figure 6.7 (A-F): Immunohistochemistry of brain tissue slices after microdialysis probe implantation into the lateral ventricle with saline (left; *n* = 1) infused once a day for 10 days, Fasudil (middle; *n* = 3) infused once a day for 14 days, or Lonafarnib (right; *n* = 1) infused once a day for 10 days in 14-month-old 3xTg mice. Examples of fibrillar Aβ42-stained (OC; green) amyloid plaque number and size quantification in the dSub of a saline-infused mouse (A-B), a Fasudil-infused mouse (C-D), and a Lonafarnib-infused mouse (E-F). Amyloid plaque quantification was performed manually using Zen Blue Microscope Software. Abbreviations; dSub: dorsal subiculum; DAPI: 4′,6-diamidino-2-phenylindole.

6.4 Appendix D– Immunohistochemistry protocols

6.4.1 Cresyl violet (Nissl) staining

1. Dehydrate sections – 10 dips in each: 50, 70, 80, 90, 100, 100, and 100% ethanol
2. Leave in xylene for 2min
3. Rehydrate sections – 10 dips in each: 100, 100, 100, 90, 80, 70, and 50% ethanol
4. Quick wash in running water
5. Leave sections in Cresyl Violet for 3min on shaker
6. Dip sections in running water 3x, then citric acid 3x, then running water 3x
7. Leave sections in Cresyl Violet for 2min on shaker
8. Repeat step 6
9. Dehydrate sections – 10 dips in each: 50, 70, 80, 90, 100, 100, and 100% ethanol
10. Leave in Xylene for at least 5min
11. Coverslip with Xylene + Entellan

6.4.2 Fluorescent immunohistochemistry

1. Do heat-induced antigen retrieval (HIAR) at 60 degrees celsius for 2 hours in PB
    1. Use 80-100ml of PB in glass jars
    2. Set the heating stirrer plate to 82 degrees celsius
    3. Warm glass jars to 60 degrees celsius in microwave
2. Wash 3x10min in PBT
3. Incubate for 1 hour in PBT with 5% goat serum
4. Incubate primary antibodies in PBT with 5% goat serum for 4 hours in fridge (5 degrees celsius) - 1:1000 (0.1%) concentration
5. Leave in PB overnight
6. Wash 3x10min in PBT
7. Incubate secondary antibodies in PBT with 5% goat serum for 2 hours in room temperature, protected from light – 1:400 (0.25%) concentration

8. Wash 1x10min with DAPI – 1:10,000 (0.01%) concentration, protected from light
9. Wash 1x10min in Tris-HCl (skip this step if you are using a while to mount tissue), protected from light
10. Mount in Tris-HCl on slides and dry on a heating plate (at 38 degrees Celsius) for at least 4 hours, protected from light
11. Leave in Xylene for at least 5 min
12. Coverslip with Xylene+Entellan

6.4.3 3, 3'-diaminobezidine (DAB)/Peroxidase protocol

Previous research has indicated that a differential microtubule-associated protein 2 (MAP2) immunolabeling pattern can distinguish dense-core amyloid plaques from diffuse amyloid plaques using 3,3'-diaminobenzidine (DAB, Sigma-Aldrich, St. Louis, MO, USA) as a chromogen[208]. This was tested using brain sections from five old mice (three Fasudil-infused, two Lonafarnib-infused). Three to four brain sections containing amyloid-plaque abundant regions (dentate gyrus, dorsal subiculum, entorhinal cortex) were chosen from the fourth series of each animal.

1. Leave sections in 0,125M phosphate buffer (PB) at 60 degrees Celsius for 2 hours.
2. Rinse sections 2 x 10 min in PB.
3. Rinse sections 1 x 10 min in TBS-Tx
4. Incubate for 30 min with 10% goat serum in TBS-Tx
5. Draw off excess solution (do not wash)
6. Incubate with primary antibody, McSA1, 1:1000 in TBS-Tx, overnight in refrigerator (4 degrees Celsius)
7. Rinse 3x10 min in TBS-Tx. Mix secondary antibody during first wash and start dissolving DAB during second wash. Leave DAB on heated stirrer for 2 hours, then leave on bench.
8. Incubate with secondary antibody, biotinylated goat anti-mouse, 1:200 in TBS-Tx, 90 min in room temperature. Mix ABC right before next step.
9. Rinse sections 3x10 min in TBS-Tx.
10. Incubate with ABC, 90 min in room temperature.
11. Rinse 3x10 min in TBS-Tx.
12. Rinse 2x5 min in Tris-HCl.
13. Incubate with DAB for 30 minutes.
14. Rinse 2x5 min in Tris-HCl.
15. Mount sections in Gelatine on a heating plate (or Tris-HCl on Superfrost slides if doing a Nissl counterstain) and let them dry.
16. Coverslip with Toulene and Entellan.

6.4.4 List of secondary antibodies

Secondary antibody	Manufacturer	Catalog number
Goat anti-rabbit A488	Abcam	Ab150077
Goat anti-mouse A546	Thermo-Fisher	A-11030
Goat anti-mouse A647	Thermo-Fisher	A-21236

6.5 Appendix E – Lists of chemicals and solutions

Chemicals	Manufacturer	Catalog number
Dimethyl sulfoxide	VWR	23486
Entellan	Merck	107961
Glycerol	VWR	23487
Hydrochloric acid (HCl)	Merck	100317
Hydrogen peroxide solution 30%	Sigma-Aldrich	H1009
Paraformaldehyde (PFA)	Sigma-Aldrich	16005

Potassium chloride	Merck	104936
Rectified ethanol	Kiiltoclean AS	600051
Sodium chloride (NaCl)	VWR	27800
Sodium dihydrogen phosphate	Merck	106346
Sodium hydrogen phosphate dihydrate	Merck	119753
Sodium hydrogen carbonate	Merck	106329
Sodium hydroxide 35% (NaOH)	VWR	282211
Tris(hydroxylmethyl)aminomethane	Merck	108382
Triton-X-100	Merck	108603
Xylene	VWR	28975.325

DMSO
100 ml: 31.25 ml 0.4M phosphate buffer, 46.75 ml H20, 20 ml glycerin, 2 ml DMSO.

Phosphate buffer (PB) 0.4M pH 7.4
Consists of an acid (A) and a base (B).
Solution A: Sodium dihydrogen phosphate 27.6 g/500 ml H20
Solution B: Sodium hydrogen phosphate dihydrate 35.6 g/500 ml H20
Make solution A and B. Add solution A to solution B until the pH is 7.4. Store in the dark in room temperature for up to one month.

Phosphate buffer 0.125M pH 7.4
Dilute 0.4M phosphate buffer. Store at 4 degrees Celsius for up to one week.
500 ml: 146 ml 0.4 PB + 344 ml H20

Fixative 4% paraformaldehyde 500 ml
Heat 100 ml of H20 to 60 degrees in the microwave oven. Measure 10g of paraformaldehyde and add the water. Add a few drops of NaOH and leave the solution on a hot stirrer until the solution is clear. Then add 78 ml 0.4M PB and 72 ml H20.
Set the pH to 7.4 using HCl and filtrate. Everything should be carried out in a ventilated hood. Make new fixative for every perfusion.

Ringer
0.85% NaCl (4.25 g / 500 ml H20)
0.025% KCl (0.125 g / 500 ml H20)
0.02% NaHC03 (0.1 g / 500 ml H20)
Filtrate. Make fresh ringer before every perfusion.

Sucrose/saccharose
Dissolve 30g sucrose/saccharose in 31.25 ml 0.4M PB and 68.75 ml H20.

Tris-HCl pH 7.6
500 ml: 3.03 g Tris in 500 ml H20
Use HCl to adjust the pH to 7.6. Store in refrigerator for up to one week.

TBS-Tx 0.5% pH 8.0
500 ml H20, 3.03 g Tris, 4.48 g NaCl, 2.5 ml Triton-X-100.
Use HCl to adjust the pH to 7.6. Store in refrigerator for up to one week.

6.6 Appendix F – QQ plots

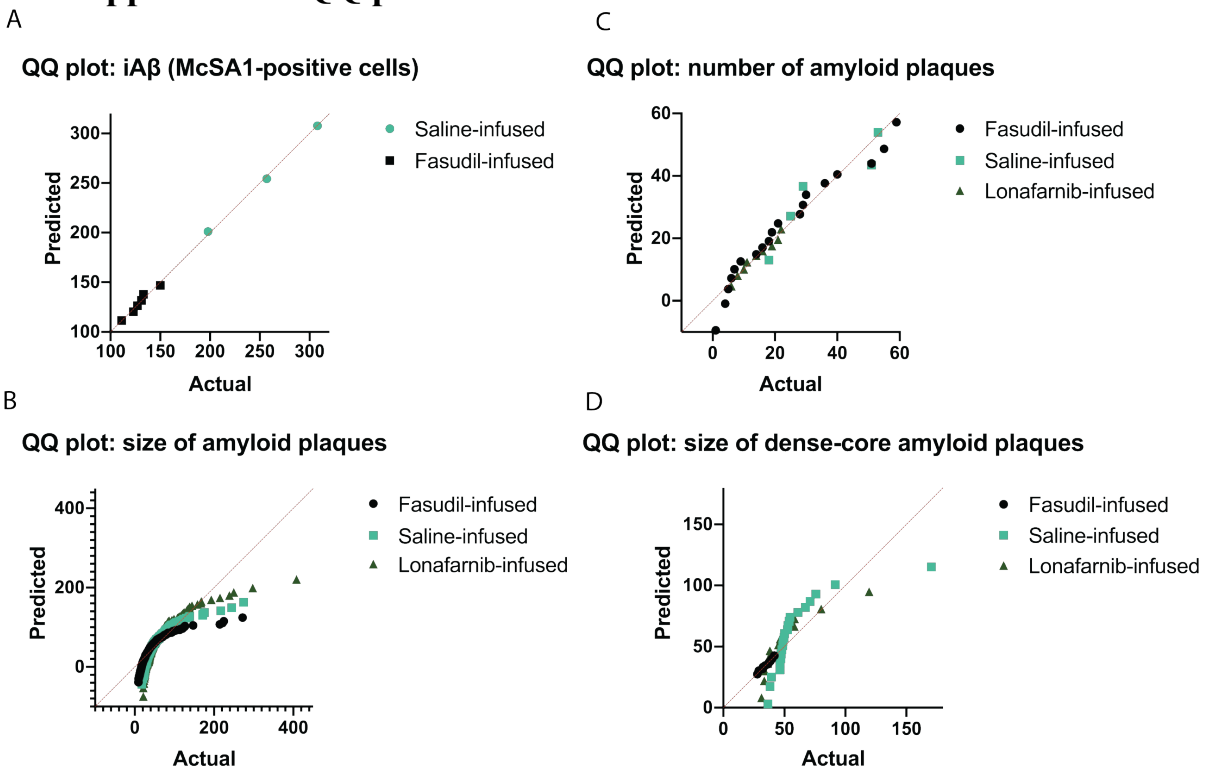

Figure 6.8. (A-D): Quartile-quartile (QQ) plots of data analyzed in this thesis. (A): QQ plot of actual vs. predicted values of McSA1-positive cells in the dSub of brain sections from 7-month-old saline-infused (n = 1) and Fasudil-infused (n = 2) 3xTg animals. Data was normally distributed, so an unpaired t-test was used to test for statistical significance between groups. (B): QQ plot of actual vs. predicted values of the size of amyloid plaques in the dSub of brain sections from 14-month-old Fasudil-infused (n = 3), saline-infused (n =1), and Lonafarnib-infused (n = 1) animals. Data was not normally distributed, so a Mann-Whitney U test was used to test for statistical significance between groups. (C): QQ plot of actual vs. predicted values of the number of amyloid plaques in the dSub of brain sections from 14-month-old Fasudil-infused (n = 3), saline-infused (n = 1), and Lonafarnib-infused (n = 1) 3xTg animals. Data was normally distributed, so unpaired t-tests were used to test for statistical significance between groups. (D): QQ plot of actual vs. predicted values of the size of dense-core amyloid plaques in the dSub of brain sections from 14-month-old Fasudil-infused (n = 2), saline-infused (n = 1), and Lonafarnib-infused (n = 1) 3xTg animals. Data was not normally distributed, so Mann-Whitney U tests were used to test for statistical significance between groups.